

20960

NATIONAL LIBRARY  
OTTAWA



BIBLIOTHÈQUE NATIONALE  
OTTAWA

NAME OF AUTHOR... *Fimer Alpaslan*

TITLE OF THESIS... *Transfer junction analysis*

UNIVERSITY... *University of Alberta*

DEGREE FOR WHICH THESIS WAS PRESENTED... *Ph.D.*

YEAR THIS DEGREE GRANTED... *1974*

Permission is hereby granted to THE NATIONAL LIBRARY  
OF CANADA to microfilm this thesis and to lend or sell copies  
of the film.

The author reserves other publication rights, and  
neither the thesis nor extensive extracts from it may be  
printed or otherwise reproduced without the author's  
written permission.

(Signed) *[Handwritten Signature]*

PERMANENT ADDRESS:  
.....  
.....  
.....

DATED *Apr. 17, 1974* ..... 19

THE UNIVERSITY OF ALBERTA

---

TRANSFER FUNCTION ANALYSIS

by

©

TÜMER ALPASLAN

A THESIS

SUBMITTED TO THE FACULTY OF GRADUATE STUDIES AND RESEARCH  
IN PARTIAL FULFILLMENT OF THE REQUIREMENTS FOR THE DEGREE  
OF DOCTOR OF PHILOSOPHY

---

DEPARTMENT OF PHYSICS

EDMONTON, ALBERTA

SPRING 1974

THE UNIVERSITY OF ALBERTA

FACULTY OF GRADUATE STUDIES AND RESEARCH

The undersigned certify that they have read,  
and recommend to the Faculty of Graduate Studies and  
Research, for acceptance, a thesis entitled TRANSFER  
FUNCTION ANALYSIS submitted by Tümer Alpaslan in  
partial fulfillment of the requirements for the degree  
of Doctor of Philosophy.

*E. R. Koronak*  
.....  
Supervisor

*Keith ...*  
.....

*G. L. Cumming*  
.....

*M. I. ...*  
.....

*.....*  
.....  
External Examiner

Date *Ap. 4. 1974*  
.....

*.....*

## ABSTRACT

The spectral ratio method is used to investigate the transmission characteristics of the crust under a group of seismic stations in Alberta. Various model crustal spectral ratios using a Haskell-Thomson matrix formulation have been compared with the experimental ones.

The implications of a simple form of seismic anisotropy in plane parallel layered media have been investigated. In the low frequency band appropriate to the P coda of most teleseismic events, transverse anisotropy does not have a significant effect on spectral ratios. A ray theory approach is used to evaluate the response of a multidipping layered media. A computerized method is used to obtain the number of terms necessary in a partial ray expansion to approximate the wave solution for a flat layered case. Model studies indicate that a flat layered assumption is valid for dip angles less than  $10^\circ$ . However, low velocity layers dipping as much as  $10^\circ$  introduce significant shift in peak positions. Complex velocities are introduced into a Haskell-Thomson matrix formulation to study the attenuation characteristics of the crust. Comparison of experimental spectral ratios with the attenuating spectral ratio model favors an average  $Q_p$  value of 500 in the crust.

Analysis of seismic station recordings near Edmonton, Pine Lake, and Rocky Mountain House suggests the presence of an approximately 35 km thick crust.

The station near Trochu and Delburne indicates a very heterogeneous structure. Azimuthal deviation measurements and record character suggest that the anomalous results are due to steeply dipping or more complicated structure in the upper crust.

Synthetic seismograms for attenuating isotropic or anisotropic layered media have been obtained for an input plane P or S wave by taking the inverse Fourier transform of the transfer function calculated by a Haskell-Thomson matrix formulation. Model seismograms have also been calculated for dipping layered media using asymptotic ray theory. When an S wave is incident at the bottom of the layered media, conversions at various interfaces cause a series of precursors to S wave. On the vertical component of displacement, the main "S" arrival may be 1-6 seconds later than the precursors for a continental crust. At some epicentral distances a sedimentary layer may generate very strong precursors up to 2 seconds before the pure shear arrival. This result appears to explain many inconsistent interpretations in the study of shear waves.

## ACKNOWLEDGEMENTS

I would like to thank my supervisor Dr. E. R. Kanasewich for his guidance.

Many thanks are also due to Dr. M. Razavy and Dr. C.H. Chapman for their excellent courses.

I express appreciation to Dr. F. Hron, for his help and cooperation.

Finally, I thank my friends Mr. and Mrs. Bates, Mr. and Mrs. Gutowski and Mrs. Mary Yiu for her job in typing.

# TABLE OF CONTENTS

		<u>Page</u>
CHAPTER I	INTRODUCTION	1
1.	Object of this work	1
2.	Previous work	2
CHAPTER II	TRANSFER FUNCTION STUDIES	6
I	Crustal investigation using spectral ratio method	6
1.	Crustal transfer function	6
2.	Haskell-Thomson matrix formulation	8
3.	Computation of experimental spectrum	14
4.	Efficiency of the spectral ratio method	18
II	Anisotropy	24
1.	Introduction	24
2.	Computation of a plane wave solution for a transversely isotropic multilayered media	29
3.	Transfer ratios for transversely isotropic layered media	37
III	Effect of dipping layers on wave transmission	48
1.	Introduction	48
2.	A ray-theory approach for computation of the response of a layered media	50
3.	Dipping layered media and transfer ratios	62
4.	Conclusions	66

	<u>Page</u>
CHAPTER II : (cont'd)	
IV Attenuation in the crust	71
1. Representation of attenuation in the solid Earth	71
2. Attenuation properties of crust	76
3. Spectral ratios for dissipative crustal models and application to earthquake data	84
4. Discussion and conclusions	93
V Crustal structure in central Alberta from spectral ratio method	97
1. Experimental data	97
2. EDM station	97
3. PIN station	113
4. RM stations	118
5. TRO and DEL stations	129
6. Conclusions	136
CHAPTER III : SYNTHETIC SEISMOGRAMS	140
I Seismograms for P waves	140
II Seismograms for S waves	148
BIBLIOGRAPHY	156



# LIST OF TABLES

<u>Chapter II</u>	<u>Page</u>
I. Table 1 - Crustal model ALTACRT-2	47
II. Table 1 - Alberta crustal model ALTACRT-3	58
II. Table 2 - Family of unconverted rays	59
II. Table 3 - List of combinations used for creation of converted rays	60
V. Table 1 - List of Earthquakes	99
V. Table 2 - Models for EDM station	106
V. Table 3 - RM crustal models	121

LIST OF FIGURES

CHAPTER II

Figure

Page

I.1	Orientation of axes and numbering of layers and interfaces	9
I.2	Theoretical spectral ratios using Parzen window and various pulse functions	19
I.3	Effect of additional phase on the spectral ratios	20
II.1	Effect of transverse anisotropy on transfer ratio	38
II.2	Effect of transverse anisotropy on transfer ratio	39
II.3	Influence of upper mantle anisotropy on the wave transmission	42
II.4	Comparison of an experimental spectral ratio with a model	44
III.1	Approximation of wave solution by ray expansion	51
III.2	Comparison of spectral ratios for a dipping model with flat one	64
III.3	Comparison of spectral ratios for dipping and flat layer model for an incident plane S wave	65
III.4	Effect of steeply dipping sedimentary layer on transmission of P waves	67
III.5	Effect of up-dipping layers on long period transfer ratios for P waves	68
III.6	Effect of dipping interfaces on long period transfer ratios	69
IV.1	Comparison of transfer ratios for attenuating models with the non-attenuating one	85
IV.2	A transfer ratio for attenuating model and its time synthesis	87
IV.3	An experimental transfer ratios for a large window length	91

CHAPTER II (cont'd)

<u>Figure</u>		<u>Page</u>
V.1	Location of array of stations	98
V.2	Long period spectral ratios for EDM station	102
V.3	Short period, combined spectral ratios for EDM station	104
V.4	Long period spectral ratio models	107
V.5	Comparison of spectral ratios	109
V.6	A few example of records for EDM station	111
V.7	Azimuthal deviations for EDM station	112
V.8	Combined long period spectral ratios for PIN station	114
V.9	Short period spectral ratios for PIN station	116
V.10	Azimuthal deviations for PIN station	117
V.11	Event 73 recorded by RM2 station	122
V.12	Some of long period spectral ratios for RM stations	123
V.13	Events from SE sector	124
V.14	Three long period spectral ratios and their comparison with RM models	125
V.15	Short period spectral ratios for RM stations	126
V.16	Azimuthal deviations for RM stations	127
V.17	Three earthquake data recorded by TRO station	130
V.18	Azimuthal deviations for TRO station	131
V.19	Azimuthal deviations for DEL station	133
V.20	Long period spectral ratios for TRO and DEL stations	135

CHAPTER III

<u>Figure</u>		<u>Page</u>
I.1	Comparison of seismograms computed by Haskell-Thomson and ray theory for P waves	143
I.2	Existing rays and their use for a 4 layered crustal model	145
I.3	Effect of dipping layers on seismogram appearance	146
II.1	Theoretical seismograms calculated using a Haskell-Thomson matrix formulation.	149
II.2	Vertical and horizontal component of surface displacement as a function of distance	151
II.3	Theoretical seismogram for a plane S wave	154

## CHAPTER I

### INTRODUCTION

#### 1. Object of this work

In seismology a study of the transmission of elastic waves has been one of the challenging search areas. This branch of Geophysics offers a direct or indirect measurement of parameters of the Earth's interior. Seismological measurements have shown that the interior of the Earth can be divided into several distinct physical and chemical shells. The outer part of the Earth which is about 50 km thick under continents and 5 km under the oceans has been named the crust. This region is separated from the upper mantle by a well recognized discontinuity called the "Moho". Rapid variations in the properties of the crust are also well known. Mountains and their roots, deep oceans and other complex tectonic features create difficulties when interpreting elastic waves that have passed through the deeper parts of the Earth.

It is useful sometimes to express the recorded teleseismic signal as a convolution of a pulse with a transfer function representing the transmission characteristics of the crust near the recording seismic station. There are a number of theoretical techniques for calculating the transfer function of layered

media. These methods have been extended to yield complete wave solutions for an incident plane wave on a plane parallel layered media in which seismic anisotropy and attenuation may exist. In this thesis the problem of a dipping layered medium has also been investigated independently. The models used in this work are assumed to be homogeneous and the layers are separated by first order discontinuities. A comparison between theory and experiment has been attempted. In this way it is hoped that the transmission characteristics of any crustal section may be determined. A number of synthetic seismograms and spectral models provided in this work should help seismologists to understand the wave modifications that are produced during transmission of a wave through a layered medium.

## 2. Previous work

Observations on the effect of the crust on wave transmission has proceeded since the early days of seismology. Among these Tomura (1929) studied the vibration of the crust using seismic waves from earthquakes; Nasu (1931) investigated the relation between the period of seismic waves and the type of soil; Gutenberg (1957) also studied earthquake damage and its relation to the type of soil; Nuttli and Whitmore

(1961, 1962) investigated the polarization angle between P and S waves and suggested frequency dependent polarization angle.

A number of authors attempted to calculate the theoretical response of crustal structure. The crust is assumed to consist of a number of layers. In the early days, great simplifications were made to obtain a solution [Sezawa and Kanai (1932, 1937)].

Thomson (1950) and Haskell (1953) were the first to formulate the frequency dependent polarization angle characteristics of a layered medium. They expressed the response of a plane parallel isotropic layered medium to an incoming plane wave at any angle of incidence using products of four by four matrices whose elements are a function of parameters of each layer and the boundary conditions. Dorman (1962) formulated the solution at a boundary between a liquid and a solid. Harkrider and Anderson (1962) obtained the response for a transversely isotropic medium.

Fast digital computers have made it practical to use the Haskell-Thomson matrix method for modelling a crustal section with any number of layers. Phinney (1964) compared the ratio of long-period spectra of vertical and horizontal seismograms with a number of models calculated using the Haskell-Thomson method.

The introduction of a spectral ratio technique was a significant breakthrough because it eliminated most of the source function effects. Hannon (1964) first attempted the calculation of long period synthetic seismograms by taking the inverse Fourier transform of the transfer function. Fernandez (1967) used spectral ratios for long-period data giving model curves to determine crustal structure. Leblanc (1967) discussed the importance of a window for the high frequency portion of the spectrum using the spectral ratio method. McCamy (1967) attempted to apply transfer function analysis to determine crustal structure using explosion sources. Ellis and Basham (1968) applied the spectral ratio method in an attempt to resolve crustal structure in central Alberta. Hasegawa (1970, 1971) used the spectral ratio method to model the structure at Yellowknife. Ibrahim (1969) made use of the spectral behavior of SH waves to determine crustal thicknesses. Kurita (1969) used long-period waves in an attempt to find crustal and mantle structure. Ishii and Ellis (1970) formulated the response of single dipping layer over a half space and Rogers and Kisslinger (1972) applied this ray theory to earthquake data. Jensen (1970) applied linear filter theory to calculate the response of a layered medium in the time domain to reduce the inefficiency of the Haskell-Thomson method.



Sprenké (1972) studied the transmission characteristics of the Alberta crust using the Haskell-Thomson method.

In this study the Haskell-Thomson matrix method and a ray theory approach were applied to earthquake data recorded by University of Alberta in 1970. Implications of an anisotropic or dipping crustal model are discussed. Comparisons are made between the completed wave solution and a partial ray expansion and criteria for a satisfactory solution have been established both in the frequency and the time domain. High frequency theoretical seismograms were obtained by Fourier inversion of Haskell-Thomson matrices using a synthetic pulse.

## CHAPTER II

### TRANSFER FUNCTION STUDIES

#### I. Crustal Investigation using the Spectral Ratio Method

##### 1. Crustal transfer function

In the time domain, according to filter theory, the transmission of a plane elastic wave through a medium can be represented as a convolution of a pulse with a transfer function representing the elastic response of the media. In the frequency domain it can be written as

$$R(\omega) = P(\omega) \cdot H(\omega) \quad (1)$$

where  $R(\omega)$  is the frequency response of the media to a pulse  $P(\omega)$  and  $H(\omega)$  is the transfer function. It has generally been assumed that crust of the Earth has been made of a number of layers separated by first and second order discontinuities. For such a layered medium, transfer function calculations can be performed by a number of methods. The Haskell-Thomson (1962) matrix formulation gives a rapid and exact calculation of a transfer function for a plane parallel multilayered medium in which seismic anisotropy may exist. Gilbert and Backus (1966) formulated another matrix method in which the Haskell-Thomson method is a special case.

One advantage of this method is that a medium with second order discontinuities is allowed (Richards, 1971).

Ray theory can be used to calculate the response of layered media (Hron, Kanasevich, Alpaslan, 1973).

A ray solution can be applied successfully to dipping or curvilinear interfaces provided that a sufficiently large number of rays are included in the response.

In this thesis both the Haskell-Thomson matrix formulation and a ray theory approach have been used to determine the response of multilayered media to a plane wave impinging on the bottom.

In equation (1), the nature of the source pulse is generally not known in practice and an incorrect assumption can seriously alter the response function. If the vertical and radial components of particle motion can be calculated, then the ratio of these two components will be independent of the source pulse:

$$\frac{R_V(\omega)}{R_R(\omega)} = \frac{H_V(\omega)}{H_R(\omega)} \quad (2)$$

Equation (2) is called the "transfer ratio" or the "spectral ratio". Both terms are used in this thesis.

In practice the vertical and horizontal components of ground velocity are generally known, then the left hand side of equation (2) can be determined and compared to the right hand side of the same equation which represents a particular model.

## 2. Haskell-Thomson matrix formulation

Periodic solutions of elastic equations of motion for the  $m^{\text{th}}$  layer may be obtained by combining the dilatational wave solution in the  $x$ - $z$  plane:

$$\theta_m = \left(\frac{\partial u}{\partial x}\right) + \left(\frac{\partial w}{\partial z}\right) = \exp[i\omega(t - \frac{x}{c})] [\theta_{od} \exp(-i\omega r_{\alpha_m} z/c) + \theta_{ou} \exp(i\omega r_{\alpha_m} z/c)] \quad (1)$$

with the rotational wave solution:

$$\Omega_m = \frac{1}{2} \left[ \frac{\partial u}{\partial z} - \frac{\partial w}{\partial x} \right] = \exp[i\omega(t - \frac{x}{c})] [\Omega_{od} \exp(-i\omega r_{\beta_m} z/c) + \Omega_{ou} \exp(i\omega r_{\beta_m} z/c)] \quad (2)$$

where  $u, w$  are the horizontal and vertical radial components of displacement,  $r_{\alpha}$ ,  $r_{\beta}$  are the  $\cos$  of the angles of direction of propagation for P or S waves from the  $z$  axis,  $\theta_{od}$ ,  $\theta_{ou}$ ,  $\Omega_{od}$ ,  $\Omega_{ou}$  are amplitudes of up and down going plane waves and  $c$  is the apparent (horizontal) phase velocity.

For layered media, the boundary conditions at the interface between two layers are that the displacements  $u$ ,  $w$ , and the normal and shear stresses,  $P_{zz}$ ,  $P_{zx}$  are continuous. Haskell (1953) has found that the velocity displacement and stress components ( $P_{zz}$ ,  $P_{zx}$ ) in matrix form at  $m^{\text{th}}$  interface are:

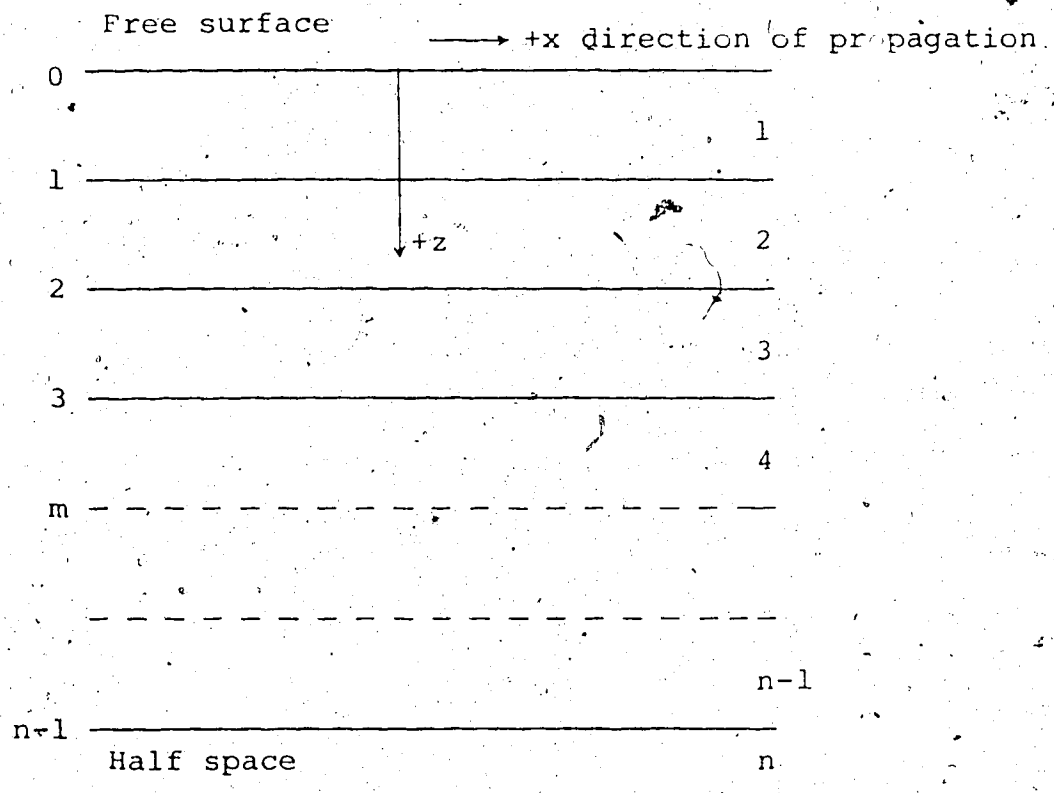


Figure I.1

Orientation of axes and numbering of layers and interfaces.

$$\left[ \left( \frac{\dot{u}}{c} \right), \left( \frac{\dot{w}}{c} \right), P_{zz}, P_{zx} \right]_m = D_m [ (\theta_{ou} + \theta_{od}), (\theta_{ou} - \theta_{od}), (\Omega_{od} - \Omega_{ou}), (\Omega_{od} + \Omega_{ou}) ] \quad (3)$$

where the factor  $\exp[iw(t - \frac{x}{c})]$  is omitted.  $\dot{u}, \dot{w}$  are time derivatives of displacements and  $D_m$  is a  $4 \times 4$  matrix whose elements are given explicitly. Equation (3) may be rewritten as

$$V_m = D_m H_m \quad (4)$$

where  $V_m$  and  $H_m$  are the column matrices. At the top of the layer, due to the boundary conditions, the equation to be satisfied is

$$V_{m-1} = E_m H_m \quad (5)$$

where matrix  $E_m$  is obtained by substituting  $z = 0$  in matrix  $D_m$ . Substitution of equation (5) in equation (4) for  $H_m$  yields:

$$V_m = D_m E_m^{-1} V_{m-1} = a_m V_{m-1} \quad (6)$$

This recursive relation can be repeated from the  $n^{th}$  layer until the surface is reached:

$$V_n = a_n a_{n-1} \dots a_1 V_0 \quad (7)$$

Using equation (5), amplitudes can be expressed as

$$H_n = E_n^{-1} a_{n-1} a_{n-2} \dots a_1 V_0 \quad (8)$$

where matrices (a) are known for each layer. If an incident plane P wave with unit amplitude is desired in the half space, this is obtained by setting  $\theta_{ou_n} = 1$  and  $\theta_{od_n} = \Omega_{od_n} = \Omega_{ou} = 0$  is the column matrix  $H_n$ . Stresses at the free surface are made to vanish by setting the components of  $V_o: (P_{zz})_o = (P_{zx})_o = 0$ . Then the surface displacement can be calculated in terms of the input amplitude for vertical and horizontal components:

$$TV_P(\omega) = \frac{2c^2 (J_{42} - J_{32})}{\alpha_n^2 D} \quad (9)$$

$$TW_P(\omega) = \frac{2c^2 (J_{41} - J_{31})}{\alpha_n^2 D r_{\alpha_n}}$$

where

$$J = E_n^{-1} a_{n-1} a_{n-2} \dots a_1$$

$$D = (J_{11} - J_{21})(J_{32} - J_{42}) - (J_{12} - J_{22})(J_{31} - J_{41})$$

$$c = \alpha_m \csc i_{\alpha_m} = \beta_m \csc i_{\beta_m}$$

(i)<sub>m</sub> is the angle of incidence in the m<sup>th</sup> layer.

Similarly for an incident plane S wave

$$TV_S(\omega) = \frac{2(J_{12} - J_{22})}{\gamma_n r \beta_n^D} \tag{10}$$

$$TW_S(\omega) = \frac{2(J_{21} - J_{11})}{\gamma_n^D}$$

where  $\gamma_n = 2\beta_n^2/c^2$ ,  $\alpha$  and  $\beta$  are the P and S wave velocities respectively.

When P and S wave velocities, density and the thickness of the layers are known, equations (9) and (10) can be evaluated numerically to obtain the response of a layered media to an input P or S waves. The behavior of the transfer function has been investigated previously (Alpaslan 1968, Sprende 1972).

The modulus of the transfer function has several peaks and troughs in the frequency domain whose amplitude and peak position change with layer thickness and the physical properties of the medium. The density of the layers and the angle of incidence do not cause a significant shift of the peaks but the amplitude changes can be notable. Therefore, for a crustal investigation using the transfer function method, a number of seismic sources located at various distances can be utilized. For a given velocity, the density of the layer can be approximated closely by using empirical data. In this thesis a velocity-density curve (Nafe-Drake, 1959) was used to specify the densities



of various layers. By varying the parameters of the media a good match may be found between experimental data and several non-unique theoretical models.

Within a given frequency band a number of models can be found to fit experimental data. This method is not a direct method for crustal investigation, however it can be applied as a diagnostic tool to choose between a number of models.

A Fourier transform of the transfer function is called an "impulse response". Since all phases can be considered as a delayed and modified form of the first arrival, all phases form a time series in which the delay times,  $\tau$ , introduce an oscillation period:

$$f = \frac{1}{\tau} \quad (11)$$

Therefore large delay times correspond to long period waves while short delay times contribute to the high frequencies. Path differences between one or more phases will determine an interference pattern in the frequency domain. For example, if  $\Delta t$  is the path difference between two rays arriving at the same receiver, then the phase at a particular frequency ( $f$ ) will be:

$$\theta = 2\pi(f\Delta t \pm n) \quad , \quad n = 0, 1, 2, \dots \quad (12)$$

When a number of rays are considered, phase contributions are much more complicated. The Haskell-Thomson matrix

formulation yields this interference pattern in a straightforward manner.

### 3. Computation of experimental spectra

In this thesis, earthquake data recorded by the Variable Aperture Seismic Array (VASA) in central Alberta, were used to compute the experimental spectra and to determine the transmission characteristics of the crust in this region. Earthquake data have three components of ground motion. One is the vertical and others are the horizontal components oriented in the N-S and E-W directions. For this study, distant earthquakes were chosen ( $\Delta > 50^\circ$ ). It can be shown that the surface of a wave front increases with the square of increasing distance from a source. Therefore plane wave assumptions are valid for these earthquakes provided that the wave front is not diffracted significantly by deeper structures of the Earth. Discontinuities in the mantle are well separated from each other. The P wave velocity in the mantle drops slowly from about 8.0 km/sec, forming a low velocity region at a depth of about 100-120 km. Thereafter the velocity increases smoothly except at depths of 400 and 700 km where there are second order discontinuities. According to wave theory, there is insignificant conversion of elastic waves at these

discontinuities for the frequencies of interest. Therefore we can assume that a pure plane P wave is incident at the bottom of the crust. Any deviation of the wave front from a plane wave will introduce errors into the spectral ratio method due to the spatial variation introduced. Earthquake sources at about  $90^\circ - 98^\circ$  away were also used. According to the geometrical ray theory, these events yield waves which graze the mantle-core boundary. It was assumed that diffraction of elastic waves due to diffraction of the mantle-core interface is negligible since waves with a wavelength of 4-80 km were being used.

Sixty seconds of digitally recorded data for each of three components have been taken for spectral analysis. The signal level in every channel has been found to vary rapidly. These variations have been corrected by bringing signal level down to the mean value. The data usually starts one second earlier than the first P arrival time. Using the horizontal components ( $r_N(t)$ ,  $r_E(t)$ ) and station-source azimuth ( $\phi$ ), radial ( $r_R(t)$ ) and transverse ( $r_T(t)$ ) components were calculated:

$$r_R(t) = r_N(t) \cos \phi + r_E(t) \sin \phi$$

$$r_T(t) = r_N(t) \sin \phi - r_E(t) \cos \phi$$

(13)

The beginning and end of the data were tapered by a cosine bell in order to reduce an amplitude contribution of a sharp discontinuity at all frequencies. Using a fast Fourier transform algorithm (Gentlemen and Sande, 1966), raw power spectrum was calculated from the Fourier coefficients. The finite length of data available imposes a time window  $W(t)$ :

$$r_S(t) = r(t) \cdot W(t) \quad (14)$$

where the window length can be varied depending on various purposes. After 60 seconds of a tapered rectangular window, another window was applied to the auto-correlation function in the time lag domain  $(\tau)$ . The window chosen is the Parzen function which has a form of

$$W(\tau) = \begin{cases} 1 - 6\left(\frac{|\tau|}{\tau_m}\right)^2 + 6\left(\frac{|\tau|}{\tau_m}\right)^3 & |\tau| < \frac{1}{2}\tau_m \\ 2\left(1 - \frac{|\tau|}{\tau_m}\right)^3 & \frac{1}{2}\tau_m \leq |\tau| < \tau_m \\ 0 & |\tau| > \tau_m \end{cases} \quad (15)$$

where  $\tau_m$  is the maximum time lag. Such a window increases the reliability of the spectra and the Parzen window has relatively small side lobes and yields a positive definite spectrum. Then the real Fourier transform of the auto-correlation function will give a smoothed spectrum:

$$R_S(\omega) = R(\omega) * \bar{W}(\omega)$$

(16)

In this procedure the window can be varied in length to eliminate any additional phases such as near source and core reflections. But the window length must be sufficiently large to obtain the proper resolution. For example, the window length used here provides a frequency resolution which will separate peaks that are 0.025- 0.033 Hz apart. In many events, additional phases were included for the sake of resolution. It is shown here that by including additional phases, some valuable information can be extracted using spectral analysis. A Parzen window yields a smooth reliable auto-correlation, however it gives poor resolution at low frequencies. Therefore, for long-period studies, another type of window may be recommended.

In equation (1), the transfer function can be written in terms of a number of components such as the instrumental transfer function, directional transfer function etc. In practice, a knowledge of the instrumental transfer function will be of great help in the interpretation of the spectrum. However, these functions have negligible effect on spectral ratios. But the gain of the channels must be known for spectral ratio studies. Gains can easily be calculated using calibration pulses and spectral component can be scaled before rotation:

$$R_R(\omega) = R_N(\omega) \sin^2 \phi + R_E(\omega) \cos^2 \phi + 2 \operatorname{Re} R_N(\omega) R_E(\omega) \cos \phi \sin \phi. \quad (17)$$

For the data used in this thesis, there was incomplete information available about instrumentation. Therefore the amplitudes of the spectral ratios are imprecise.

#### 4. Efficiency of the spectral ratio method

As seen in equation (16), the experimental spectrum is always obtained by a window and taking the ratio of components will not lead to a cancellation of this window since a convolution is involved:

$$\frac{R_{SV}(\omega)}{R_{SR}(\omega)} = \frac{R_V(\omega) * \bar{W}(\omega)}{R_R(\omega) * \bar{W}(\omega)} \quad (18)$$

According to this method the response is considered as a convolution of one or more functions (equation (1)):

$$\frac{R_{SV}(\omega)}{R_{SR}(\omega)} = \frac{[H_V(\omega) \cdot P(\omega)] * \bar{W}(\omega)}{[H_R(\omega) \cdot P(\omega)] * \bar{W}(\omega)} \quad (19)$$

As an approximation, if we can write

$$[H(\omega) \cdot P(\omega)] * \bar{W}(\omega) = [H(\omega) * \bar{W}(\omega)] \cdot P(\omega) \quad (20)$$

then in equation (19), the unknown source function will cancel, leaving only the crustal transfer ratio function where the window effect is not negligible due to convolution. Generally, the window in the frequency

Figure 1.2

Theoretical spectral ratios using Parzen window and various pulse functions. Pulses effect is negligible in the frequency band but minor differences exist towards higher frequencies.

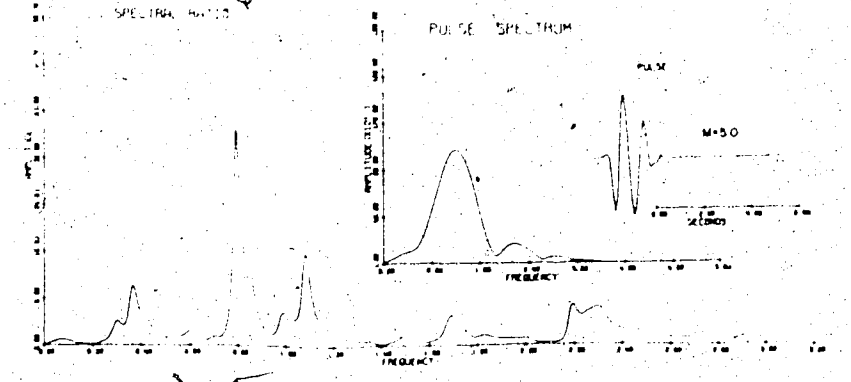
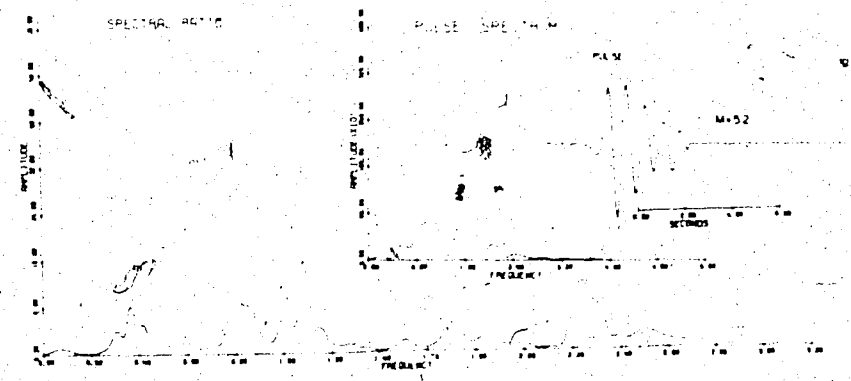
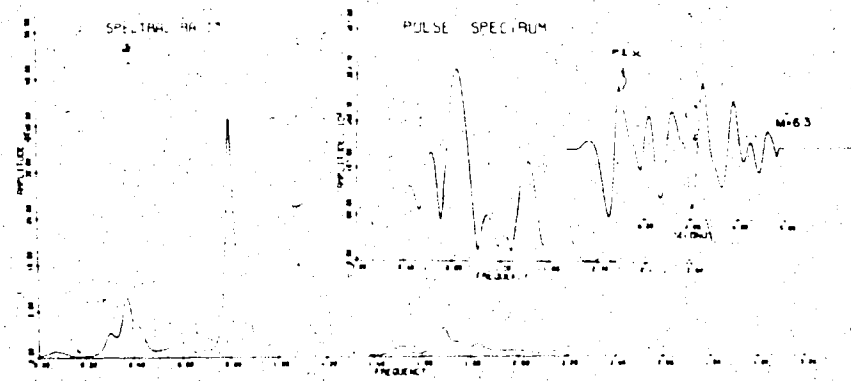
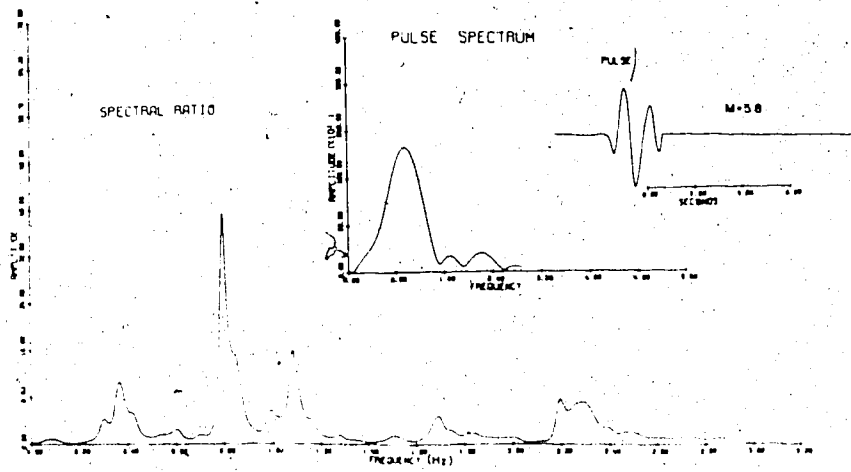
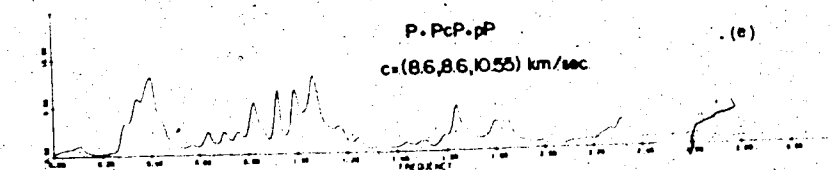
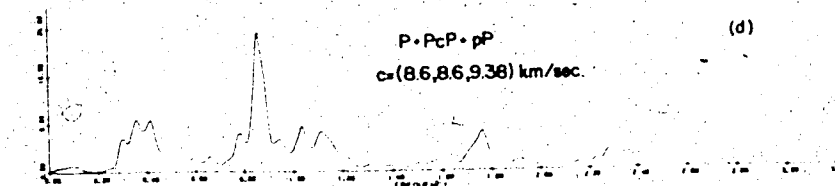
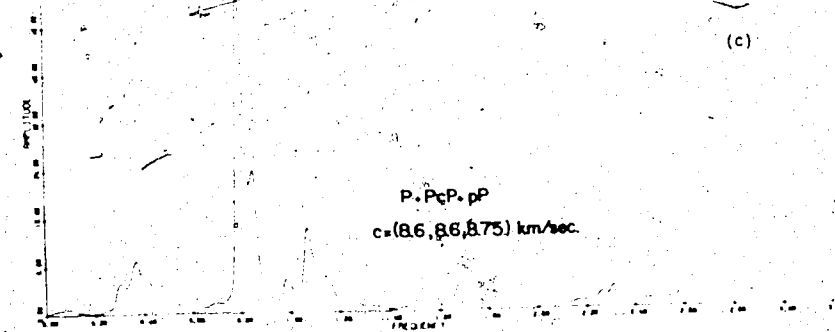
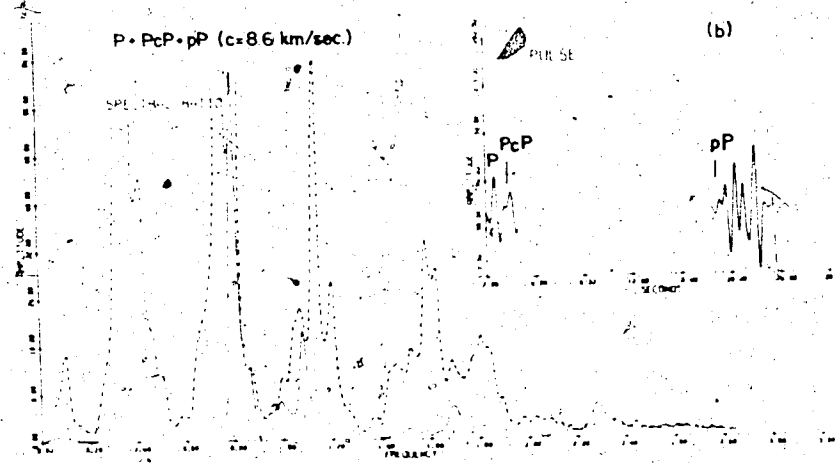
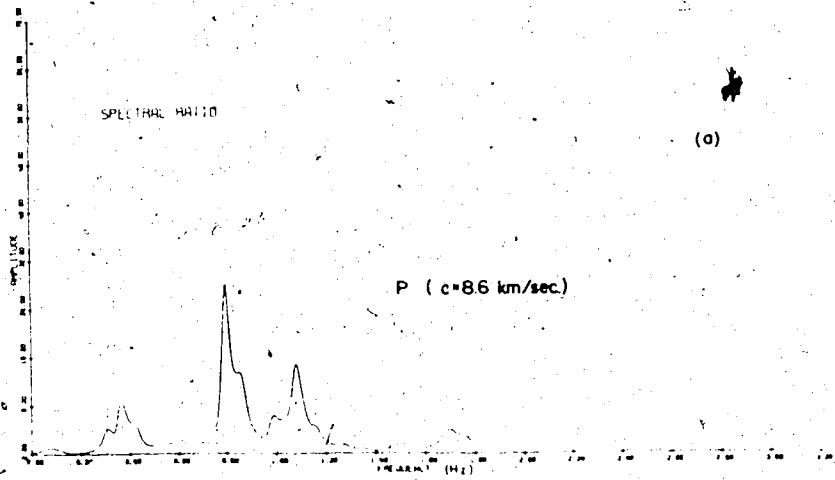




Figure I.3

Effect of additional phases on the spectral ratios.

(In figure b, broken line represents a spectral ratio with a phase velocity of 23.6 km/sec.)



domain is not a simple function and its effect on the ratios cannot be estimated theoretically. Therefore to obtain a better comparison between theory and experiment, the theoretical models have to be smoothed also by a similar window.

The approximation in equation (20) can be shown to be true for a rectangular time window and the smoothing of a theoretical model can be achieved by a double Fourier technique (Leblanc, 1967). In an earlier work (Alpaslan, 1968), this method was applied successfully to obtain a theoretical transfer function. However, when more complicated windows are used one must be assured of convergence and also that no shift in frequency is introduced. As a first step equation (19) was used for a model with a Parzen window and various pulse functions as obtained from real earthquake data using a homomorphic deconvolution technique. The results are displayed in Figure 2. Pulse functions used vary significantly in amplitude and frequency content. As can be seen spectral ratios for every case are similar. The amplitudes and shapes of the ratios at frequencies less than 1.40 Hz are exactly the same for every case. However, towards the higher frequencies small differences exist due to the variable spectral content of the source pulses. In general, it can be said that variation in the pulse produces negligible

variations in the spectral ratio. The most reliable ratios were obtained only at low frequencies. In this process it is essential that the window length is larger than the pulse duration in time.

In practice a seismologist can rarely obtain data which satisfies all the assumptions discussed earlier. For example, after the P arrival, additional phases such as pP and PcP arrive within the window length. These multiple pulses create holes and distortions in the experimental spectra destroying valuable information. If one can choose earthquakes having a great depth ( $>150$  km) and distance ( $\Delta > 55^\circ$ ), about 40-50 seconds of data will be free of multiple phases. In this thesis if such data were chosen, only one or two events would be available. Therefore these phases were included in this study, but many spectral ratios were combined to obtain ratio that approached the true one. In Figure 2, many models with additional phases have been displayed. Additional phases were introduced to the theoretical Haskell-Thomson formulation:

$$R(\omega) = R_{c_1}(\omega) + R_{c_2}(\omega) e^{i\omega\Delta t_{pP}} + R_{c_3}(\omega) e^{i\omega\Delta t_{PcP}} \quad (21)$$

$\Delta t$  is the time delay of a particular phase and  $c_1, c_2, c_3$  are the phase velocities. All pulses used here were

taken from real data using a deconvolution technique, therefore amplitude of these phases were not assumed. In Figure 3.b, all phases are assumed to have the same phase velocity as it can be seen that the spectral ratios are only affected in amplitude by comparison with a single pulse case (Figure 3.a). In Figure 3.c,d,e, the phase velocity of pP is increased steadily. It is clear that the spectral ratios change their appearance due to the increasing difference between main P and pP phase velocities and the delay time will determine amount of distortion. Therefore, it is concluded that the spectral ratios are still useful even when multiple pulses exist within the window length provided that the phase velocity of pulses does not differ significantly.

For spectral ratio analysis, data with high signal to noise ratio must be chosen. Noisy data will produce extra peaks in the spectral ratio which cannot be modelled by a structural effect. This is one of the possible reasons one obtains different spectral ratios for the same station when using various events.

## II. Anisotropy

### 1. Introduction

A large amount of evidence about the seismic anisotropy of certain regions of the solid Earth have been accumulated for a long time. Neuman (1930), during a study of various earthquakes, observed an impulsive activity before the main S arrival. He compared this motion to the Love wave type and after the main S arrival, he identified Rayleigh wave motion. Byerly (1934-38) has noted the change of S motion from transverse to the vertical plane. He suggested that a double refraction phenomenon occurs in the surface layers of the Earth. Measurements of seismic anisotropy on rock samples confirmed the variation of the velocity with direction (Koefford et al, 1963). The degree of anisotropy was found to vary for a different rock samples. Khalevin and Koshkina (1966) measured the sound velocity in rock samples collected from the Ural region of the U.S.S.R. Among these rock samples, metamorphic rocks showed 300 % anisotropy. The variation of velocity is observed in three directions; one is the perpendicular to the cleavage; the second is parallel to the cleavage and parallel to the lineation; and the third direction is parallel to the cleavage and perpendicular to the lineation. Their results showed that the velocity in

the second direction is larger than that in other directions. Compact textured samples (granoblastic) showed small anisotropy.

Small scale anisotropy has been measured by a number of authors in situ (McCallum (1932), Weatherby (1934), Ricker (1953), Vanderstoep (1966), Cherry et al (1968)). Yegorkino (1969) used recordings of a distant earthquake at four stations separated by 7-10 km, to determine the anisotropy in a sedimentary layer in the northern region of Caspian Basin of the U.S.S.R., using travel time and polarization analysis for converted phases ( $PS_H - PS_V$ ) at the bottom of the sedimentary layer. He was able to measure 0.5-0.7 seconds time differences in arrival times of  $PS_V$  and  $PS_H$  waves. He concluded that the  $S_H$  wave velocity was 10-15 % larger than the  $S_V$  wave velocity in this sedimentary layer.

Anisotropy has been shown as a possible cause for obtaining "non geological" boundaries in a number of seismic field measurements (Layat et al, 1961). Khalevin and Tavrin (1965) could not find any correlation between boundaries obtained with the deep seismic sounding method and those established by stratigraphic and lithographic studies in the upper part of the crust (450-850 m) in Urals of the U.S.S.R. They believed that the main reasons for this was the

varying degree of metamorphism in the rocks of the upper part of the crust.

A theoretical description of general anisotropy can be made in terms of 21 elastic parameters (Love, 1944). Backus (1970) offered an interpretation of these parameters. However, a complete physical interpretation of all 21 parameters is not possible at this time. Using various symmetry relations, a number of simpler forms of anisotropy can be stated. The simplest form of anisotropy allows a physical interpretation and might partially explain anisotropy measurements. One such type of anisotropy is the transverse isotropy in which the propagation of elastic waves perpendicular to an axis of symmetry is equivalent to waves propagating in an isotropic media. This symmetry axis is called the unique axis. Only five elastic parameters are sufficient to describe this kind of anisotropy in which SH and SV waves can travel with different velocities and P waves can have three different velocities of propagation (Stonely, 1949). Surface waves exist in a transversely isotropic media as is the isotropic case (Buchwald, 1961). A number of features of surface wave dispersion have been explained by transverse isotropy (Kovach, 1965; Kanimura, 1966; Crampin, 1966).

Transverse isotropy can generally be divided into two groups: (a) transverse isotropy with a vertical



unique axis. In this group SH and SV waves travel with a different velocity. (b) transverse isotropy with a symmetry axis other than vertical. This kind of anisotropy predicts azimuthal variation in P wave velocity. Hess (1964) reported  $P_n$  velocity variation with azimuth in the Mendocino fractured zone, off California. Raitt (1969) measured anisotropy as a function of azimuth in the Pacific ocean. Backus (1965) derived a relation for an anisotropic medium in which the P wave velocity varies with azimuth. He showed that measurements of velocity in five different azimuths will determine the anisotropy. This method has been applied by Christensen, Crosson (1968) and Raitt (1969).

It can be stated that the formation of transverse isotropy in the real Earth may form in two ways. One is the sedimentation and metamorphism of Earth material (Khalevin et al, 1965). The other is the orientation of crystals under anisotropic stresses. Macdonald (1960) studied orientation of anisotropic minerals in a stress field. He showed that in a stress field each mineral tries to take an orientation in which the potential energy of the system is minimum. The direction of orientation is shown to be the same as the one with the lower elastic wave velocity in the minerals. Christensen (1965) measured the compressional wave

velocity in various metamorphic rocks at high pressures. He observed a variation of velocity with direction as a result of mineral orientation. Silaeva and Bayuk (1967) measured the P wave velocity and anisotropy in rock samples at a high pressure and temperatures. They have concluded that anisotropy depends on the stress state of the rocks. Corlet and Emery (1959) measured the vertical and horizontal pressure in sedimentary rocks. They have found that the horizontal pressure is 0.5-0.75 of the vertical pressure. In tectonically young and active regions comparatively low sub-crustal velocities of longitudinal waves (7.5-7.9 km/s) are partly due to the incomplete orientation of the medium (Babuska, 1970). Generally, in tectonically active regions such as young mountain ranges, suboceanic trenches etc. at least triaxial pressure is proposed. Therefore one may have a transverse isotropy with a unique axis not vertical. For a tectonically quiet structure, assuming a vertical biaxial pressure, transverse isotropy with a vertical axis is the usual form of anisotropy.

In this thesis the possible implications of anisotropy on the transfer function have been investigated. The purpose of this study is not to determine the anisotropy in an Alberta crustal section but to clarify the uncertainty imposed by the assumption of

isotropy during the determination of crustal parameters using a transfer ratio method. The study of anisotropy has been achieved in two steps. In the first step, experimental transfer functions calculated at each station in Alberta have been classified according to the direction of wave approach. Spectral analysis has been carried out for each quadrant at every station. In this way the possible structural anisotropy in azimuth is investigated. The result of this study depends on the number of reliable experimental data. The conclusions and diagrams for this study are presented in another section where interpretation of experimental results are discussed. In the second step which is presented in this section, the transfer ratios for transversely isotropic media with a vertical-unique axis have been calculated using a matrix method. Models are assumed to be two-dimensional, homogeneous, plane and parallel layered media. Various degrees of anisotropic models have been compared with isotropic models and differences have been discussed in terms of the structural interpretation.

## 2. Computation of a plane wave solution for a transversely isotropic multilayered media

The equation of motion for elastic waves may be written (neglecting body forces) as

$$\rho \frac{\partial^2 U_i}{\partial t^2} = \frac{\partial P_{ij}}{\partial x_j} \quad j = 1, 2, 3 \quad (1)$$

where  $\rho$  is density,  $U$  is displacement. We assume an elastic body that is, it produces internal stresses when subjected to an external force that causes deformation. The stress components  $P_{ij}$  can be written as a function of strain ( $e_{pq}$ )

$$P_{ij} = P_{ij}(e_{pq}) \quad (2)$$

where

$$e_{pq} = \frac{1}{2} \left( \frac{\partial U_p}{\partial x_q} + \frac{\partial U_q}{\partial x_p} \right) \quad p, q = 1, 2, 3$$

If the strain components are small and we can assume absolute elasticity, which means that the stress becomes zero in the absence of deformation, then expansion of equation (2) into a Maclaurin series leads to a linear relationship between stress and strain, which is known as Hooke's law

$$P_{ij} = c_{ijpq} e_{pq} \quad i, j, p, q = 1, 2, 3 \quad (3)$$

where

$$c_{ijpq} = \left( \frac{\partial P_{ij}}{\partial e_{pq}} \right)_{e_{pq} \rightarrow 0} \quad \text{are called elastic parameters.}$$

$P_{ij}$  and  $e_{pq}$  are second rank tensors and  $c_{ijpq}$  is a three-dimensional fourth-rank tensor, independent of the choice of a cartesian coordinate system. This has

81 independent components. Then the equation of motion becomes

$$\rho \ddot{U}_i = c_{ijpq} U_{p,qj} \quad (4)$$

The 81 parameters are reduced to 21 by the symmetry relations

$$c_{ijpq} = c_{jipq} = c_{ijqp} = c_{pqij} \quad (5)$$

The elastic parameters  $c_{ijpq}$  are dependent on whether the process is adiabatic or isothermal. It is necessary to assume a positive definite function  $\phi$  exists (Love 1944), such that

$$P_{ij} = \frac{\partial \phi}{\partial e_{ij}} \quad (6)$$

where

$$\phi = \frac{1}{2} c_{ijpq} e_{ij} e_{pq}$$

The function  $\phi$  is termed as elastic potential per unit volume. It is the density of potential energy in an elastically deformed body and is defined in terms of the thermodynamical conditions of the body.

A plane wave solution of equation (4) can be written as

$$U_i = a_i \exp[i\omega(t - m_p x_p)] \quad (7)$$

$i = 1, 2, 3$   
 $p = 1, 2, 3$

where

$\vec{m}_p = \left(\frac{1}{\omega}\right) \vec{k}_p$ ,  $\omega$  is the radial frequency,  $\vec{k}$  is the propagation vector of plane waves in a cartesian coordinate system. Then the equation of motion (4) will be

$$\left[ \frac{1}{\rho} c_{ijpq} m_i m_j - \delta_{ip} \right] U_i = 0 \quad i, p = 1, 2, 3. \quad (8)$$

Equating the determinant of equation (8) to zero, the displacement components can be calculated. For 21 elastic parameters, the evaluation of these equations is tedious. However, for a particular crystal system, the determinant can easily be expanded.

Transverse isotropy has a symmetry which is equivalent to a hexagonal crystal. A six fold symmetry axis exists. The elastic parameters are unchanged by rotation about this axis and most of the parameters vanish or become equal to each other, leaving only five independent elastic moduli. In a cartesian coordinate system where the  $x_j$  axis is downward, the components of the elastic parameters will be

$$c = \begin{pmatrix} c_{1111} & c_{1122} & c_{1133} & 0 & 0 & 0 \\ c_{1122} & c_{1111} & c_{1133} & 0 & 0 & 0 \\ c_{1133} & c_{1133} & c_{3333} & 0 & 0 & 0 \\ 0 & 0 & 0 & c_{2323} & 0 & 0 \\ 0 & 0 & 0 & 0 & c_{2323} & 0 \\ 0 & 0 & 0 & 0 & 0 & \frac{c_{1111} - c_{1122}}{2} \end{pmatrix} \quad (9)$$

A separation of the equation of motion into longitudinal and transverse components is not possible. Therefore, the distinction between P and S waves, cannot, in general, be done, except in certain directions. An expansion of the determinant of equation (8) yields relations between the velocity of wave propagation and the elastic moduli (Stoneley, 1949). Considering wave propagation in certain directions, an interpretation of five elastic parameters can be made. Following Stoneley (1949) and Anderson (1961), some directions of wave propagation in a transversely isotropic media are comparable to the isotropic case:

a) For a direction of propagation along the unique axis ( $x_3$ ), pure compressional and shear waves with horizontal particle motion are the solutions of the determinant of the coefficients:

$$PV = \left( \frac{c_{3333}}{\rho} \right) \quad SV_H = \left( \frac{c_{2323}}{\rho} \right) \quad (10)$$

b) Propagation in any direction perpendicular to the unique axis, yields the following solutions:

$$PH = \left( \frac{c_{1111}}{\rho} \right)$$

$$SV_H = \left( \frac{c_{2323}}{\rho} \right) \quad (11)$$

$$SH_H = \left( \frac{c_{1111} - c_{1122}}{2\rho} \right)$$

PV, PH can be considered as P wave velocities in the vertical and horizontal directions,  $SV_H$  is the velocity of a vertically travelling S wave with horizontal particle motion and  $SH_H$  corresponds to an S wave travelling perpendicular to the direction of  $SV_H$  waves with a horizontal particle motion. The fifth parameter can be determined if the velocity in any other direction is known (usually  $45^\circ$  from the vertical axis):

$$c_{1133} = [(2\rho P_A^2 - L)^2 - H^2]^{1/2} - c_{2323} \quad (12)$$

where  $P_A$  is the P wave velocity in a direction other than the ones parallel to the axis, and

$$L = \frac{1}{2}(c_{1111} + c_{3333} + 2c_{2323})$$

$$H = \frac{1}{2}(c_{1111} - c_{3333})$$

For a real velocity, the determinant of equation (8) yields six roots for every  $m_p$ . These roots might be real or form complex conjugate pairs. Every root contributes to the displacement (equation (7)) and the theoretical implications of these roots have been investigated by Synge (1957), Kraut (1963) and by a number of other authors. However, the solution of a wave equation can, in general, be written in terms of



existing up and down travelling waves (Anderson, 1961) in the  $(x_1-x_3)$  plane:

$$U_j = U_{upj} e^{kr_P x_3} + U_{dpj} e^{-kr_P x_3} + U_{usj} e^{kr_S x_3} + U_{dsj} e^{-kr_S x_3} \quad (13)$$

where the common factor  $\exp[i(\omega t - kx_1)]$  is omitted.

Each term in equation (13) represents plane waves travelling in  $x_3$  direction which is pointing downwards.

$U_{up}$ ,  $U_{dp}$ ,  $U_{us}$ ,  $U_{ds}$  are the amplitudes of up and down going P and S waves.  $r_P$  and  $r_S$  are the cot. of angle of direction of P and S waves from  $x_3$  direction.  $k = \omega/c$ , and  $c$  is the phase velocity.

By substitution of equation (13) into equation of motion and equation (6), displacement and stress components can be written in terms of input amplitudes. It is more convenient to use dimensionless velocity for the displacements (Harkrider, Anderson, 1964). Then at the  $m^{\text{th}}$  interface the solution can be written

$$\begin{aligned} \left(\frac{\dot{U}}{c}\right)_m &= ik[U_{o1} \cos P + iU_{o2} \sin P + U_{o3} \cos Q + iU_{o4} \sin Q]_m \\ \left(\frac{\dot{U}}{c}\right)_m &= ik[-U_{o1} \gamma_P \sin P + iU_{o2} \gamma_P \cos P - U_{o3} \gamma_S \sin Q \\ &\quad + iU_{o4} \gamma_S \cos Q]_m \end{aligned} \quad (14)$$

where

$$P = kr_P x_3, \quad Q = kr_S x_3$$

$$U_{oj} = U_{uh} + (-1)^{j+1} U_{dh} \quad \begin{array}{l} j = 1, 2 \quad h = P \\ j = 3, 4 \quad h = S \end{array}$$

and

$$\gamma_h = \frac{(c_{1133} + c_{2323}) \cdot r_h}{\rho c^2 - c_{2323} - c_{3333} r_h^2} \quad h = P \text{ or } S$$

The stress components will be

$$(P_{33})_m = ik [iX_P U_{o1} \cos P - X_P U_{o2} \sin P + iX_S U_{o3} \cos Q - X_S U_{o4} \sin Q]_m \quad (15)$$

$$(P_{13})_m = ik [iY_P U_{o1} \sin P - Y_P U_{o2} \cos P + iY_S U_{o3} \sin Q + Y_S U_{o4} \cos Q]_m$$

where

$$X_h = c_{3333} \gamma_h \gamma_h + i c_{1133}$$

h = P or S

$$Y_h = c_{2323} (\gamma_n - i \gamma_h)$$

For a plane parallel multi-layered media, equations (14) and (15) can be written in matrix form. Recursive relation for a number of interfaces can be formed in the same way as it has been done in section I, to find the surface amplitude in terms of the input amplitude and the vertical and horizontal transfer functions can similarly be written for a (n-1) layered media, the n<sup>th</sup> layer being a half-space (m = 0, 1, 2, ..., n). Then, the transfer function for an incident P wave

will be

$$TW_P(\omega) = \frac{2iV_P \gamma_P}{c_n D r_{P_n}} (J_{31} + J_{41}) \quad (16)$$

$$TU_P(\omega) = - \frac{2V_P}{c_n D} (J_{32} + J_{42}) \quad (17)$$

D and matrix J are similar to the ones calculated in section I.

### 3. Transfer ratios for transversely isotropic layered media

Equations (16) and (17) are the surface responses of a transversely isotropic multi-layered media to an input P wave with unit amplitude in a form convenient for numerical evaluation for a number of layers. In Figure 1 the transfer ratios which are the ratios of the vertical component to the horizontal one, have been shown for an Alberta crustal model using two different angles of incidence. Anisotropic factors have been shown as the ratio of velocities:

$$\phi = \frac{P_V^2}{P_H^2} \quad (\text{PHI})$$

$$\eta = \frac{P_A^2}{P_H^2} \quad (\text{ETA})$$

$$\xi = \frac{S_H^2}{S_V^2} \quad (\text{XI})$$

Figure II.1

Effect of transverse anisotropy on transfer  
ratio as a function of angle of incidence:

$\text{PHI} = 0.83$ ,  $\text{ETA} = 0.83$  in the crust.

Broken line indicates isotropic model.

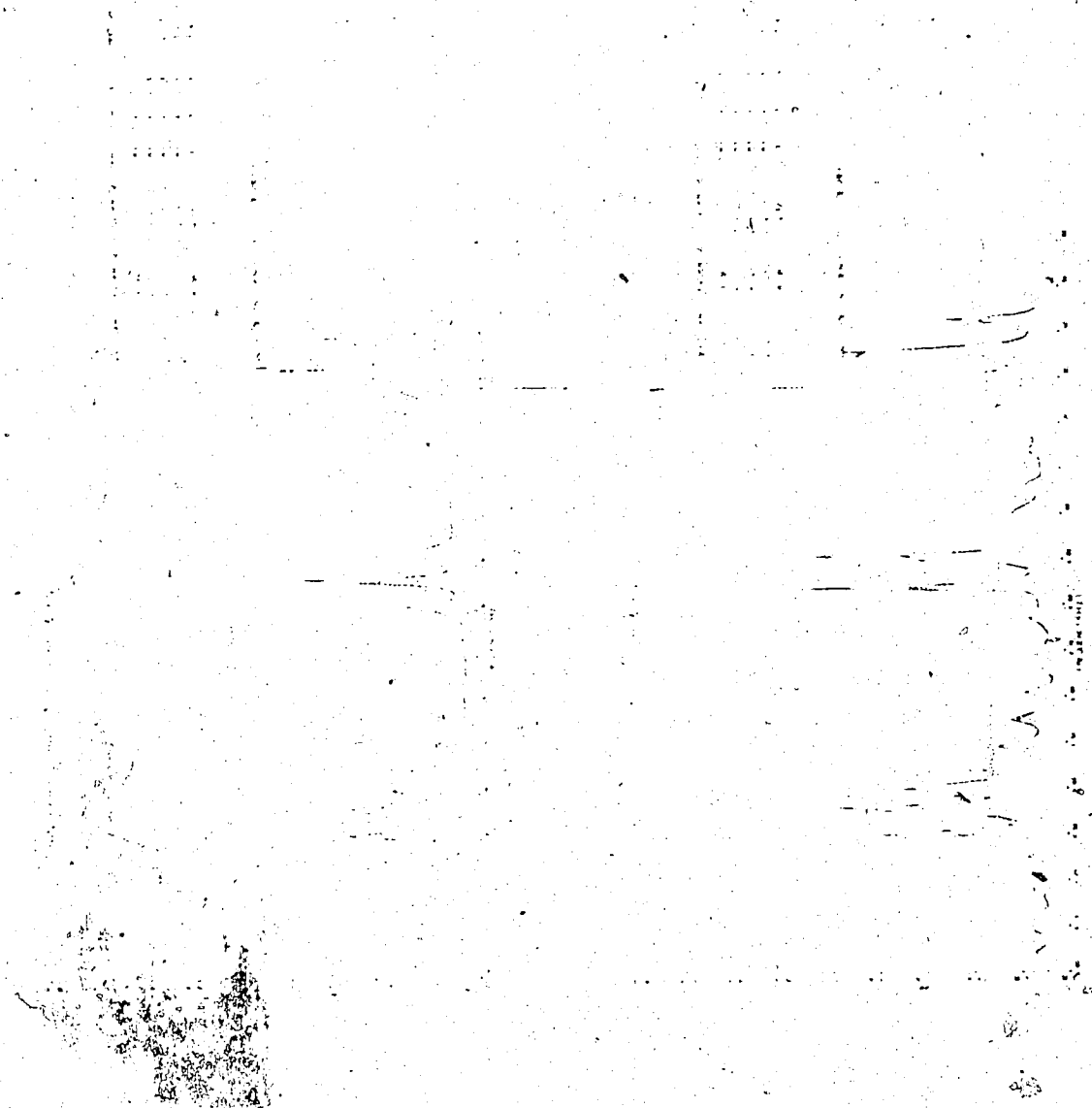
.....  
.....  
.....  
.....  
.....

.....  
.....  
.....  
.....  
.....

.....  
.....  
.....  
.....

Figure II.2

Effect of transverse anisotropy on transfer ratio as a function of angle of incidence:  
PHI = 0.83, ETA = 0.91 in the crust.  
Broken line indicates isotropic model.



All models presented in this thesis are two dimensional, therefore the factor (XI) should not be considered on these figures. Models presented in Figure 1 have 10 % anisotropy in which the  $P_H$  velocity is higher than  $P_V$  velocity and the half space is assumed to be isotropic. By comparison with the isotropic case, peaks and troughs are shifted to higher frequencies indicating shallower or higher velocity structure. This can be explained in terms of energy propagation, since in an anisotropic media, energy does not necessarily propagate perpendicular to the wavefront. It may even propagate parallel to the wavefront with a higher velocity (Lighthill, 1960). If the energy flux vector or Poynting vector is divided by the total energy density of the wave, the velocity of energy propagation (group velocity) is obtained. The relation between group velocity and phase velocity is found to be (Musgrave, 1954):

$$\bar{V}_g \cdot \hat{n} = \bar{V}_p \quad (18)$$

where  $V_g$  is group velocity,  $V_p$  is the phase velocity and  $\hat{n}$  is the normal to the wavefront. In an anisotropic media the direction of displacement vectors and the Poynting vector must be considered at the same time when reflection and transmission of an elastic wave is studied. The critical angle phenomenon



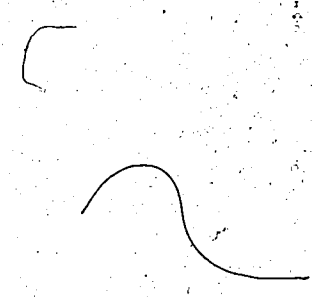
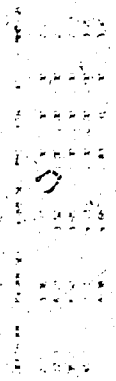
is more complex in an anisotropic media and needs more explanation in terms of these vectors.

It is clear that when the horizontal distance travelled by the wave in an anisotropic media, is significant with respect to a vertically travelling wave, the effect of anisotropy will be greater, when transmission of a plane wave through an multilayered anisotropic media is considered. The angle of wave approach at the bottom of the media is important since a variation of velocity with direction will be felt easily by the wave for grazing angles of incidence. A larger number of models, than shown in this section, have been calculated. Even small anisotropy introduces important changes in the shape of the transfer ratios for large angles of incidence. However, for experimental transfer ratio studies, distant earthquakes are chosen in this thesis. Most of these teleseismic events should yield waves with an angle of incidence less than 35 degrees at the bottom of Alberta crust, according to the Jeffrey-Bullen tables (Phinney, 1964).

The anisotropy factor ( $\eta$ ) will determine the state of transverse isotropy in a model. Models shown in Figure 1 have an intermediate velocity ( $P_A$ ) which is equal to the vertical velocity ( $\eta = 1$ ). This sharp velocity change in horizontal direction

Figure II.3

Influence of upper mantle anisotropy on the wave transmission. Broken line indicates isotropic model.

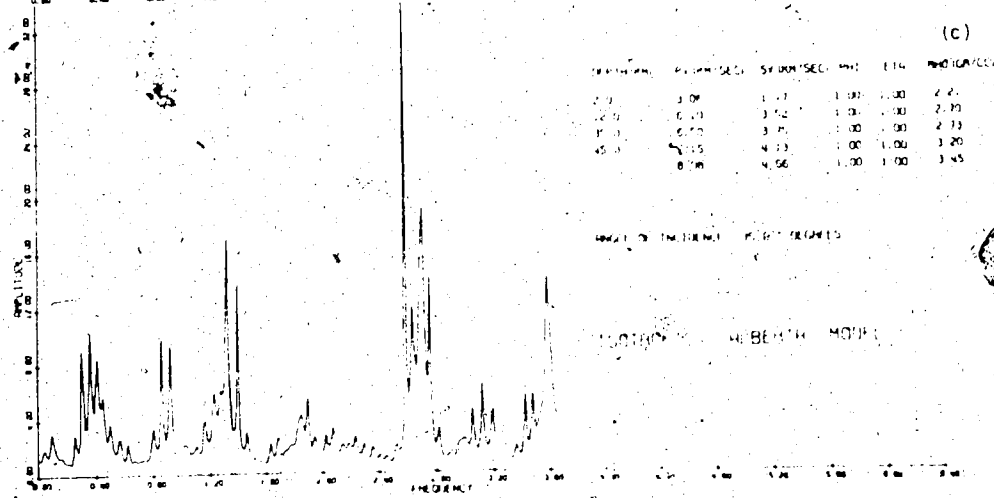
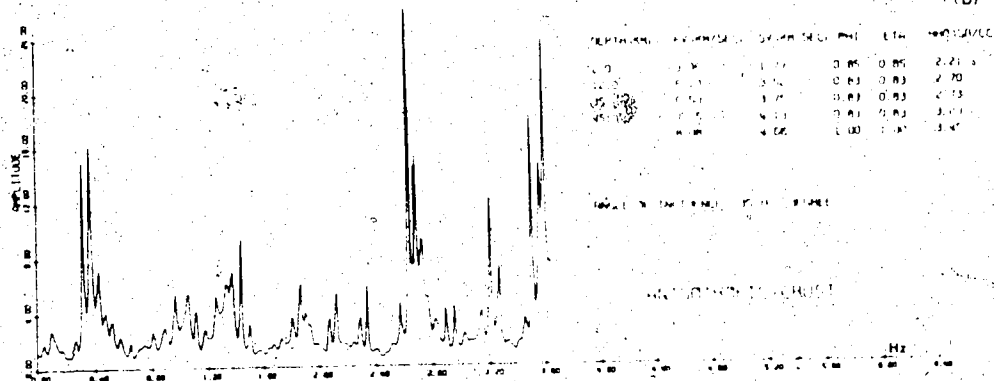
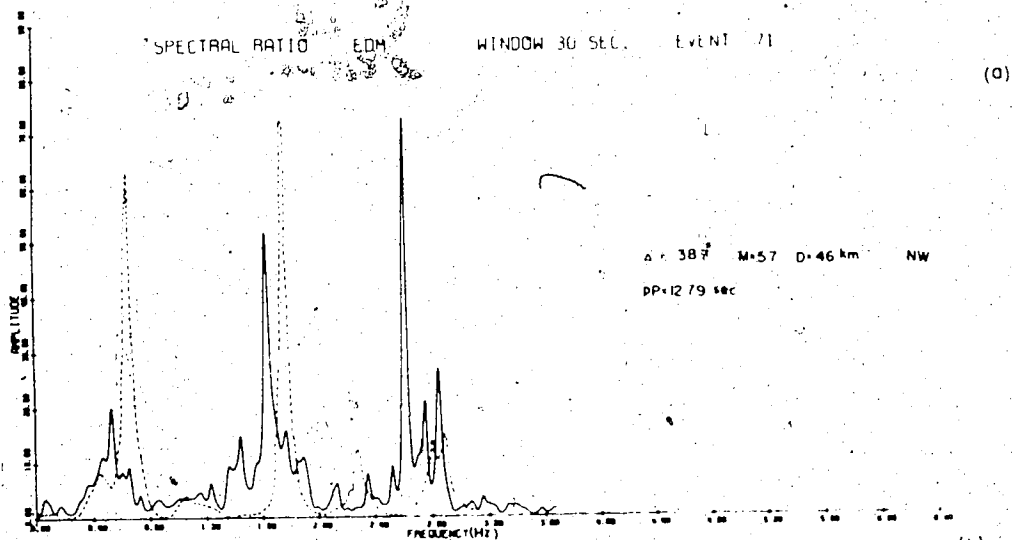


corresponds to highly laminated media. The degree of lamination can be introduced by a factor  $\eta$ . For example, models shown in Figure 2 have a smooth velocity variation from the horizontal to the vertical direction ( $\eta = 0.91$ ). This model showed no significant shift of peaks in frequency but only amplitude changes. From the comparison of Figure 1 with Figure 2, it can be stated that the transfer ratios are much more influenced when  $\eta = 1$ . The transverse isotropy introduces no additional peaks into the transfer ratios by comparison with the isotropic case. The effect of transverse isotropy on transfer ratios is not so severe for low frequencies. For frequencies less than 0.26 Hz, the maximum frequency shift in peak position is observed to be 3 mHz and the amplitude changes are found to be 20-30 % from the isotropic case.

Since the angle of wave approach at the bottom of the media is important for transversely isotropic media, the anisotropy of the half space will be one of the contributing factors. In Figure 3, an isotropic crustal model over the transversely isotropic half space has been studied. This transfer ratio has been calculated assuming that a purely incident P wave exists. Existence of a purely P wave in an anisotropic media may be questionable, however, it can be assumed that due to an anisotropic process at the source, deep

Figure II.4.

Comparison of an experimental spectral ratio  
with an Alberta crustal model (ALTACRT-1).  
For unsmoothed models amplitudes refer to  
square root of power.



isotropic structure of the Earth or by some kind of mechanism, a pure P wave is introduced into a transversely isotropic space below the crust. Investigation of these assumptions will not be done here since this model is only of theoretical interest at this time. This showed that 50 % amplitude changes (Figure 3) with respect to the isotropic wave indicating the importance of the angle of incidence.

For long period elastic waves, if the amplitude changes can be ignored, the effect of transverse isotropy on the transfer ratios is negligible. However, for short period waves, a study of transfer ratios is no longer independent of the angle of incidence and anisotropy may be one of the significant factors to overcome some difficulties in application of this method to the real data (Ellis and Basham, 1968). In Figure 4.b-c, an Alberta crustal model (Cumming and Kanasewich, 1966) has been compared with an experimental transfer ratio. The experimental spectral ratios have been calculated using an earthquake recorded at the EDM Station in Alberta (section I). This spectral ratio is smoothed by a 30 second Parzen window in order to increase the reliability of the spectrum. By comparison with the isotropic model, it can be said that the experimental and theoretical transfer ratios are not completely similar. However, the anisotropic

model makes a comparison much easier. This anisotropic crustal model has a vertical Poisson's ratio  $\sigma_V = 0.24$  and a horizontal one  $\sigma_H = 0.35$  in the crustal layers. There is no other evidence for various Poisson's ratio values in this crustal model, therefore, this model must be verified. Both models yield a very poor comparison with the experimental transfer ratio at both frequencies. This may mean that the model has to be modified. The models shown in Figure 4.b-c were not smoothed because small peaks in the experimental curve have very low reliability. In Figure 4-a, another model with six layers over a half space (Table 1) has been displayed. This model is smoothed by a similar window. Comparison with the experimental data is more favorable than for a four layer model. This may suggest that significant alteration has to be made in the sedimentary layers of the model. In the Alberta plains, a thick sedimentary layer is a common feature of the crust and anisotropy in these layers may significantly affect the transmission characteristics of the crust.



Table 1

## Crustal Model ALTACRT - 2

<u>h(Thickness)</u>	<u>P(km/sec)</u>	<u>S(km/sec)</u>	<u><math>\rho</math>(gr/cc)</u>
1.3	3.00	1.5	2.20
0.8	5.20	3.0	2.60
0.5	4.30	2.48	2.50
10.0	6.10	3.52	2.70
23.0	6.50	3.75	2.73
10.0	7.15	4.13	3.20
-	8.08	4.66	3.45

### III. Effect of Dipping Layers on Wave Transmission

#### 1. Introduction

In the study of the structure of the crust one of the simplifying assumptions has always been the existence of plane parallel layers. It is most likely that this assumption is not satisfied in many crustal sections. As far as we know, Kuhn (1961) was the first to study the time response of a dipping layered structure using a laboratory model. Kane (1966) applied ray methods to determine the response of a single dipping layer over a half space and Fernandez (1967) discussed the effect of dipping layers on the transfer function. Ishii and Ellis (1970) formulated the solution of time transformed wave equation for a dipping layer over a half space in the cylindrical coordinate system. Rogers and Kisslinger (1972) have used this ray method to calculate the response of a single layered dipping model in the frequency domain and attempted to determine a dipping crustal structure in U.S. They have also made a model study. Tsukuda (1972) has attempted to determine the response characteristics of a single dipping layered analog model. He has concluded that for dip angles less than 5-10 degrees, there is no significant change in the transfer function for plane P waves. His results are concordant with the ones obtained by Rogers and Kisslinger.

An analog model study can be considered as a complete wave solution for that particular media. However, an analytic complete wave solution for a dipping layered media cannot be formulated as in the case of a parallel layered media (section I). In this section, a ray-theory approach has been used to evaluate the response of a multi-dipping layered media in the time domain. The transfer ratios have been calculated from the Fourier transform of the impulse response. The wave solution can be expanded into an infinite number of series, and each term represents a physical ray (Spencer, 1960; Cisternas et al, 1973). For numerical evaluation, the ray expansion has to be terminated; therefore, a comparison between the complete wave and a ray solution has to be made to determine the proper number of terms in the ray expansion for a suitable approximation. The Haskell-Thomson matrix formulation (section I) is an exact wave solution and has been used to determine the accuracy of a ray expansion. A comparison of the two solutions has been carried out in both the time and the frequency domain. After determining the optimum number of terms in the ray expansion to obtain the best approximate solution economically, a ray method has been used to calculate the response of a dipping layered media to a plane wave impinging on the bottom. Using an efficient algorithm for ray

generation (Hron, 1972), the transmission of a plane wave through a multi-dipping layered media has also been studied. In this section only the transfer function studies have been presented as the time domain studies will be discussed later.

## 2. A ray-theory approach for computation of the response of a layered media

In an isotropic homogeneous media, the displacement vector can be written as a sum of longitudinal and transverse components (Bullen, 1963). Each component satisfies a wave equation of type (section I)

$$\Delta \bar{U} - \frac{1}{c^2} \bar{U}_{tt} = 0 \quad (1)$$

where  $\Delta$  is Laplacian and  $U_t$  is time derivative of displacement  $\bar{U}(x, y, z, t)$ . A general solution of the wave equation for a disturbance travelling in the positive direction with a velocity,  $c$ , and whose position in space is given by a surface  $W(x, y, z)$ , can be written as

$$\bar{U}(x, y, z, t) = \bar{H}(x, y, z, t) f\left(t - \frac{W(x, y, z)}{c}\right) \quad (2)$$

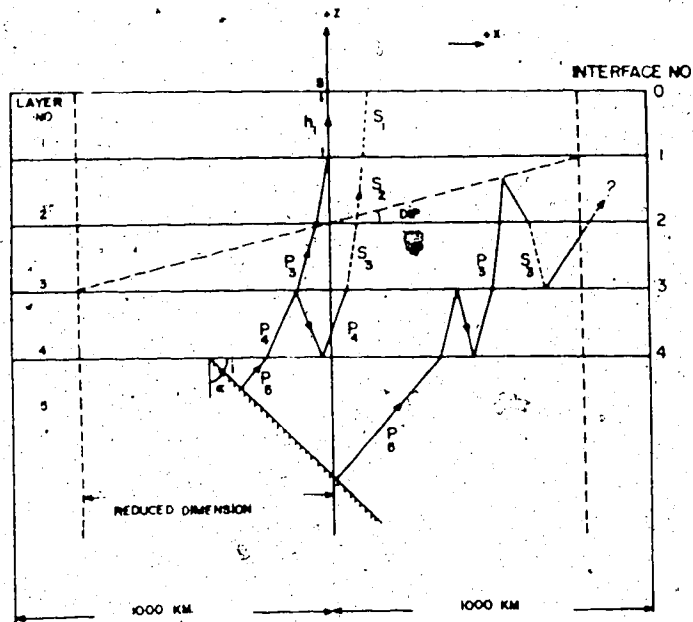
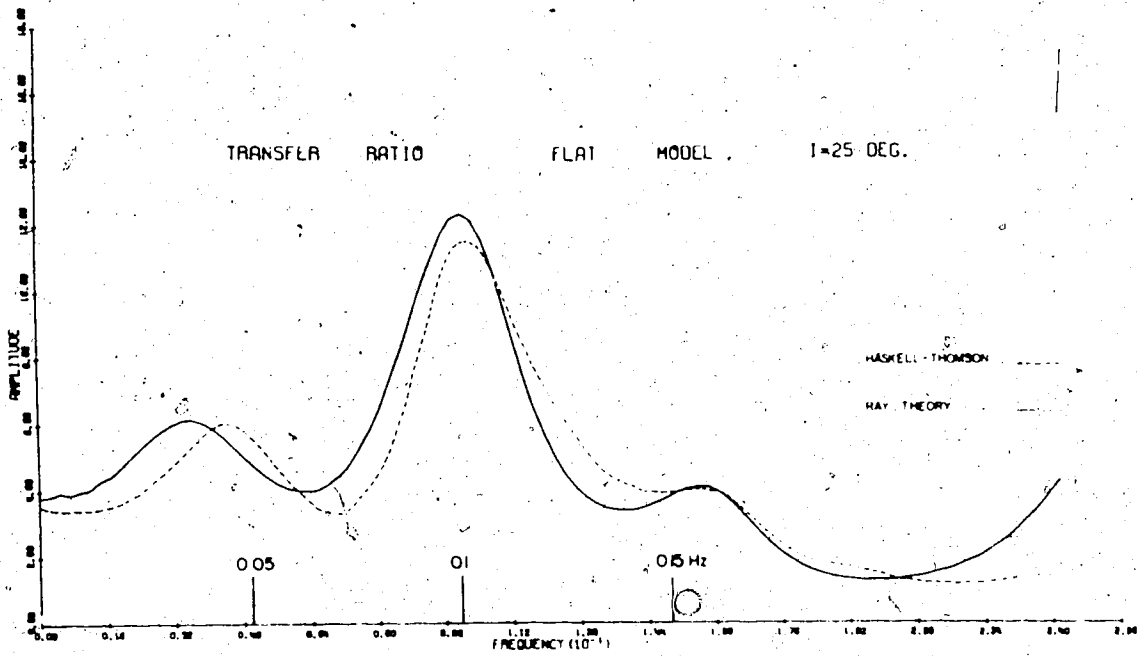
where the function  $f(t)$  represents the disturbance and it may be discontinuous at  $t = 0$ . The position of the surface,  $W(x, y, z)$ , at any time ( $t$ ) is given by

$$t = T(x, y, z) = \frac{W(x, y, z)}{c} \quad (3)$$

Figure III.1

Approximation of wave solution by ray expansion.

The long period spectrum was calculated using a time series of 35 seconds long.



The expansion of equation (2) in a Taylor series near the surface,  $W(x, y, z)$ , ( $t = \tau + \Delta\tau$ ) leads to the following equation:

$$\bar{U}(x, y, z, t) = \sum_{n=0}^{\infty} \frac{1}{n!} \left[ \frac{\partial^n H}{\partial t^n} \right]_{t=\tau(x, y, z)} \cdot (\Delta\tau)^n f(t - \tau(x, y, z)). \quad (4)$$

In this equation the amplitude of the disturbance is no longer time dependent. For the particular case of a harmonic wave solution, where the amplitude is expanded as a power series in  $(1/i\omega)$ , it can be taken as (Hron and Kanasevich, 1971)

$$\frac{1}{n!} (\Delta\tau)^n f(t - \tau) = \frac{e^{i\omega(t - \tau)}}{(i\omega)^n}. \quad (5)$$

Then the solution can be written in terms of only space dependent amplitudes  $\bar{A}(x, y, z)$ :

$$\bar{U}(x, y, z, t) = \sum_{n=0}^{\infty} \bar{A}_n(x, y, z) \frac{e^{-i\omega(t - \tau)}}{(i\omega)^n}. \quad (6)$$

Equation (6) can be generalized for an arbitrary source function  $S_n(t)$ .

$$\bar{U}(x, y, z, t) = \sum_{n=0}^{\infty} \bar{A}_n(x, y, z) S_n[t - \tau(x, y, z)] \quad (7)$$

where  $S_n(t - \tau)$  is given by

$$S_n(t - \tau) = \frac{1}{\pi} \int_{\omega_0}^{\infty} \frac{S(\omega)}{(i\omega)^n} e^{i\omega(t - \tau)} d\omega \quad (8)$$

$S(\omega)$  is the Fourier transform of  $S_n(t)$  and defined to be zero from  $\omega = 0$  to  $\omega_0$ . Equation (7) is known as an asymptotic ray expansion.

If we assume a solution of the wave equation in the form of equation (2), for a specific wave whose velocity of propagation is  $v$ , then substitution of equation (2) into equation (1) leads to the following equation:

$$\left(\frac{\partial w}{\partial x}\right)^2 + \left(\frac{\partial w}{\partial y}\right)^2 + \left(\frac{\partial w}{\partial z}\right)^2 = \frac{v^2}{c^2} \quad (9)$$

where it is assumed that velocity is independent of space coordinates. Equation (9) is known as the "Eikonal" or "characteristic equation" of the wave equation and it is a first order differential equation, the solutions are

$$W(x, y, z) = \text{const} \quad (10)$$

These are surfaces in three dimensional space, which are called wavefronts. Since rays are defined as normals to the wavefront, then equation (9) leads to the concept of a "ray". Solution of equation (9) must also be solution of the wave equation. When it is not, some limitations should be imposed on the solution such as the wavelength being smaller than layer thickness, negligible change in the curvature of the wavefront and amplitude of the wave over wavelength. In equation



(7) terms of (17) are the corrections to the first term due to such limitations. For a plane wave, a solution of the Eikonal equation is also a solution of the wave equation, provided that wavelengths are much smaller than layer thickness. Only  $n = 0$  in equation (7) will be sufficient to obtain a wave solution using first order ray theory. Proof of this is given and discussed by Červený and Ravindra (1971). Equation (7) can be applied to any media if the source function is known at time  $t = 0$ . Rays can be drawn in space using Fermat's principle. When there is a discontinuity in parameters of the media, continuity of displacement and stress components are the boundary condition to be satisfied and the amplitude of the ray is predicted by coefficients of reflection and transmission (Knott, 1899). In an isotropic media it can be assumed that energy flows in the direction of the ray. For a plane wave, the cross section of a ray bundle (ray tube) is constant at any time and it can easily be shown that energy is conserved at any instant. Therefore, for this simple case, a geometric expansion factor is not necessary (Červený and Ravindra, 1971). For a ray which is reflected and transmitted a number of times, the amplitude,  $A(x, y, z)$ , in equation (7) will be the product of reflection and transmission coefficients (Spencer, 1960). For a plane wave solution,

the density of rays will be important and the sum of existing rays will constitute a solution of the wave equation. However, for numerical evaluation of a solution, the number of rays to be summed must be chosen from an infinite number of rays.

A program developed by Hron et al (1973) is used to determine the optimum number of rays necessary to evaluate economically the response of a layered-media to a plane wave impinging on the bottom. The validity of the solution has been tested by comparison with the one calculated using a matrix method (Haskell, 1953) which can be considered as a complete wave solution. Rays with up to 13 segments for a four layered Alberta crustal model (Table 1), have been shown in Table 2. Segment number 5 represents the ray impinging on the bottom of the layered media. Each segment is represented by a number corresponding to the layering sequences (Figure 1). For example, ray number 1 has five segments and represents the ray transmitted directly from bottom to the surface. Rays with a large number of segments can be constructed from ray number 1, by adding two more segments to it in any layer. For this model, the total segment number in a ray will be an odd integer starting from 5. The ray classification is based on the number of segments

in a ray (NSEG). The maximum number of conversions of a ray will be  $JCONV = NSEG - 1$ . A list of converted phases constructed from Table 1 has been shown in Table 3. For example, if one conversion is to be allowed for ray number 1 which has 5 segments, then possible conversions may be at one of the four interfaces from bottom to the top ( $JC = 1, 2, 3, 4$ ). The total number of converted rays with NSEG segments and JCONV conversions is given by the equation (Hron, 1971):

$$C_{\text{JCONV}}^{\text{NSEG}-1} = \frac{(NSEG - 1)!}{JCONV! (NSEG - 1 - JCONV)!} \quad (11)$$

Therefore, the number of rays increases rapidly. For example, from the unconverted rays with 13 segments, one can construct about half a million rays. For a plane wave solution, kinematic and dynamic analogs of rays are not necessary since phases are well separated in time. The number of conversions to be used on each set of rays for a satisfactory seismogram is found empirically as given in the following table:

<u>NSEG</u>	<u>Set</u>	<u>No. of conversions</u>
5	1	4
7	2	4
9	3	4
11	4	3
13	5	1

Generally, ray amplitudes decrease with increasing number of reflections as well as number of conversions. In this thesis, the minimum amplitude for a ray to be included was taken to be  $1/300$  of the existing maximum ray amplitude. The impinging point and offsets on the bottom of the layered media has been calculated and the only rays of any impinging within 1000 km of the receiver have been taken into consideration for a flat layered model (Figure 1). For a dipping layered model the 1000 km region on both sides of the receiver has been reduced further to exclude the vertex. The radiation from the wedge shaped structure is ignored as it is assumed that waves propagate out of the open end of the layer. Using the tests given above, accepted rays are determined with respect to existing rays. When less than a certain given percentage (7 %) of the rays are accepted in a group, no other rays in a higher set are taken into consideration in order to save computing time.

The response of a model (Table 1) calculated using ray theory has been compared to the one calculated by a matrix method in both the time and frequency domain. The time domain comparison is presented in another chapter and gives a very good comparison over the initial interval of the coda, however, small differences exist at larger times. The lower end of the frequency is the most imprecise because this corresponds to large

reverberation times. In Figure 1, the transfer ratio for an Alberta crustal model (ALTACRT-1) calculated using ray theory has been compared to the one calculated using a matrix method. The worst part of this comparison is at about 0.04 Hz. In this model, wavelengths are about 6-15 times larger than layer thickness, however, there is no change in the position of major peak and only amplitude differences exist.

Table 1

Alberta Crustal Model ALTACRT-3

<u>h(km)</u>	<u>V<sub>P</sub>(km/sec)</u>	<u>V<sub>S</sub>(km/sec)</u>	<u>ρ(gr/cc)</u>
1.10	2.31	1.33	2.04
0.92	3.06	1.77	2.21
31.38	6.50	3.75	2.73
9.8	7.15	4.13	3.20
	8.08	4.66	3.45









### 3. Dipping layered media and transfer ratios

A ten degree dip was introduced into model ALTACRT-1 into the basal interface (Figure 2). The sign convention was that a positive (negative) sign indicated an up-dipping (down-dipping) interface with respect to a wave approaching at the bottom of the layered media. The difference between a flat and a dipping model mainly occurred in the amplitude of the transfer ratio and there were no significant frequency shifts. In this model a peak at about 1.28 Hz has been affected most and the down-dipping model shows a decrease in amplitude with respect to the flat layered model, which is opposite to amplitude change for an up-dipping case. For frequencies larger than 15 Hz, very significant differences appeared. The effect of dipping layers on an incident S wave is more serious (Figure 3) and this can be explained in terms of particle motion. For P waves interfaces dipping as much as  $10^\circ$  introduced no significant shift of peaks in frequency. However, when low velocity sediments have dips about  $10^\circ$ , the most significant effects are observed. The important shift of peaks occurs at all frequencies as well as amplitude changes. Here, an important feature of program must be mentioned; when a thin layer at the top of the model is dipping severely, the region on which rays impinging will be reduced to

a very small value, for example, for  $+10^\circ$ , it will be (Figure 1)  $-56.7 < x < 11.3$  km. Therefore, a number of the rays will be excluded in the response. For example, in Figure 4, the peaks around 0.90 Hz does not exist. When the same layer has a dip of  $-10^\circ$ , the same important phases such as  $P_5 P_4 P_3 P_2 P_1$  do not reach to the surface due to the above reasons, raising some question about the solution. When all the layers in a model are dipping concordant, the interpretation of the transfer ratio in terms of real Earth is difficult (Figure 4, bottom). For this case a frequency shift of about 24 MHz was observed at very low frequencies (0.1 Hz) (Figure 5). Generally, about 30-40 seconds of experimental data are used to calculate spectral ratios, this time length corresponds to a plane wave impinging on about 100 km region of the bottom of the layered media. Dipping of sedimentary layers as much as  $10^\circ$ , brings serious restrictions on the ray solution, or this may mean that radiation from the wedge shaped structure is not negligible. For this model on which sedimentary layer has a severe dip, the peaks at very low frequency band were shifted to the higher frequencies, however, this shift is found to be unstable with changing angle of incidence. If Figure 6-d, model ( $i = 35^\circ$ ) showed a shift of peaks towards the low frequencies with respect to flat layered model, the

Figure III.2.

Comparison of vertical ratios for a dipping  
model with a zone.

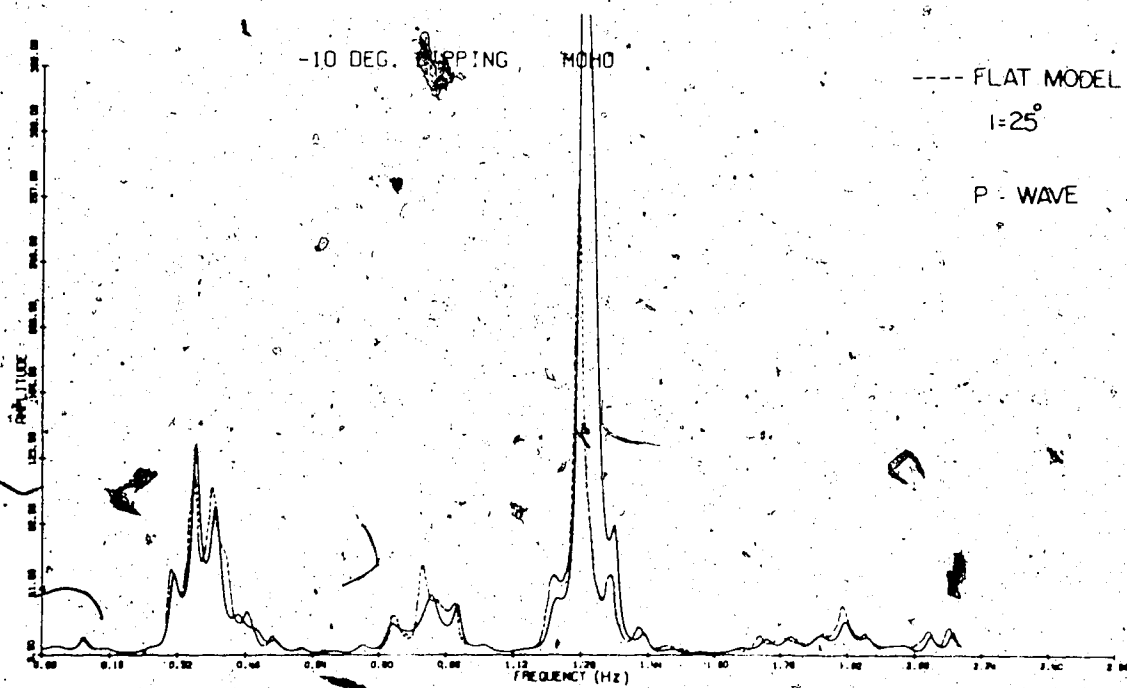
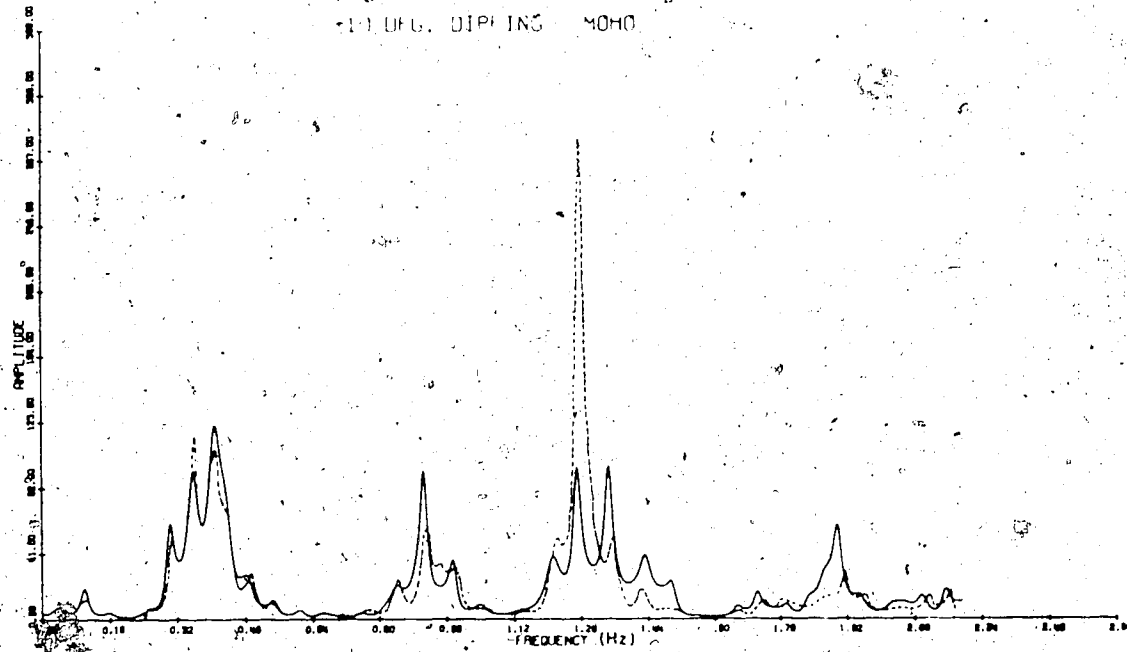
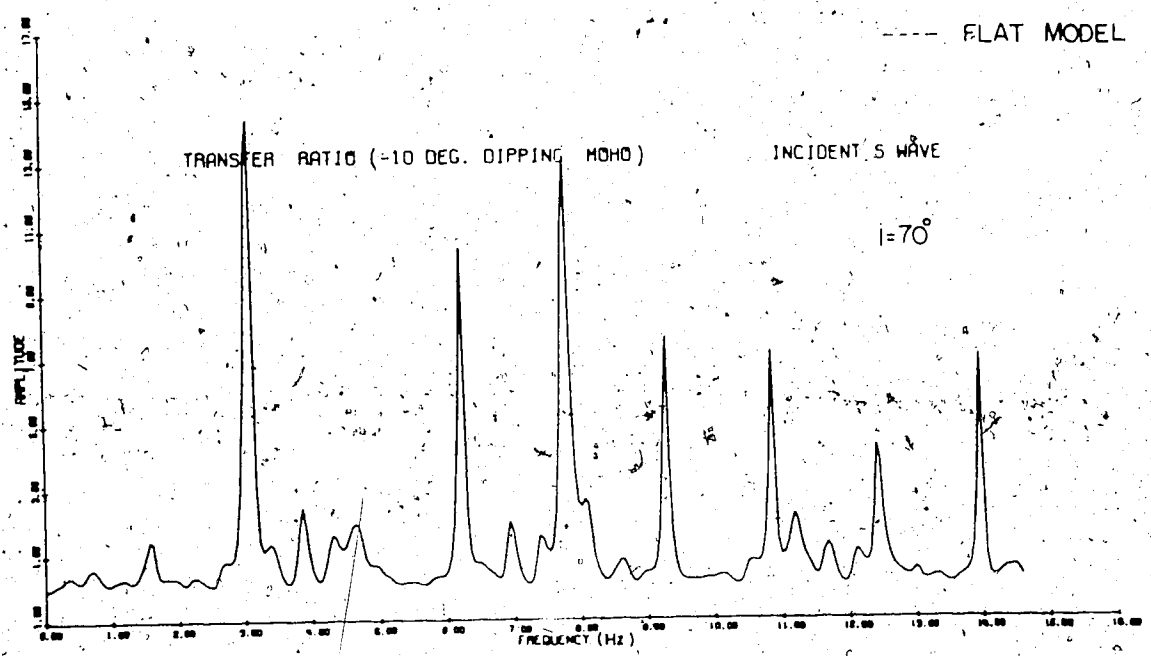
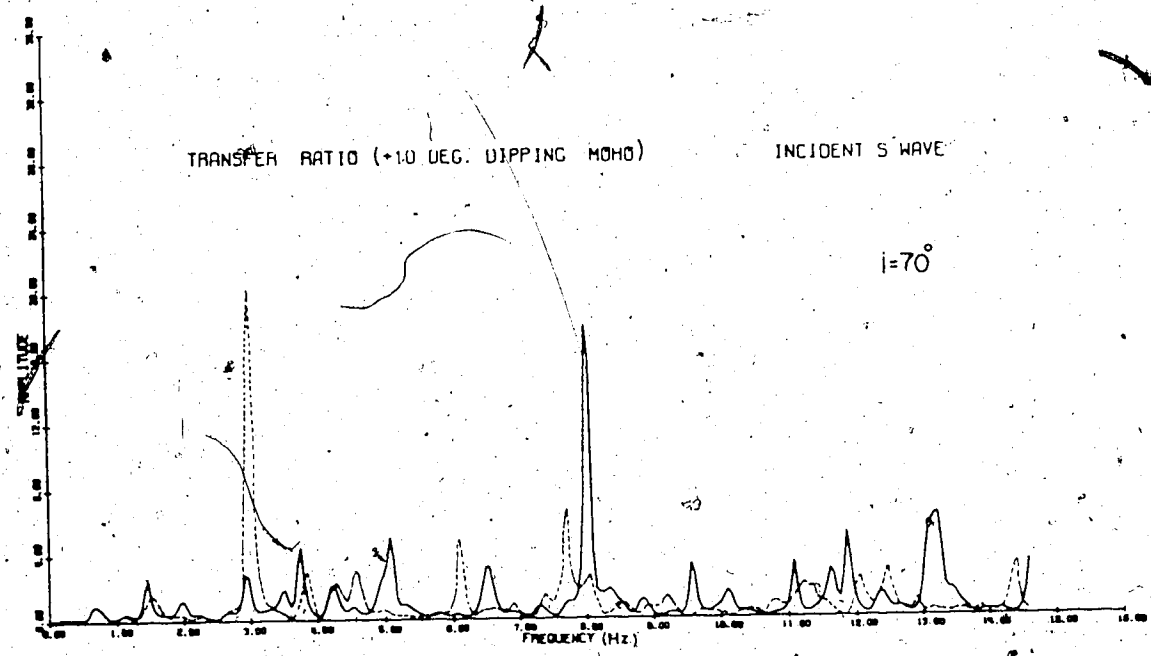


Figure III.3

Comparison of spectral ratios for dipping  
and flat layer model for an incident plane  
S wave.



interpretation of this amount of shift in terms of real Earth can be done if the total thickness of the crust is varied about 5 km.

#### 4. Conclusions

For dipping interfaces of thick layers with a high velocity, the transfer ratios are not affected significantly for dip angles of as much as 10 degrees in the frequency range of interest. In flat layered media, a layer with a thickness less than one wave-~~length~~ introduces no significant frequency shift into the transfer ratio. However, there are significant shifts when steeply dipping low velocity layers are present. For example, an up-dipping sedimentary layer as much as 10 degrees causes a shift to the higher frequencies. This is expected, because the low velocity layer affects travel time of the wave significantly. For a down-dipping sedimentary layer it is expected to have a frequency shift to lower frequencies due to larger travel time of wave in this layer. However, for large down-dipping thin layers, the region on which wave impinges on the bottom of the layered media is very small, therefore the number of rays used is very low and the solution cannot be evaluated using this program. In both cases, the amount of shift introduced by low velocity layer on transfer ratios is not certain

Figure III.4

Effect of steeply dipping sedimentary layer  
on transmission of P waves.



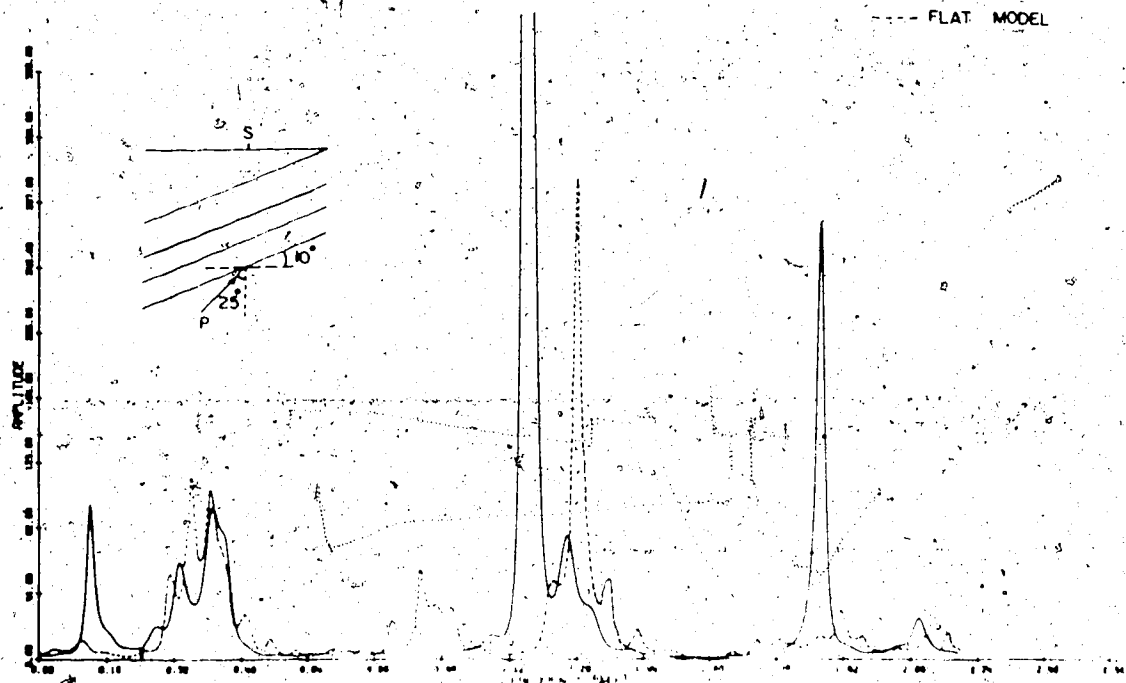
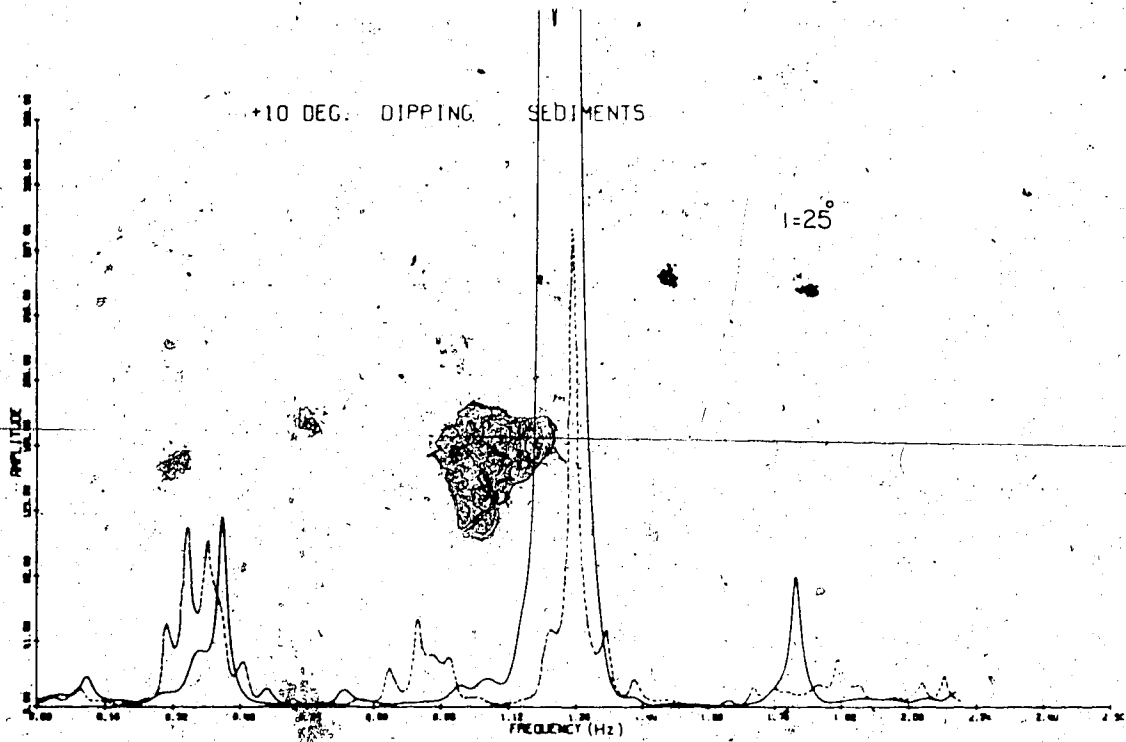
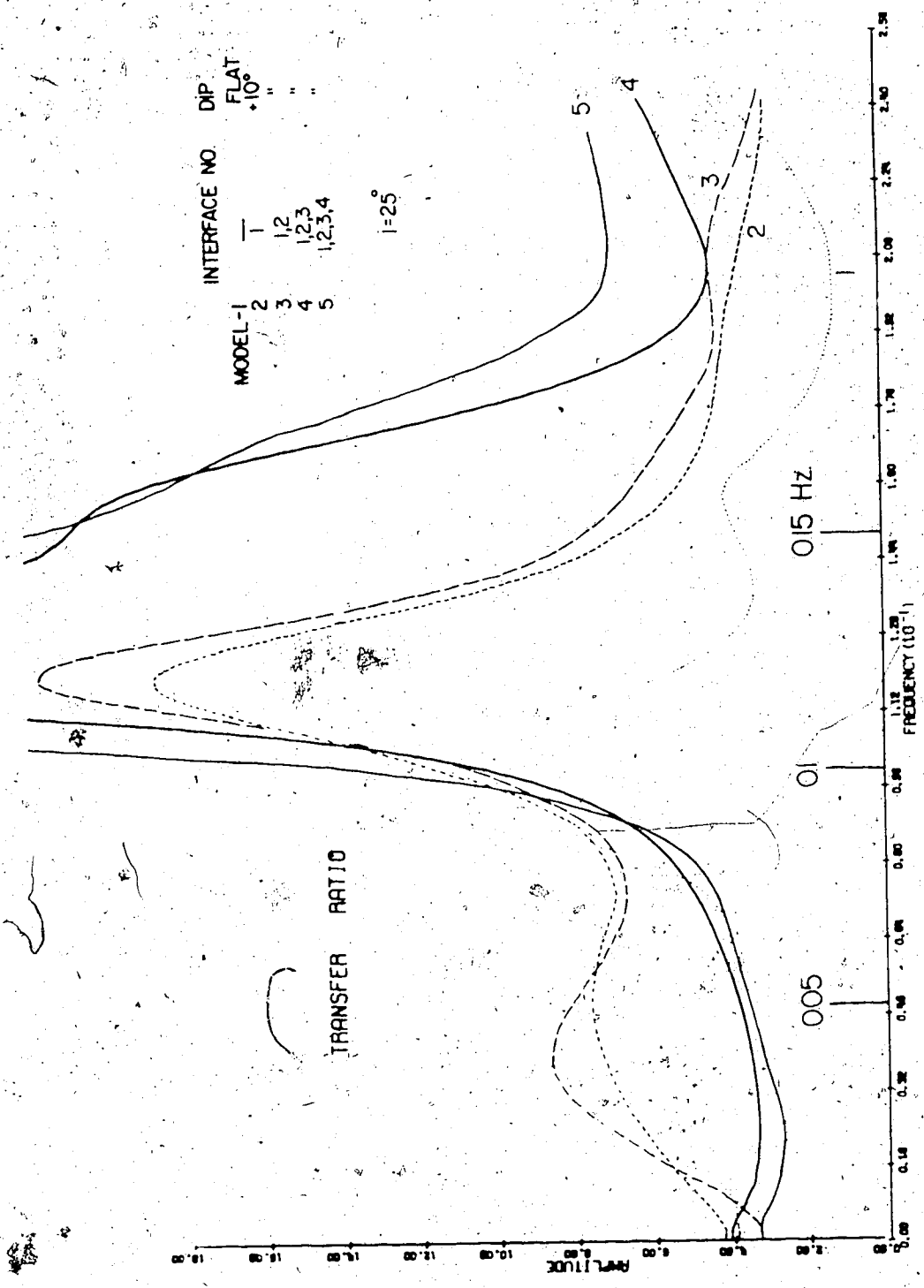


Figure III.5.

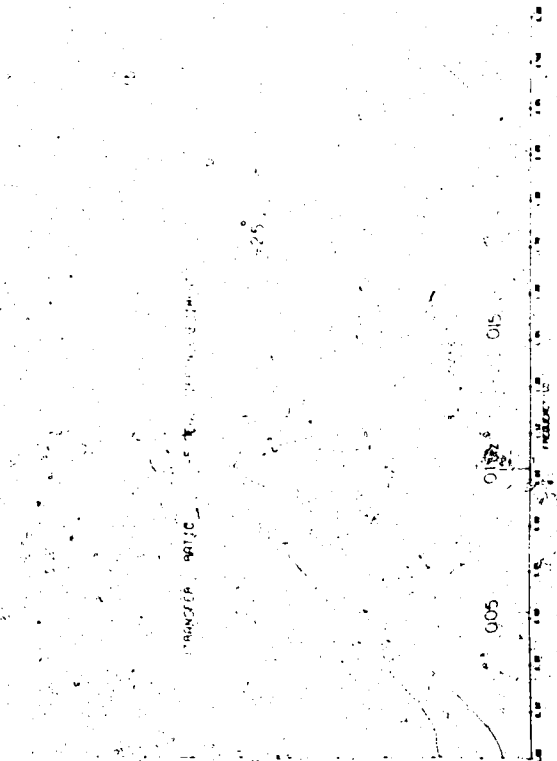
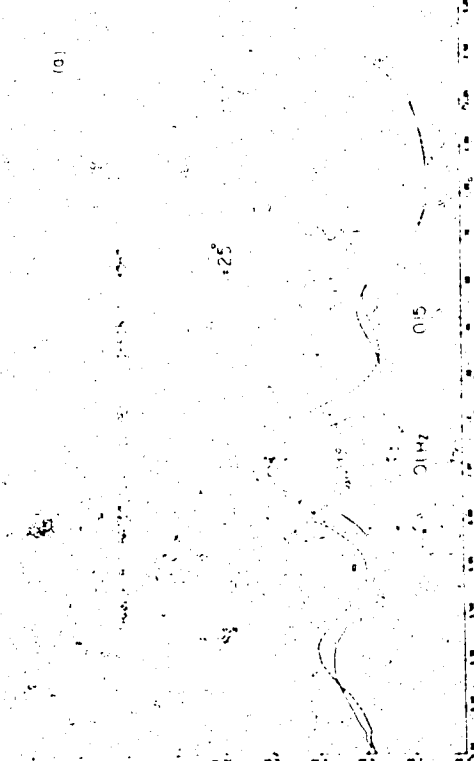
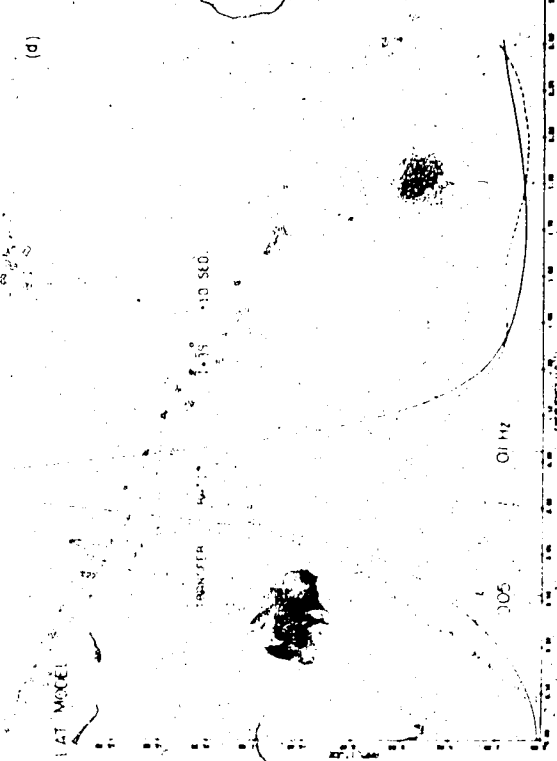
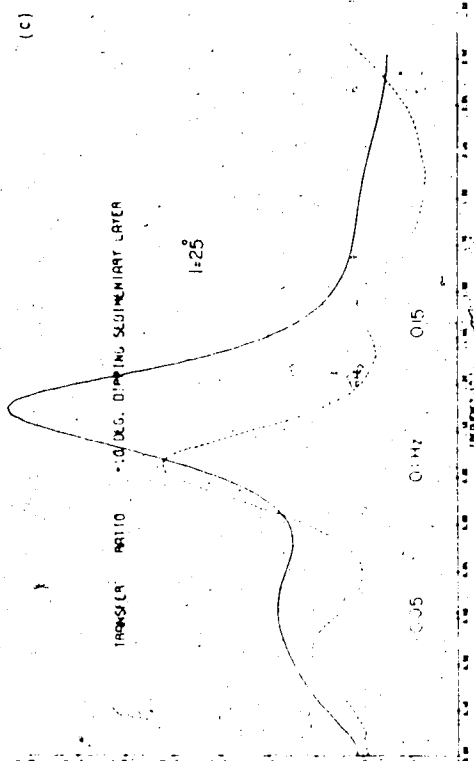
Effect of up-dipping layers on long period  
transfer ratios for P waves (model ALTACRT-I).



G

Figure III.6

Effect of dipping interfaces on long period transfer ratios and its variation with angle of incidence.



because it is also a function of terms used in ray expansion and this depends on the region in which rays are to be evaluated. Long period spectrum is very sensitive to the terms used in ray expansion and it is clearly also dependent on angle of incidence of the wave. For severely dipping interfaces, short time interval or high frequencies should be made of use.

Dip determination using spectral ratio method requires important assumptions. For even a simple crustal structure, the experimental transfer ratios for various azimuths have to be studied to determine the amplitude changes indicative of a possible dipping structure. If short period data is used to study dipping interfaces, assumption of non-attenuating and isotropy of the media is necessary and velocity of the media and angle of incidence of the wave have to be known with sufficient accuracy. For a multi-dipping layered media the spectral ratio method can then be used to obtain a better fit between theory and experiment, if additional evidence exists for dipping layers.

#### IV. Attenuation in the Crust

##### 1. Representation of attenuation in the solid Earth

The study of seismic wave attenuation in the solid Earth has developed recently into one of the more interesting research areas. In many seismic studies attenuation has been neglected for the sake of simplicity. However, a number of researches have shown that a study of the loss mechanism brings additional information about the physical state of the interior of the Earth. The nature of the loss mechanism is very important when inversion of observed data is attempted because a seismologist would like to interpret his findings in terms of a real Earth.

It has been customary to represent a lossy media in terms of a delayed strain due to an applied stress. This can be written in the time domain as a convolution of strain with a memory function or in the frequency domain it will be

$$P(\omega) = e(\omega) \cdot m(\omega) \quad , \quad \omega = 2\pi f \quad (1)$$

where  $P(\omega)$ ,  $e(\omega)$  and  $m(\omega)$  are the Fourier transform of stress, strain and a memory function respectively. Here the memory function,  $m(\omega)$ , describes the nature of the loss mechanism such as viscosity, solid friction, etc. The memory must be an even function of frequency

in order to have energy dissipated equally over positive and negative frequencies. There are a large number of models suggested to describe the loss mechanism since Maxwell (1866). They are usually expressed in the time domain by a suitable approximation of laboratory measurements. By calculating the Fourier components of the time model, attenuation is also defined in the frequency domain. A large number of laboratory measurements on solid materials (Knopoff, 1964) showed that, for strains less than  $10^{-6}$ , attenuation is independent of amplitude of strain and linear for sufficiently large frequencies but non-linearity occurs around zero frequency.

According to Hooke's law, the ratio of stress to strain is a parameter called the modulus of elasticity. Then in equation (1), the memory function is nothing else than a complex modulus. One way of treating the problem is to express an elastic modulus as a complex function in the frequency domain. For example, in isotropic lossy media the two elastic parameters will be

$$\lambda = \lambda_R + i \operatorname{sgn} \omega \lambda_I \quad (2)$$

$$\mu = \mu_R + i \operatorname{sgn} \omega \mu_I$$

$$\operatorname{sgn} \omega = \begin{cases} +1 & \omega > 0 \\ 0 & \omega = 0 \\ -1 & \omega < 0 \end{cases}$$



where  $\lambda$  and  $\mu$  are Lamé constants and the sign  $\omega$  function is required so that there are real space-time loss mechanisms and stress components. This approach can be thought of as a modification of Hooke's law. As will be shown below, introducing complex elastic moduli is equivalent to having a spatially damped motion in frequency. In equation (2), the elastic parameters have been assumed to be independent of frequency. This is equivalent to having frequency independent velocities. However, Futterman (1962) calculated the Fourier transform pairs for a model in which body waves are dispersive.

For the frequency independent case, the wave velocity in a lossy media can be expressed as (Bullen, 1953)

$$v^2 = \frac{M_R + i \operatorname{sign} \omega M_I}{\rho} \quad (3)$$

where  $\rho$  is the density of the media and  $M$  is a complex elastic modulus. As an example for P (compressional) waves

$$M_R = \lambda_R + 2\mu_R, \quad M_I = \lambda_I + 2\mu_I \quad (4)$$

From the definition of a phase angle

$$\theta \approx \frac{M_I}{M_R} \quad \text{for} \quad M_I \ll M_R$$

The inverse of the phase angle,  $\phi$ , is defined as

"quality factor,  $Q$ ". This dimensionless quantity has been used as a measure of attenuation in electrical circuit theory and many branches of physics. There are a number of different definitions of  $Q$  in the literature, however, by making use of various physical quantities, it can be shown that they are equivalent. For example, it can be defined as

$$Q = \frac{2\pi E}{\Delta E} \quad (5)$$

where  $\Delta E$  is the energy dissipated and  $E$  is the maximum energy stored in the system per stress cycle. Another definition is that in a spatially damped motion where the restoring force is proportional to the amplitude of vibration, the natural logarithm of the amplitude ratio of successive oscillations (logarithmic decrement) is proportional to the inverse of  $Q$

$$\delta = \frac{\pi}{Q} \quad (6)$$

In all these definitions, an exponential type attenuation results. If we consider a plane wave propagating in the  $z$  direction in isotropic lossy media with a certain velocity, then at a time  $t = 0$ , it can be written as

$$e^{-i\omega(\rho/(M_R + i \operatorname{sgn}\omega M_I))^{1/2} z} = e^{-|\omega|z/2CQ} e^{-i\omega z/C} \quad (7)$$

This represents a plane wave propagating with a velocity,

C, whose amplitude is damped with distance z in an amount determined by the frequency and the factor,

The phase velocity is given by

$$\frac{1}{C} = \text{Re} \left\{ \left( \frac{\rho}{M_R + i \text{sgn} \omega M_I} \right)^{1/2} \right\} \quad (8)$$

and the spatial attenuation constant will be

$$\alpha = \frac{\omega}{2CQ} = \omega \text{Im} \left( \frac{\rho}{M_R + i \text{sgn} \omega M_I} \right)^{1/2} \quad (9)$$

Equation (7) is a particular solution of the differential equation of motion of a medium possessing solid friction (Knopoff, 1956)

$$\rho \frac{\partial^2 \bar{U}}{\partial t^2} = (\lambda + 2\mu) \left\{ 1 + \frac{1}{|\omega| Q_\alpha} \frac{\partial}{\partial t} \right\} \nabla \nabla \cdot \bar{U} - \mu \left\{ 1 + \frac{1}{|\omega| Q_\beta} \frac{\partial}{\partial t} \right\} \nabla \times \nabla \times \bar{U} \quad (10)$$

where  $Q_\alpha$  and  $Q_\beta$  are quality factors for P and S waves respectively.

Solid friction is one of the physical models for attenuation where the phase velocity and the quality factor Q are not a function of frequency.

This model is strongly suggested for solid materials due to laboratory measurements but there is no theory to explain every aspect of solid friction.

We have seen that attenuation can be sufficiently described by having complex velocities. Using equations (8) and (9),  $M_I$  can be eliminated:

$$\left(\frac{M_R}{\rho}\right)^2 = C \frac{4Q^2}{[4Q^2 + 1]} \quad (11)$$

If  $Q \gg 1$ , then approximation will be

$$\left(\frac{M_R}{\rho}\right)^2 \approx C \quad (12)$$

On the other hand, using same equations (8) and (9), it can be written

$$\frac{1}{C} = \frac{2\alpha Q}{\omega}$$

or

$$\operatorname{Re}\left\{\left(\frac{\rho}{M_R + i \operatorname{sgn} \omega M_I}\right)^2\right\} = -2Q \operatorname{Im}\left\{\left(\frac{\rho}{M_R + i \operatorname{sgn} \omega M_I}\right)^2\right\} \quad (13)$$

and we have

$$\left(\frac{M_I}{\rho}\right)^2 = -\frac{1}{2Q} \cdot \left(\frac{M_R}{\rho}\right)^2$$

using

$$V_I = \left(\frac{M_I}{\rho}\right) \quad V_R = \left(\frac{M_R}{\rho}\right)$$

$$V_I = -\frac{V_R}{2Q} \quad (14)$$

Then equations (12) and (14) determine the real and imaginary part of velocity.

## 2. Attenuation properties of crust

In many research works, attenuation properties of the crust has been treated together with attenuation

in the mantle or attenuation characteristics have been used by comparison of laboratory measurements.

However, it is difficult to imitate physical states of the interior of the solid Earth in a laboratory. Born (1941) discussed the nature of solid friction and viscous friction and attempted to verify his discussions by experiments using bar type sample rocks. Oscillatory motion has been set up at one end of the bar and motion is detected at the other end by a coil. From the damped resonant motion of the bar, he calculated the logarithmic decrement using the width of the resonance curve. His results can be summarized as in the following table:

	<u>Resonant freq. (K.Hz)</u>	<u>Q</u>
Sylvan Shale	12.80	70
	6.58	75
	3.36	73
Hunton Limestone	10.55	60
	2.82	72
Amherst Sandstone	1.26	55
	0.93	157

Born used the above seven dry samples and concluded that losses are due to solid friction but unconsolidated sediments near the surface may exhibit plastic behavior.

Therefore, there could be viscous losses. Similarly, under laboratory conditions Birch and Bancroft (1938) studied forced resonant vibration of a long column of Quincy granite. They used longitudinal, flexural and torsional waves to measure dependency of velocity and attenuation on frequency. Their result showed a Q value between 100-200 over a frequency range 140-1600 Hz. However, the same authors (1938b) measured a Q value of 1200 for torsional vibrations of a small granite rod at a frequency about 7.0 K.Hz under a pressure of 4000 atm and a Q value of 180 for a pressure of 200 atm at the same frequency. Knopoff and Porter (1963) determined  $Q = 80$  for Westerly granite from the Rayleigh wave analysis in the frequency range of 100-400 K.Hz. There are a number of research work done in measurement of attenuation in situ. Among these, McDonald et al. (1953) have done a detailed study of attenuation in the Pierre shale near Limon, Colorado. They measured attenuation of vertically travelling compressional waves using signals recorded by five detectors positioned in the bore holes at various depths in the formation, which was about 4000 ft. thick. An empirical frequency decay law is stated using the frequency spectra of recorded signals in the frequency range 50-500 Hz. They concluded that attenuation is a function of the first power of frequency contradicting the work of Ricker (1953) at the same

site, who found an attenuation relation which is a function of the square of frequency. The McDonald et al. result showed a Q value of about 10-23 for Pierre shale and no dispersion observed. However, they have noted that dispersion may be important in the weathered zone. Collins and Lee (1956) used a limited number of strain recording taken over a small distance to determine attenuation parameters in sandstone. Their results gave a Q value of 7 over the frequency range 100-900 Hz for compressional waves. However, they could not make any conclusions due to insufficient data.

Many laboratory measurements for attenuation have been performed at large frequencies. One obtains a high resolution in the data and so determines the dispersion relation with frequency. It is well agreed among a number of authors that attenuation is linear for these high frequencies. However, the seismological spectrum is centered at about 1 Hz which is well below the range of laboratory measurements. On the other hand, it is well known from experimental seismology that waves with a frequency near 50 Hz create great problems in interpretation since at these high frequencies elastic waves are very sensitive to inhomogeneity and anisotropy of the crust and scattering becomes important. The first low frequency attenuation experiment has been performed by

Peselnick et al. (1961). They have attempted to measure internal friction in shear modulus of Solenhofen limestone over a frequency range of  $4-10^7$  Hz. Using torsional waves for a limestone sample whose density is 2.67 gr/cc and shear velocity is 3.1 km/sec, their results showed higher Q values:

	<u>f</u>	<u>Q<sub>s</sub></u>
Solenhofen	3.89 Hz	850

Later, Donato et al. (1962) performed attenuation measurements in the laboratory using a wide range of frequencies including very large periods. For low frequencies, the specimen was made to vibrate as a beam clamped at both ends and then compared with a standard steel beam.

Young's modulus and attenuation have been measured.

They found that while Young's modulus remains constant within 5% for all frequencies, the Q varies at low frequencies, but it is constant for high frequencies.

Variation of Q at low frequencies is noted to increase by a factor of two as compared to the value at high frequencies. Their results are as follows:

	<u>f</u>	<u>Q</u>
Upper Oolite Limestone	< 2 Hz	360
	20-40 Hz	180±18
	10-80 K.Hz	310 <sup>12</sup> ±15



	<u>f</u>	<u>Q</u>
Dolerite	<2 Hz	360
	2-40 Hz	180 ± 18
Hard Chalk	<2 Hz	220
	11-66 K.Hz	70 ± 8

Tullos (1969) has used transfer function analysis to measure attenuation in Gulf Coast sediments. Analysis has been carried out using vertically travelling waves in a sedimentary layer of 1000 ft. thick, recorded in a frequency range of 50-400 Hz by array of seismometers. Q values have been found to be high for these sediments for which the velocity structure is well known:

	<u>d(ft)</u>	<u>Q<sub>p</sub></u>
Loam-sand-clay	1-10	5
Clay-sand	75-100	420
Sandy clay	100-500	165
Clay sand	500-1000	315

There is a large amount of research on the attenuation of the Earth's interior. In those works where researchers treated the crust as a part of the mantle crustal attenuation is found to be severe.

There is a small number of published works dealing with attenuation only in the crust. Press (1964) determined Q values for the crust from nuclear explosions

in Nevada. He made use of channel waves and assumed that seismic wave energy decreases with the first power of distance. His average for  $Q$  from  $L_g$  waves is  $\bar{Q} = 450$  and  $\bar{Q} = 260$  from  $P_g$  phases. He interpreted low  $Q$  values for  $P_g$  waves not as a property of crustal structure but as an energy loss due to mode conversions. Fedetov (1963) studied attenuation of shear waves whose frequency is 0.2-0.5 Hz propagating in the crust near southern Kurile island. He found a  $Q$  value with a large uncertainty:  $Q_s = 400 \pm 200$ . Anderson et al. (1965) estimated a  $Q$  value of 1000 for the crust using surface waves with periods 50-300 seconds. O'Brien (1968) estimated a  $Q$  value of 1000 for compressional waves using Early Rise refraction data near Superior Lake. Sumner (1967) made use of earthquake shocks located at a depth of 20-180 km, to study attenuation of  $P$  waves in southern Peru. He calculated a  $Q$  value of more than 1000 for the crust and upper mantle. Clowes et al. (1970) determined crustal attenuation from deep reflections. His results showed a  $Q$  value of 200 for sedimentary layers and 1500 for the lower crust. Hill (1971) used published head wave amplitude data to determine  $Q$  values in central north America. His results from amplitude distance curves of  $P_g$  and  $P^*$  arrivals, gives a  $Q$  value greater than 1000 for the crystalline crust and intermediate layer in the west coast normal heat flow provinces and

Q values are smaller for high heat flow provinces. He attributed low Q values to the scattering of head waves, temperature dependent Q values and negative velocity gradients in the upper part of crystalline crust associated with high geothermal gradient. In his work, he used a crustal model with 2 km low velocity sedimentary layer ( $V_p = 3.0$  km/sec), overlying crystalline basement ( $V_p = 6.0$  km/sec).

Brian (1973) utilized 4-40 sec period surface waves to determine attenuation in central north America. He estimated an average Q value for shear waves of about (75-300) for upper 15-20 km portion of the crust,  $Q = 2000$  for deeper part of the crust. He interpreted this rapid jump in Q values as a possible temperature increase and change in chemical constitution of the crust at intermediate depth. However, he was not able to predict a Q value for P waves.

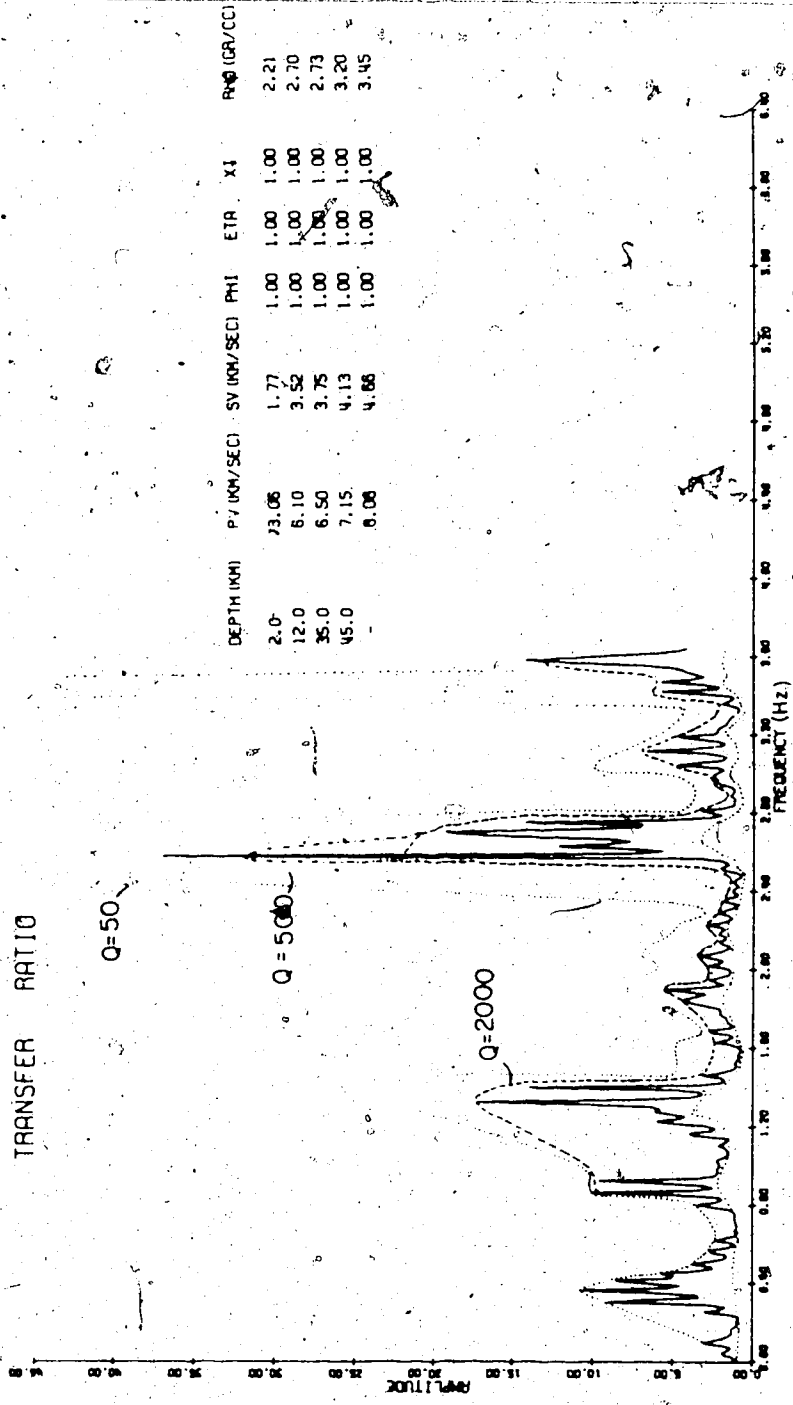
In a tectonically complex area, O'Neill and Healy (1973) reported very low  $Q_p$  values along the San Andreas fault region. For the uppermost part of the crust they have estimated Q values of 35-100. In some region Kurita (1973) has elucidated  $Q_s$  values about 90-160 for the upper 6 km of the crust and for sedimentary rocks it is as low as 35-40.

### 3. Spectral ratios for dissipative crustal models and application to earthquake data

In one of the attenuation models, the memory function in equation (1) is expressed as a logarithmic function in time which fits a linear behavior of attenuation over a large range of frequencies. In this model phase velocity and quality factors are functions of frequency (Futterman, 1962). However, a cutoff frequency is introduced to approximate laboratory measurement. Above the cutoff the  $Q$  is linear with frequency, while below the cutoff frequency,  $Q$  is assumed to be infinite. Wuenschel (1965) and Jensen (1970) applied this model to real materials and spectral ratios. In this thesis, frequency independent  $Q$  value and phase velocities are used. Attenuation is introduced in the Haskell-Thomson formulation by making use of complex velocities. Attenuation is allowed to be independent of the sign of frequency and distance travelled by the wave in the  $z$  direction. The proper sign is chosen for the exponent to account for the correct direction of transmission for a wave incident at the bottom of layered media. In Figure 1, the transfer ratios for one of the isotropic Alberta models are shown for different  $Q$  values. In this figure, the solid line represents a non-attenuating model. The attenuating models are only shown by their envelopes on the graphs.

Figure IV.1

Comparison of transfer ratios for attenuating models with the non-attenuating one.



Very small values of  $Q$  cause the spectral level to increase with increasing frequency. For example, for  $Q = 50$  significant differences from the non-attenuating model occur at about 1.2 Hz, 2.60 Hz and 3.40 Hz.

Among these, the one at 2.60 Hz is the most indicative for attenuation. This peak has an 800% larger amplitude than the second larger peak at a frequency of 3.40 Hz.

Models for  $Q = 500$  and  $Q = 2000$  have very little differences in amplitude from a non-attenuating model at all frequencies. Letting  $Q$  increase with depth in the crustal section (Figure 2a) creates no distinct differences from a non-attenuating model. All models have negligible differences in amplitude for frequencies less than 0.80 Hz for 35 degrees of angle of incidence.

For angles of incidence of  $5^\circ$ , all models are almost the same at frequencies less than 0.3 Hz. Among these calculated models, dissipative ones have shown no

frequency shift for a sampling frequency of 0.0122 Hz with respect to non-dissipative models for long periods.

But major peaks which are indicative of attenuation at higher frequencies are displaced as much as two samples.

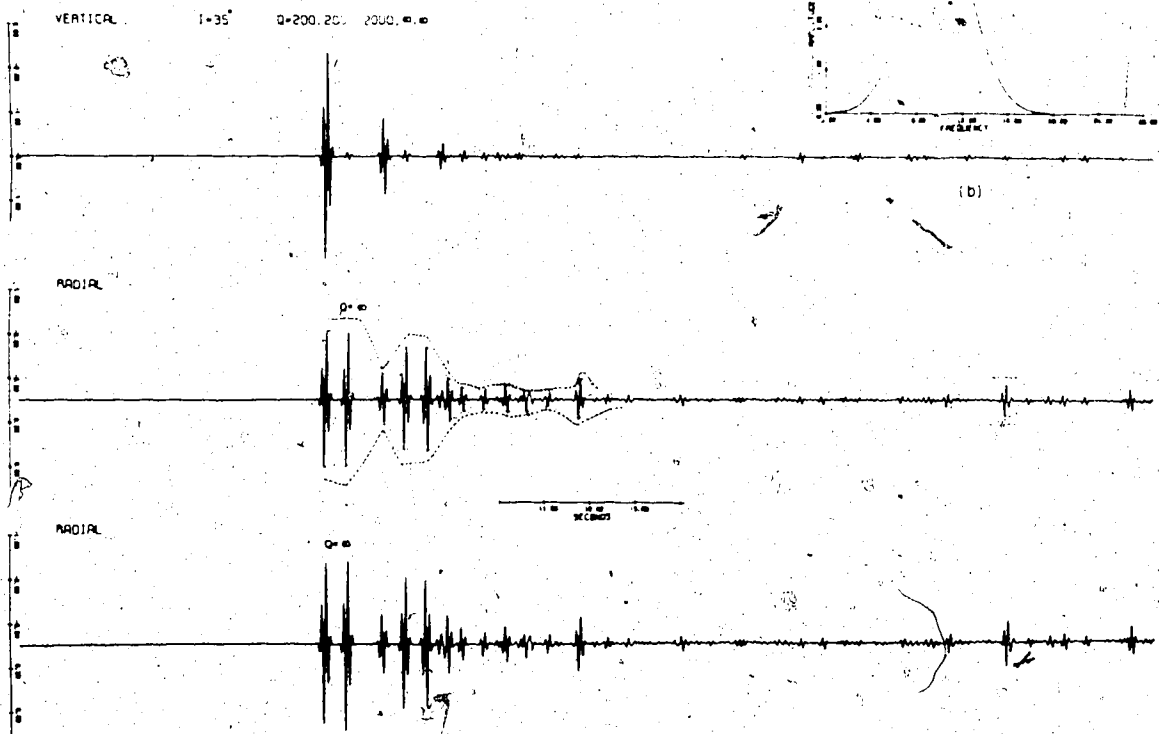
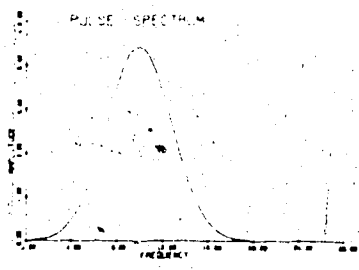
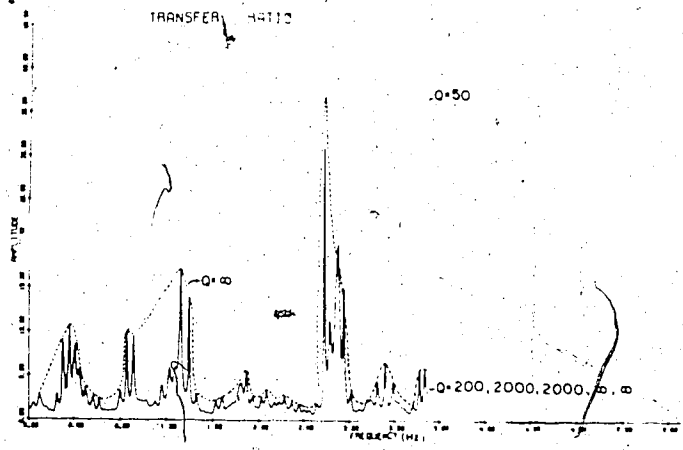
Here, it is assumed P and S velocities have the same quality factors. However, if we were to use a different quality factor for S waves following Knopoff, 1971, it would be

$$Q_P \approx \frac{9}{4} Q_S \quad (14)$$

Figure IV.2

A transfer ratio for attenuating model  
and its time synthesis.





then more distinct amplitude changes will occur in the transfer ratios. This is due to exponential factor:

$$e^{-\omega z / 2V_S Q_S} \quad (15)$$

where  $V_S < V_P$  and  $Q_P > Q_S$ . Then the exponent will be larger than the similar exponent for P waves for the same frequency and distance  $z$ . Therefore, the horizontal component will be damped faster than the vertical component for all frequencies.

A synthetic seismogram can be studied for an attenuating model by taking a Fourier inversion of the transfer function, provided that the true phase is known at each frequency. In Figure 2b, a synthetic seismogram is determined for an Alberta model including attenuation. There are significant amplitude differences from the non-attenuating model. The time synthesis was obtained by a convolution of a pulse with the crustal transfer function calculated using Haskell-Thomson matrix formulation. The source pulse is a sine function which has a decaying envelope in time and the frequency of the pulse is centered at 10 Hz. More detailed calculations of theoretical seismograms will be discussed in another chapter. What is clear from Figure 2b is that the amplitudes of different phases are decreased with respect to the non-attenuating model.

However, the relative amplitude decrease among phases is nearly constant. This makes determination of a Q factor, by making use of the amplitude ratio of two or more phases in time domain using experimental seismograms, very difficult. When very low values of Q are used, the shift of many phases is about 0.3 sec in the time domain. This is because large phase shifts are introduced in the frequency domain when Q values are small. Large phase variation due to severe attenuation might make Fourier inversion unsuccessful when time synthesis of a model is required.

When determination of attenuation is desired for a crustal structure using transfer ratios, exact amplitude correlation between observed and theoretical responses is necessary. This requires a well calibrated recording system. On the other hand, for a given crustal structure, if there is a sedimentary low velocity layer, velocity and thickness for the layer must be known accurately and velocity contrast between layers has to be reasonably known in order to interpret large amplitude variation in the transfer ratios. Nevertheless, modelling of large amplitude variations as in Figure 1 for the case of  $Q = 50$ , by using velocity contrast or various Poisson's ratio is difficult since

these quantities generally have an upper and lower limit for a realistic Earth's crust. On the other hand, due to finite experimental data, a calculated spectra using real data is convolved by a kind of window. Generally, this window is not a simple one in order to increase reliability of the calculated spectrum. For a better comparison of theoretical and experimental spectrum amplitudes, similar windows must be applied to both spectra since the window is a significant factor for amplitudes as well. A spectral window less than 50 seconds, eliminates completely large spikes as in the case of  $Q = 50$  in Figure 1 and makes the transfer ratios indistinguishable for various  $Q$  values. However, for spectral windows of more than 50 sec length, spectral amplitudes are independent of window length and only in these cases more convincing comparisons of amplitudes between theoretical and experimental spectral ratios are possible.

Another significant factor affecting the amplitudes of experimental spectral ratios is additional phases such as near source or core reflections. These additional phases create multiple pulse problem in a combined layered response. Even when these additional phases arrive with same velocity, spectral ratio amplitudes are found to increase significantly. If deep earthquakes are used for the study of attenuation, then additional phases can be neglected in the analysis since these

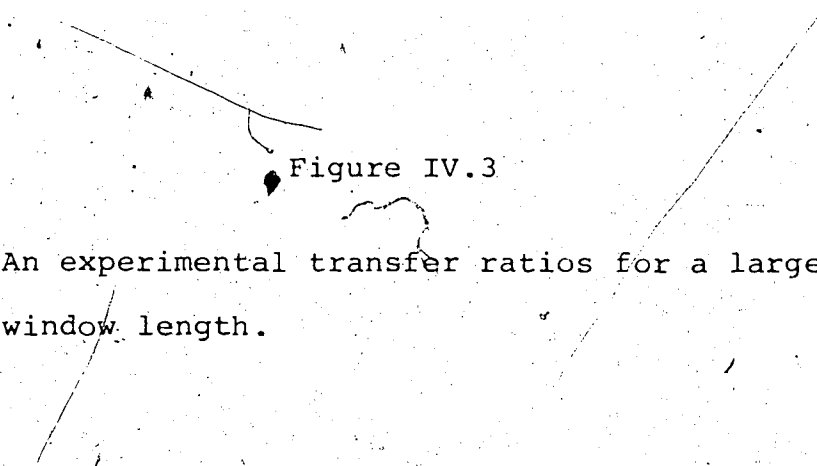
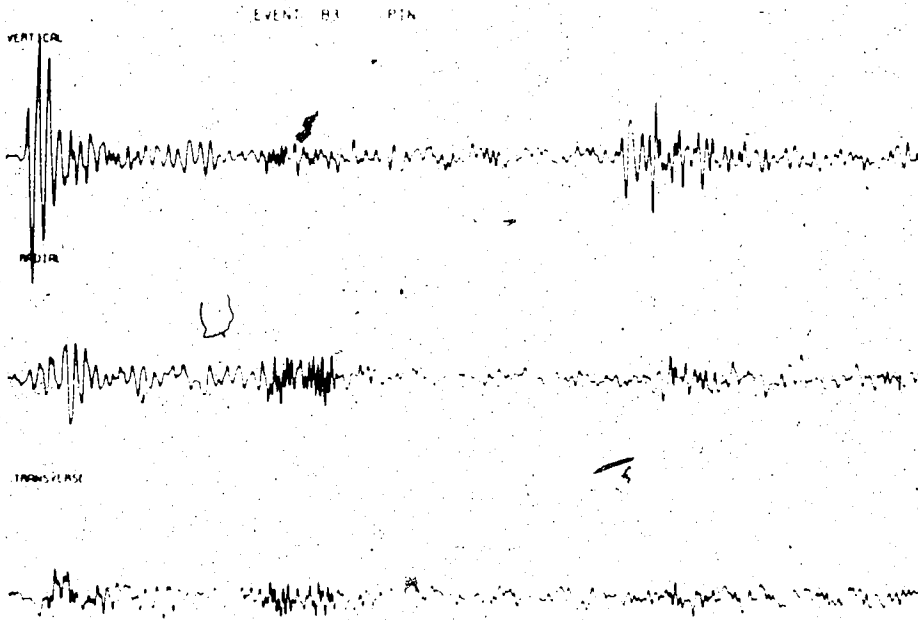
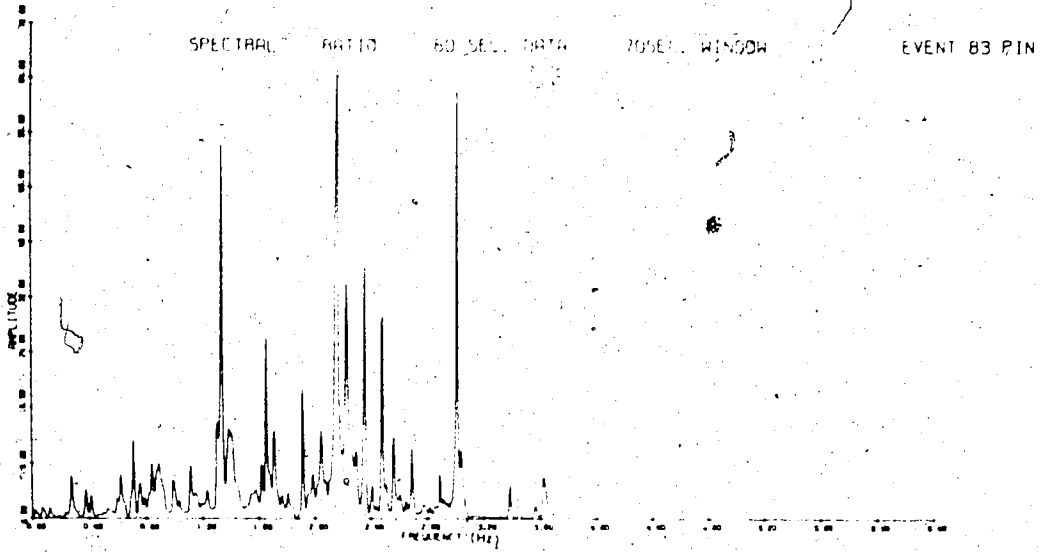


Figure IV.3

An experimental transfer ratios for a large window length.



phases arrive out of the window length for earthquakes which occurred at far distances and large depth. Effect of additional phases and earthquake magnitude on the amplitude of spectral ratios will be discussed extensively in another section of this thesis. During the spectral analysis of 1970 earthquake data recorded by the VASA stations in central Alberta, an attempt was made to determine attenuation. Several earthquakes had no additional phases incident within 50-70 seconds of time. One of the results recorded at Pine Lake is shown in Figure 3. This seismogram has no predicted additional phases up to 102 seconds when the pP reflection arrives. The core reflections are incident at the same time as the main pP arrival but this has no effect on spectral ratios (this will be shown in another section). Spectra of vertical and radial motion have been calculated by inversion of the smoothed auto-correlation function. Smoothing has been achieved by a 70 second Parzen window. The earthquake was located at  $77.6^\circ$  distance away and the predicted angle of incidence at the bottom of crust is about  $25-30^\circ$ , corresponding to a phase velocity about 19.25 to 16.16 km/sec. This spectral ratio was comparable to the theoretical one for a model shown in Figure 2a. Distinct features of the model for different attenuations are almost kept

unchanged. If we study the experimental ratios shown in Figure 3, there are no features resembling the model with  $Q=50$  but agree fairly well with the one with  $Q \geq 500$ . For this interpretation, assumption of constant phase velocity and the well known velocity variation with depth as shown in the model is necessary.

Spectral ratio models do not discriminate against various attenuating models for a source distance less than  $16^\circ$ . However, differences between non-attenuating and severely attenuating models are still significant for small angles of incidence.

From the study of peak positions in experimental and theoretical spectral ratios, it is clear that there are significant differences. Perhaps it would be possible to say more about attenuation when a better fitting model is found at higher frequencies and if gains of recording instrument and other information are available, absolute match of amplitudes may be attempted.

#### 4. Discussions and conclusions

From the review of published research, a number of conclusions can be reached. Laboratory measurement of attenuation cannot be accepted as a representative value for the real Earth. The consensus of opinion is that



for high frequencies, attenuation factor is linear. However, nonlinear attenuation exists around zero frequency and the exact cutoff frequency is not certain. Unfortunately the range of our seismic spectrum lies in this nonlinear region and there is a larger scatter of data in this band of the spectrum. Mechanism of loss in solid materials and the Earth is still an unresolved problem. Today one of the two principal theories proposed to explain anelasticity is solid friction, where  $Q$  and phase velocities are not a function of frequency (Knopoff, 1956), the other is causal dispersive attenuation (Futterman, 1962). There are a large number of experimental data supporting non-dispersive attenuation in solids. However, Wuenschel (1965) showed that very small dispersion can significantly affect attenuation characteristics. Both theories have a model for the nonlinear attenuation region, but no firm experimental evidence exists to support any of these.

The nature of the loss mechanism in the real Earth can be divided in two parts:

- a) Losses due to rock formations in natural states.
- b) Losses due to other causes.

In this classification, part b) covers a wide range of causes such as reflection, transmission, scattering,

etc. In general, this is a representation of the real Earth in terms of wave propagation. Part a) represents attenuation, for which measurements have been attempted, that is stress relaxation due to the atomic or macroscopic structure of rocks. In an experimental attempt on the real Earth, these two causes generally are inseparable. For a correct measurement of the Q factor, the Earth has to be modelled to a sufficient degree of approximation. Channel waves and head waves, due to their propagation patterns, are sensitive to the lateral inhomogeneities in the Earth. Attenuation measurements using these waves, generally, show large variations even for the mantle region of the Earth.

Q values increase with increasing pressure and temperature but after a certain temperature, thermo-friction becomes important (Knopoff, 1971). It is most likely that the attenuation mechanism becomes more complex in the deeper part of the crust.

A solid friction loss mechanism predicts a lower Q values for S waves. This is due to the argument that permanent creep is almost never observed in a deformation experiment in which the sample is compressed hydrostatically but not fractured (Knopoff, 1971). This argument is against the other theories of loss mechanism (Walsh, 1969). There are a large number

measurements which showed larger  $Q_S$  than  $Q_P$  (White, 1965). On the other hand, from surface wave study, Anderson et al. (1965) observed that  $Q$  values for P waves are 2.4 and 2.6 times larger than  $Q$  values for S waves.

In view of the experimental data mentioned in section 2, it will be fair to assume  $Q_P = 200-250$  for a 2 km thick sedimentary layer composed of a series of shale, sandstone, dolomite, limestone, etc. and  $Q_P = 1000-1500$  for a granite basement and lower crust in Alberta. During the analysis of 1970 earthquake data recorded by the VASA stations, experimental spectral ratios have been compared with various dissipative theoretical transfer ratios. This comparison suggests an average value of  $Q_P \geq 500$ . However, the results are not conclusive due to an insufficient amount of reliable data. More reliable  $Q$  values as a function of depth cannot be determined at this time, using the spectral ratio method.

91

V. Crustal Structure in Central Alberta  
from the Spectral Ratio Method

1. Experimental data

In this thesis, an attempt is made to resolve crustal structure in Alberta using about 50 earthquakes recorded by various seismic stations (Figure 1). The data were recorded on a magnetic tape digitally with a sampling rate of 12.5 samples per second. Spectra were calculated using the method mentioned in section I. Experimental spectra have been compared with the two dimensional theoretical ones. Azimuthal deviations have been measured at every station to determine the effect of wave scattering in a three dimensional case. Station residuals have been used in the interpretation of spectral ratios.

2. EDM station

Event 73 recorded in 1970 has no additional phases predicted within the window length. This event has a prominent peak at 0.1 Hz (Figure 2). Other events have a peak at about the same frequency but small differences in peak position exist. Events 71, 92, 93 showed anomalous shifts in peak position at lower frequencies indicating a thicker crust. However,

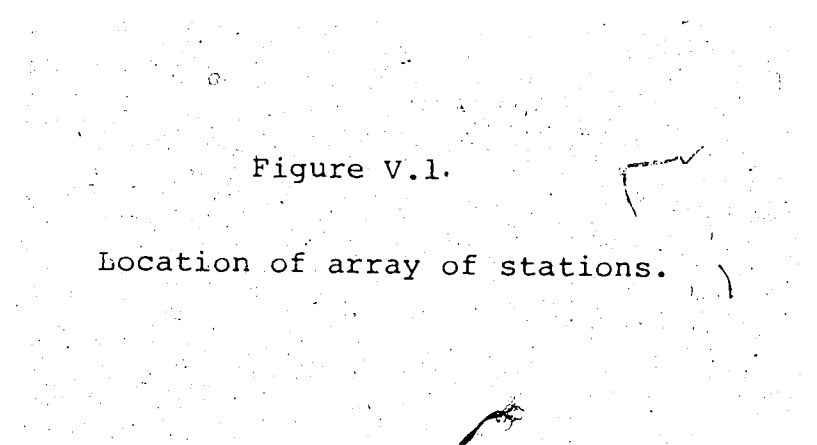


Figure V.1.

Location of array of stations.

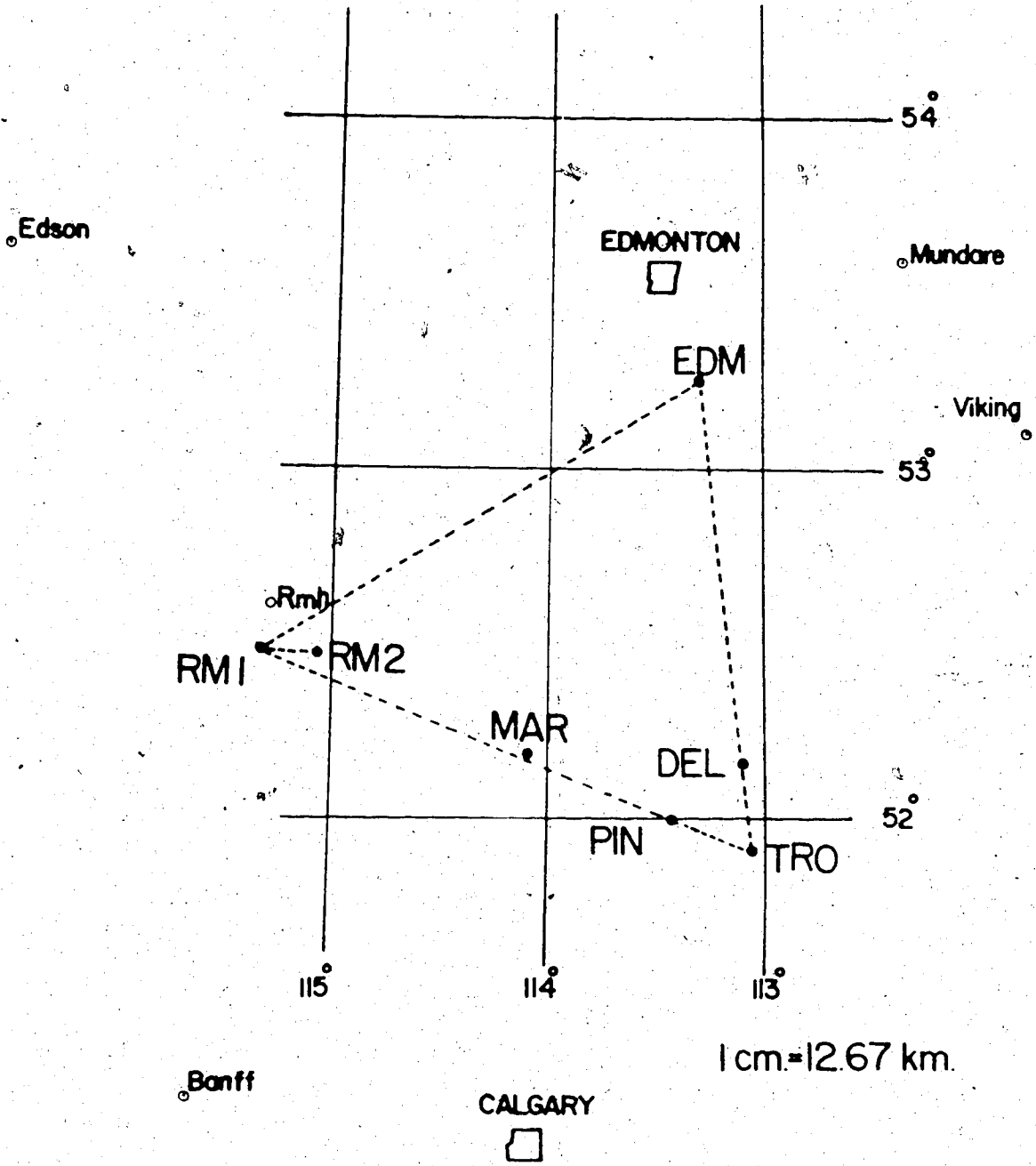


Table I

EDM (53°13'.37, -113°20'.9) h = 0.730 km

Event	Location		Date (1970)	Time		Depth (km)	M	Δ°	Azm. (deg)	Im (deg)	pP-P (sec)	PcP-P (sec)	PP-P (sec)	
	Lat.	Long.		h	s									
71	51.4	-178.5	18.7	1	48	38.9	46	5.7	38.7	294.44	26.3	12.8	127	91
73	6.8	-73.0	20.7	17	44	57.6	163	5.0	56.7	129.71	32.1	38.6	54	132
84	32.2	131.7	25.7	22	41	10.7	34	6.1	78.0	308.19	22.4	10.2	10	178
86	32.2	131.8	26.7	7	10	36.0	35	6.1	77.9	308.12	22.4	10.4	11	179
92	26.0	95.4	29.7	10	16	19.3	59	6.5	97.3	334.13	19.1	17.2	1	237
93	37.8	55.9	30.7	0	52	19.5	19	5.7	88.9	8.50	19.0	5.8	6	207
112	-7.9	158.7	3.8	7	01	11.9	67	5.9	95.0	263.64	19.6	19.1	1	232

PIA (52°0'.36, -113°27'.0) h = 0.952 km

48	18.0	-64.6	8.7	4	49	10.6	150	5.8	51.1	112.88	32.1	34.0	135	121
53	43.8	148.4	9.7	12	11	58.9	48	5.5	61.4	305.27	28.5	13.3	41	139
68	-1.8	-77.3	17.7	17	49	59.5	182	4.9	61.7	137.95	28.4	42.5	42	141
71	51.4	-178.5	18.7	1	48	38.9	46	5.7	39.1	295.76	36.3	12.8	127	90
73	6.8	-73.0	20.7	17	44	57.6	163	5.0	56.0	128.98	30.4	37.6	59	135
74	36.5	70.5	21.7	1	18	5.2	210	5.2	91.8	355.34	19.6	52.0	-	104
83	28.9	139.0	25.7	11	4	43.7	462	4.9	77.6	301.14	23.6	101.7	-	180
92	26.0	95.4	29.7	10	16	19.3	59	6.5	98.3	333.97	19.1	17.2	7	243
106	46.7	152.5	2.8	1	36	10.6	60	5.0	57.3	304.06	29.9	15.8	56	130

Table I (cont'd)

RM1 (52° 29'.47, -115° 24'.3) h = 1.076 km

Event	Location Lat. Long.	Date (1970)	Time h m s	Depth (km)	M	$\Delta^\circ$	Azm. (deg)	Im (deg)	PP-P (sec)	PcP-P (sec)	PP-P (sec)
5	63.4 146.2	5.6	10 31 54.6	33	5.5	48.2	323.32	33.1	10.0	88	110
7	52.2 159.6	10.6	22 40 23.1	33	5.5	49.0	305.63	32.9	10.0	85	114
10	44.9 149.5	10.6	16 17 48.7	57	5.7	58.8	304.14	29.4	15.3	48	132
11	24.5 -68.5	11.6	6 2 54.9	112	6.3	86.9	138.22	20.4	29.4	1	206
13	56.6 -152.1	12.6	4 54 31.4	33	5.2	21.5	295.63	-	9.0	243	24
17	-19.4 -69.2	14.6	9 38 2.1	125	5.0	82.0	136.53	21.3	32.7	6*	198
36	53.4 160.4	28.6	11 1 53.5	23	5.8	47.9	306.56	33.2	7.6	78	101

RM2 (52° 26'.78, -115° 17'.44) h = 1.045 km

51	43.9 148.4	9.7	8 11 9.7	51	5.4	60.2	304.06	29.0	14.0	46	135
52	43.9 148.4	9.7	11 24 39.5	41	5.4	60.1	304.00	29.0	11.8	46	135
53	43.8 148.4	9.7	12 12 58.9	48	5.5	60.2	303.98	29.0	13.2	46	135
71	51.4 -178.5	18.7	1 48 38.9	46	5.7	37.9	294.41	36.7	16.6	144	103
73	6.8 -73.0	20.7	17 44 57.6	163	5.0	57.1	127.29	30.5	38.3	53	129
84	32.2 131.7	25.7	22 41 10.6	34	6.1	77.5	306.94	22.2	10.2	14	179
86	32.2 131.8	26.7	7 10 36.0	35	6.1	77.5	306.86	22.2	10.4	14	179
88	-21.7 -174.6	28.7	4 47 47.7	33	5.2	90.0	233.10	19.8	10.4	2	216
92	26.0 95.4	29.7	10 16 19.3	59	6.5	97.4	332.41	19.1	17.2	12	260
93	37.8 55.9	30.7	0 52 19.5	19	5.7	89.8	6.97	19.9	6.3	1	215



Table I (cont'd)

DEL (52° 9' .49, -113° 3' .31) h = 0.831 km

Event	Location		Date (1970)	Time		Depth (km)	M.	Δ°	Azm. (deg)	Im (deg)	pP-P (sec)	PcP-P (sec)	PP-P (sec)
	Lat.	Long.		h	m								
54	61.5	-146.5	10.7	9	16	44.2	35	20.3	310.46	-	9.30	251	18
72	-3.8	158.4	19.7	9	22	40.1	20	95.7	271.20	20.0	6.65	1	237
73	6.8	-73.0	20.7	17	44	57.6	103	55.9	129.40	30.0	38.6	58	131
86	32.2	131.8	26.7	7	10	36.0	35	78.7	308.45	21.8	10.4	8	181

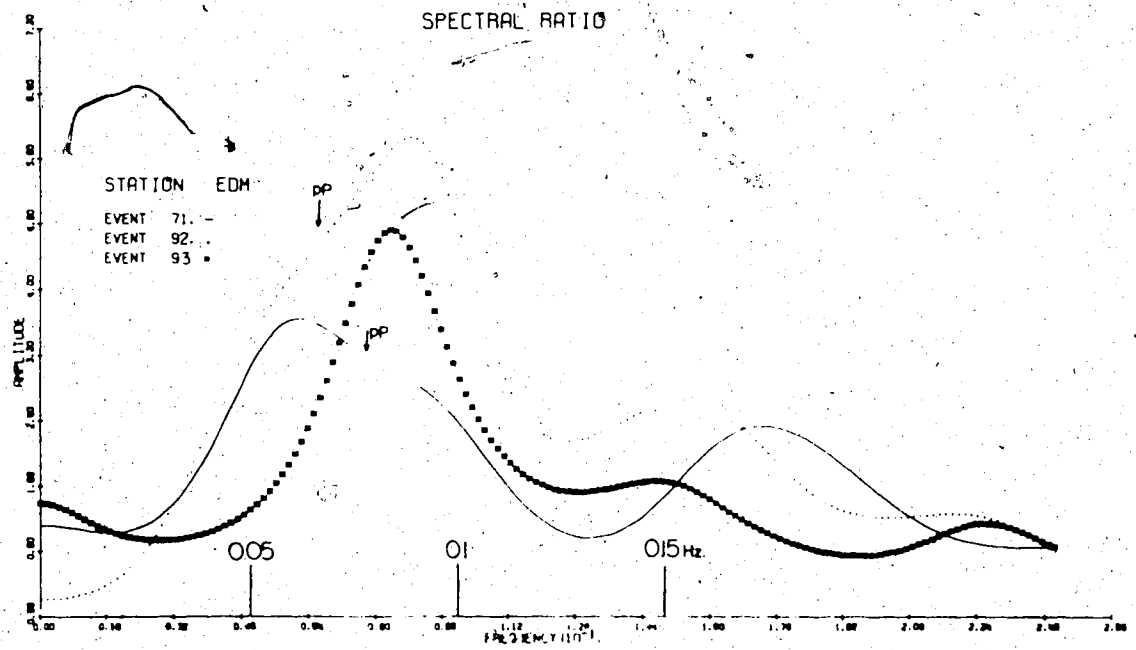
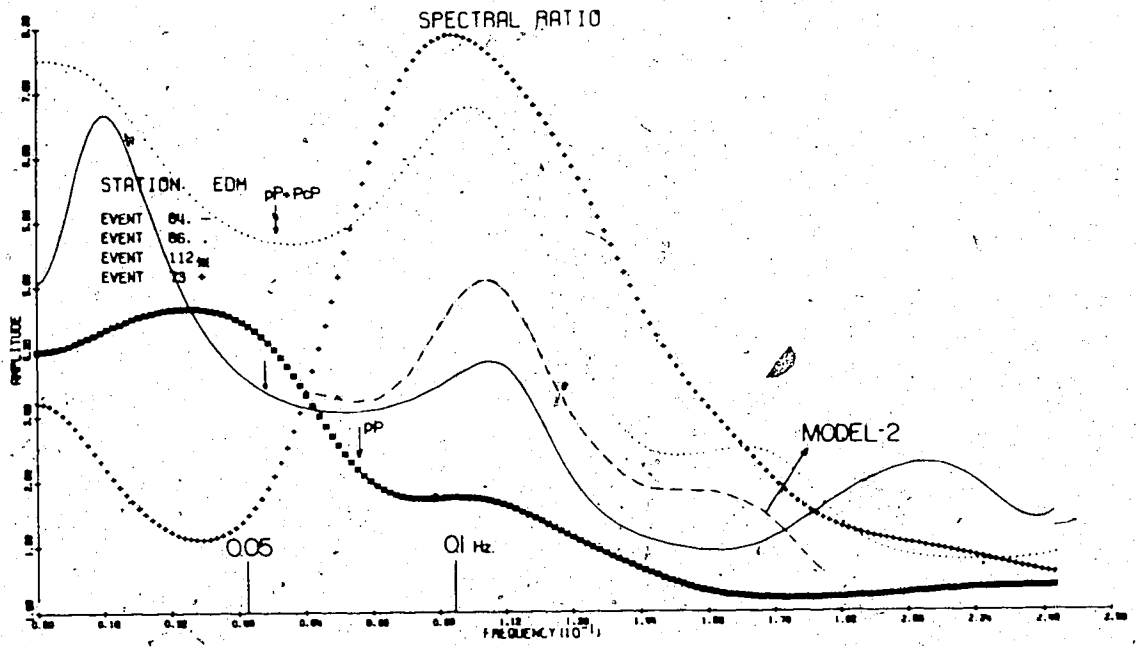
TRO (51° 53' .77, -113° 3' .37) h = 0.831 km

19	24.8	121.8	19.6	12	44	6.2	84	89.8	312.0	19.9	23.1	2	261
20	15.4	-45.9	19.6	14	25	18.4	33	64.0	98.34	27.5	10.0		
21	-26.6	-114.4	20.6	11	40	39.2	33	78.1	181.23	22.4	10.0	10	178
29	-7.9	158.7	25.6	5	13	58.6	69	95.1	263.75	19.6	19.6	~0	231
45	-7.7	-74.3	7.7	6	3	45.6	140	68.0	138.0	25.8	34.7	17	154
48	18.0	-64.6	8.7	4	49	10.6	150	50.8	113.18	32.0	34.0	135	121
55	17.5	-101.0	10.7	13	14	50.9	46	35.6	159.99	38.0	12.8	208	137
56	28.7	129.3	10.7	16	16	57.3	63	83.0	308.36	20.9	17.3	63	193
59	60.4	-152.0	13.7	16	0	41.4	104	23.0	306.96	-	22.4	229	34
64	-19.2	-173.5	16.7	21	17	44.2	33	88.1	235.34	20.2	10.0	54	209
67	51.0	-171.3	17.7	7	32	10.1	33	35.5	292.2	38.0	10.0	149	80
68	-1.8	-77.3	17.7	17	49	59.5	182	61.4	138.32	28.5	40.5	41	140
71	51.4	-178.5	18.7	1	48	38.9	46	39.4	296.06	36.2	12.8	128	95
76	-15.9	-173.1	21.7	6	21	33.5	33	85.2	236.79	20.7	10.0	4	202
83	28.9	139.0	25.7	11	4	43.7	462	77.9	301.44	22.4	101.7	-	185
84	32.2	131.7	25.7	22	41	10.7	34	78.9	308.61	21.9	10.2	9	181

Figure V.2

Long period spectral ratios for EDM station.

Frequency of expected holes in the spectral ratios has been indicated by the arrows.



all these events suffer distortion due to additional phases such as pP and PcP. These additional phases produce holes in the spectra, which distort the ratios, but the large observed frequency shift of 10 mHz cannot be attributable only to the additional phases.

Short periods of spectra were found to be more sensitive to the noise. By noise we mean signal generated noise such as anomalous conversions in crustal layers or surface wave type noise. A large peak at about 0.5 Hz was very well duplicated on all events (Figure 3). A second peak at 1.60 Hz was also well established but it has a lower amplitude. A third peak at about 2.5 Hz was not seen from all the events. However, according to event 73, it must certainly exist. Averages of all spectra were used to display in Figure 3 the most probable peaks and their positions.

In Alberta a large number of crustal investigations have been carried out in the past. However, most of these studies have been done in the southern part of the province. In earlier spectral ratio studies (Alpaslan, 1968; Sprende, 1972), a southern Alberta crustal model (ALTACRT-2) has been used as a starting model. This model did not fit the observational spectral ratios as shown in section III. A reflection study (Ganley and Cumming, 1974) near EDM has brought some clarification to the crustal structure in this

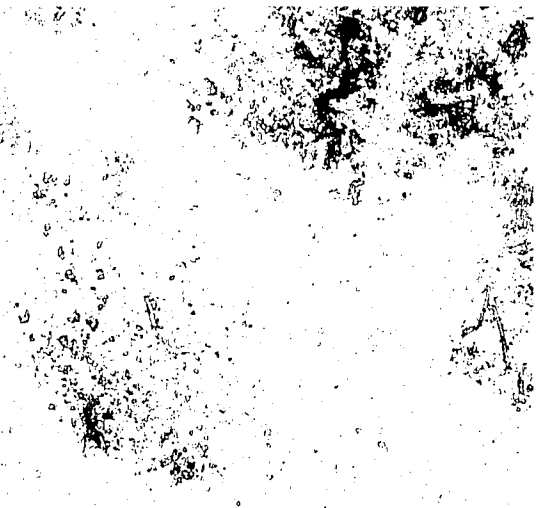

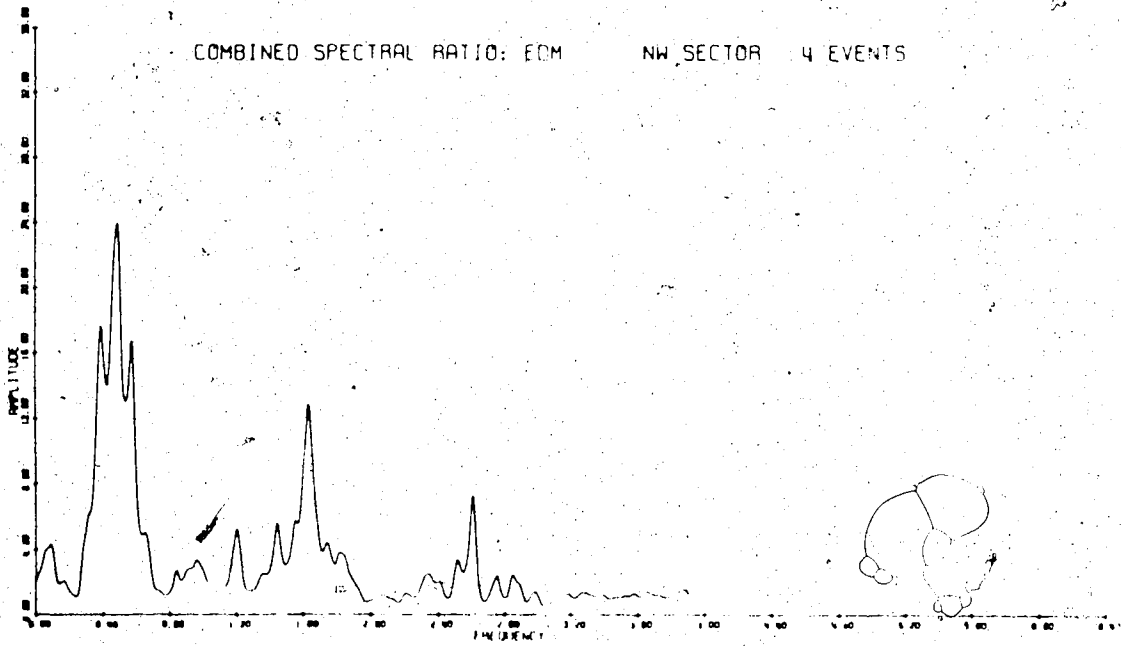
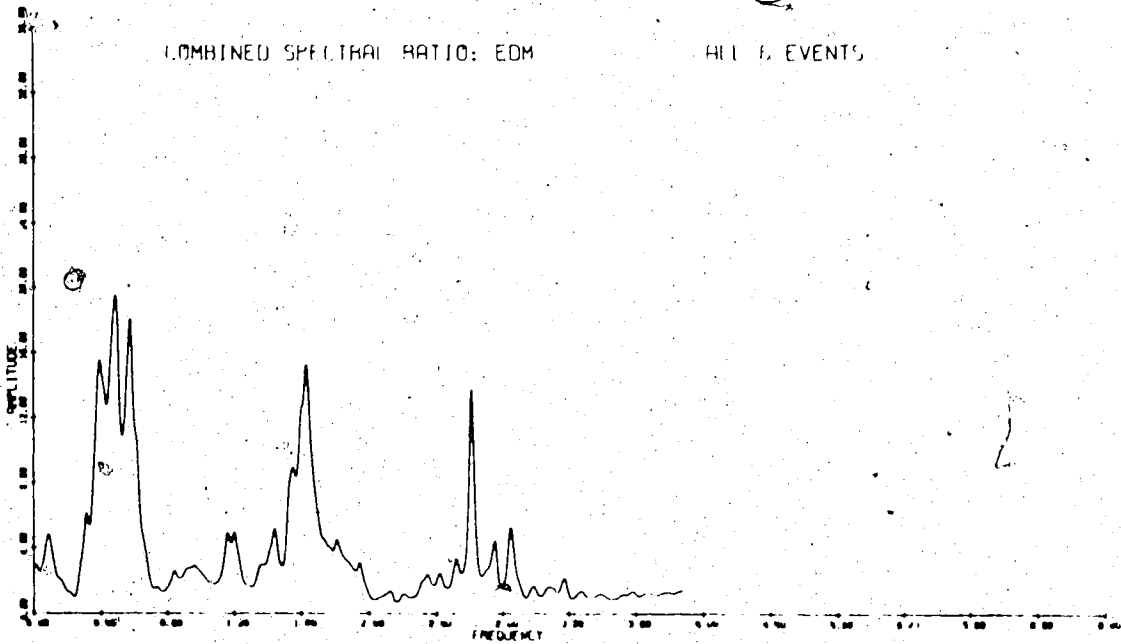


Figure V.3

Short period combined spectral ratios for EDM station.





region. Although this work is not complete, clear reflections have been identified at 3.5, 7.5 and 10.7 seconds. According to this work a model has been constructed for this area (Table II) which has a total thickness of 36 km. A low velocity layer of 2.3 km has also been included. In Figure 4, possible models have been displayed. A low velocity layer did not have a pronounced effect in this band of spectrum. Removal of the sedimentary section does not influence peak position but significantly affects the shape of the spectrum. By removing a 4 km thick intermediate layer (model 3), the peak position is displaced by about 4 mHz towards the lower frequencies. This is an expected phenomenon because the high velocity layer is displaced by a lower velocity layer which decreases the travel time. In this frequency band, layers with velocities of 6.4 and 6.5 km/sec are not distinguishable. In Figure 2, the experimental spectral ratios were compared with model 2. It is clear that the peak of event 73 has been slightly displaced to the lower frequencies. If we keep the crustal thickness constant at 36 km the experimental spectrum favors a simple layered crustal model.

Then, is there really an intermediate layer with a high velocity? Same model can be produced if we have thinner crust with a low velocity or thicker crust with

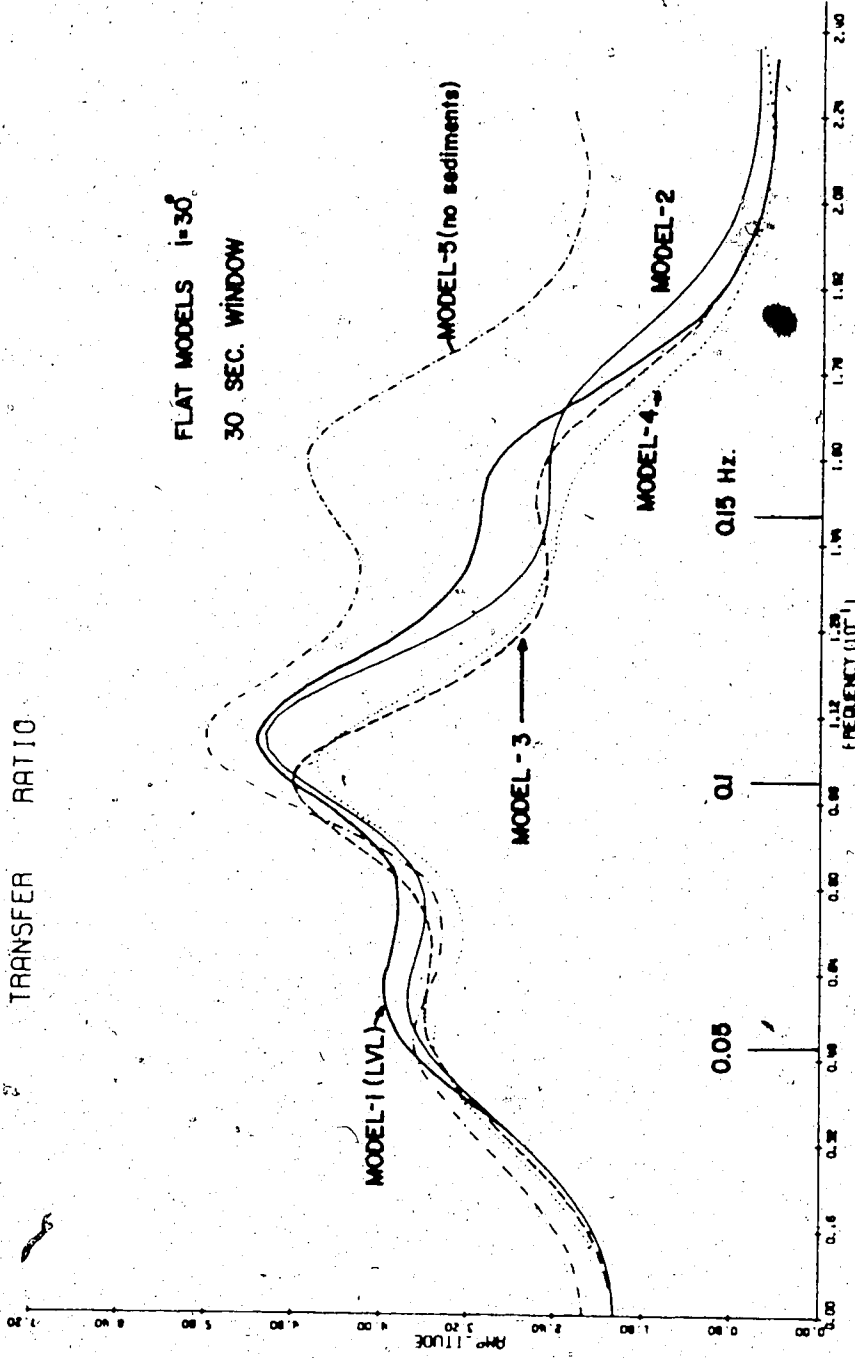
Table II

h (km)	Model 1			Model 2	Model 3	Model 4	Model 5	Dipping model
	V <sub>p</sub>	V <sub>s</sub>	ρ	h (km)	h (km)	h (km)	h (km)	Dip
1.32	2.68	1.43	2.2	1.32	1.32	1.32	-	0.0
1.31	4.81	2.88	2.6	1.32	1.31	1.32	-	-0.5
16.07	6.4	3.70	2.67	18.37	18.37	-	-	-0.5
2.30	5.7	3.30	2.65	-	-	-	-	+15.0
11.00	6.5	3.73	2.85	11.00	-	33.37	36.0	+15.0
4.00	7.2	4.17	3.15	4.0	15.00	-	-	-2.0
-	8.1	4.68	3.40	-	-	-	-	-2.0



Figure V.4

Long period spectral ratios from models given in  
Table II.

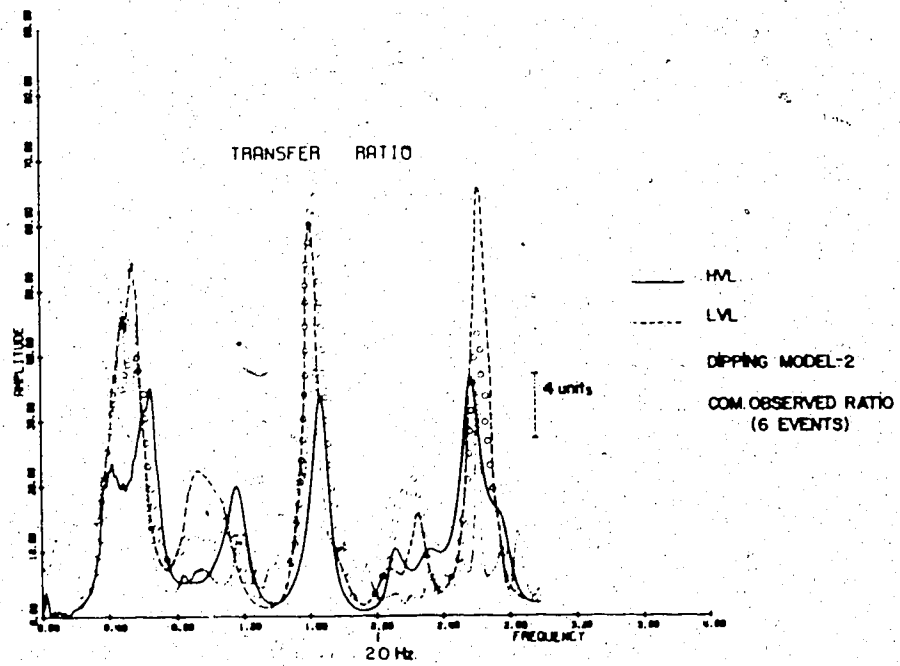
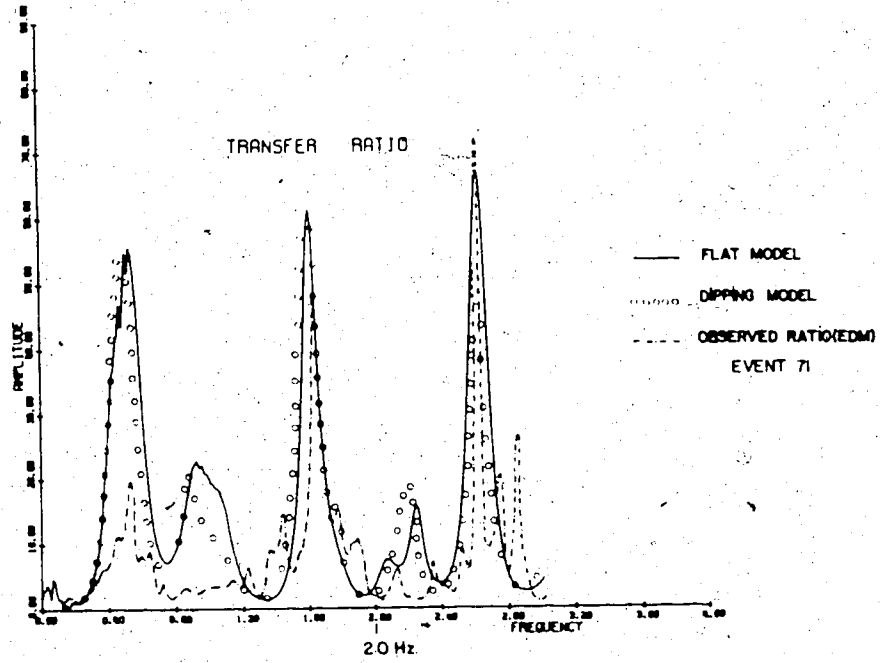


a high velocity as in Figure 7. Residuals at this station show an early arrival at all quadrants. Therefore, a thicker crust with a high velocity zone is possible but the amount of the residuals does not suggest any large changes in thickness-velocity relations.

The sedimentary layers of the model control the shape of the spectrum at higher frequencies. The deeper layers of the model have an influence on the amplitude of the spectral ratios. A two layer sedimentary structure has been found to be satisfactory to produce the basic pattern of interference which is observed (Figure 5). In this figure, event 71 has a peak of very large amplitude at about 2.5 Hz. This is due to the presence of additional phases. Dipping models produce no significant shift in peak position with respect to the flat model but only the amplitude of the peaks changes. A very thin low velocity layer does not have significant effect on the spectral ratio at this frequency. Therefore, this band of the spectrum is not sufficient to resolve a thin LVL as suggested by Somerville and Ellis (1972). This conclusion perhaps is not surprising that a thin layer like this LVL can be resolved for wavelengths less than layer thickness, that is a frequency band larger than 2.5 Hz should be used. Small peaks in Figure 5 do not compare with the

Figure V.5

Comparison of experimental spectral ratios with the theoretical models. At the bottom diagram all models represent a dipping crustal model. Models with a thin LVL and HVL have been shown for comparison.



model as well as large peaks; a better sedimentary model can be found when larger amount of reliable spectra are available. In many ways amplitudes of the peaks can yield more information, but for this kind of comparison all information regarding instrumentation must be known. Inexact gains of experimental spectrum component have made amplitude comparison doubtful. Record character for this station was poor (Figure 6) in the sense that additional phases change the appearance of record as well as the frequency content of it. Arrivals with a larger amplitude than main P arrival is a general character of the records. As can be seen, large transverse motion for all events is a common factor. This suggests that a two dimensional model is too simple for this area.

If the crust were a homogeneous media transverse motion would be zero. However, inhomogeneities will produce transversely polarized shear (SH) motion which should have a minimum in same direction. Starting from this assumption horizontal energy ratios were calculated (Kurita, 1972):

$$\theta_E = \frac{\int_{\omega_1}^{\omega_2} |E_T(\omega)|^2}{\int_{\omega_1}^{\omega_2} \{ |E_R(\omega)|^2 + |E_T(\omega)|^2 \}} \quad (1)$$

Figure V.6

A few examples of records for EDM station.

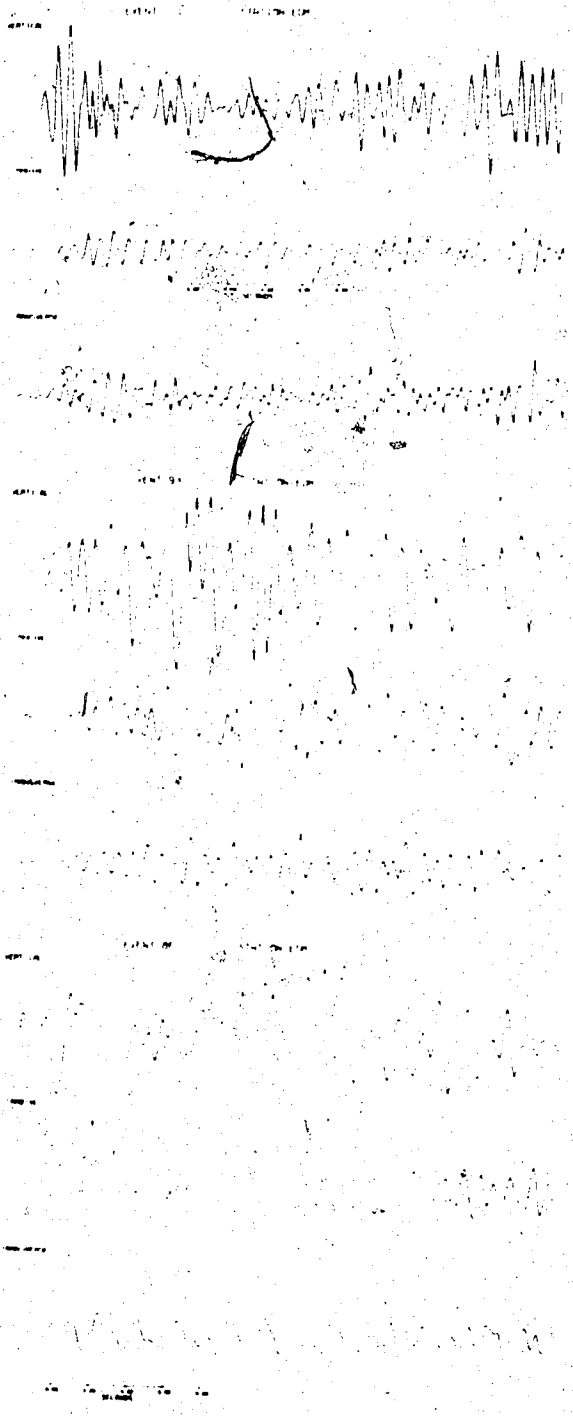
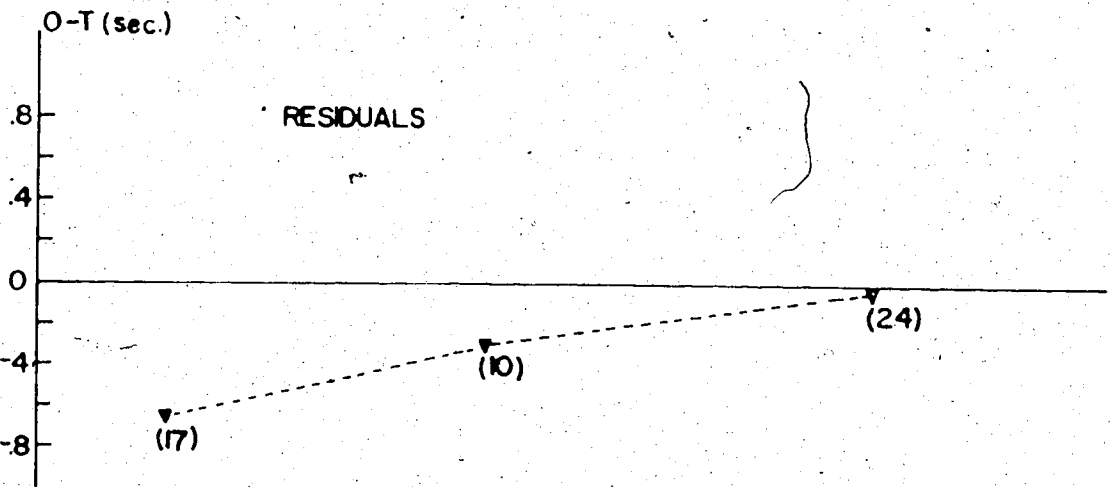
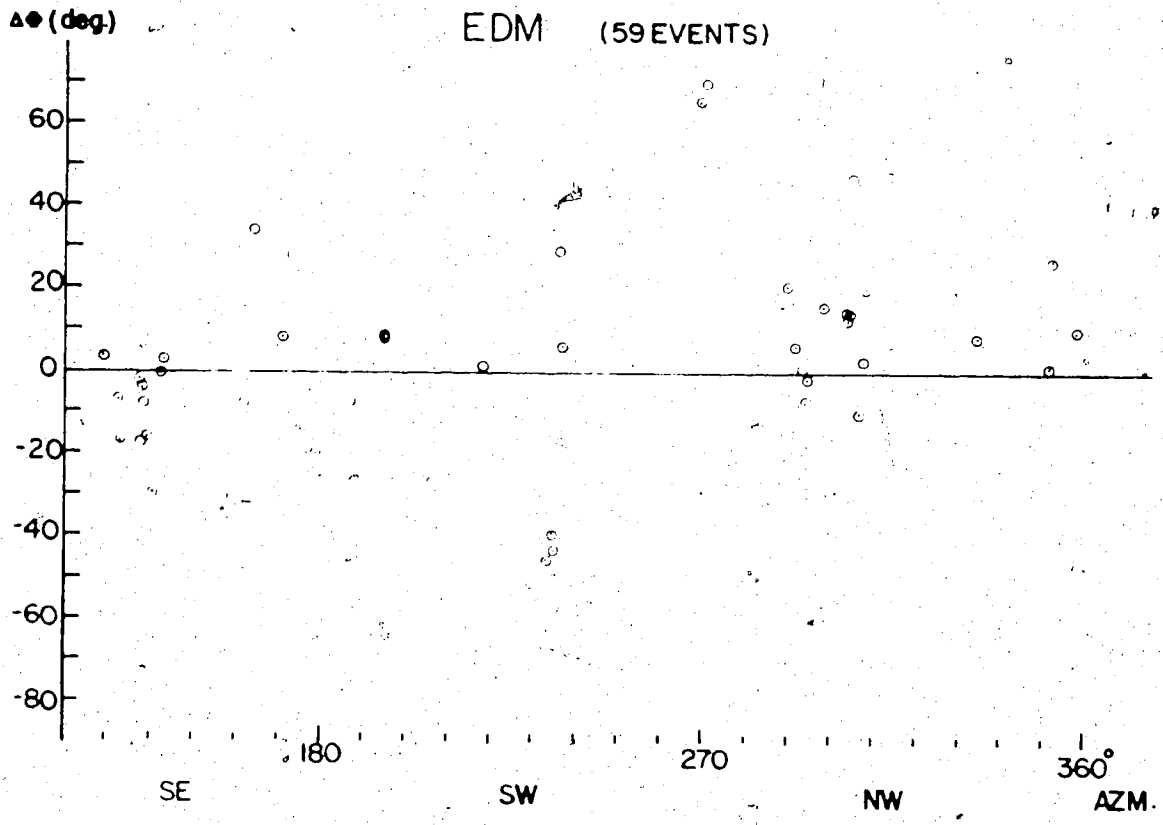




Figure V.7

A graph of azimuthal deviation versus azimuth and station residuals. For this diagram all available events were used. For residuals J-B tables were used.



where  $E_R$  and  $E_T$  are the radial and transverse amplitude spectra respectively. Using the known station-source azimuth as a starting angle, data were rotated to obtain the minimum  $\theta_E$  value which can be considered as a true wave approach. The sum in equation (1) was performed from 0 Hz to 4 Hz to obtain the minimum energy for the transverse component. The azimuthal deviation was measured for all available earthquake data. As seen in Figure 7, a large amount of variation exists. However, one should remember that this method includes possible ~~misplacement~~ misplacement of seismometers and mislocation of the epicentre. Therefore, the pattern of azimuthal deviation is more important than the magnitude.

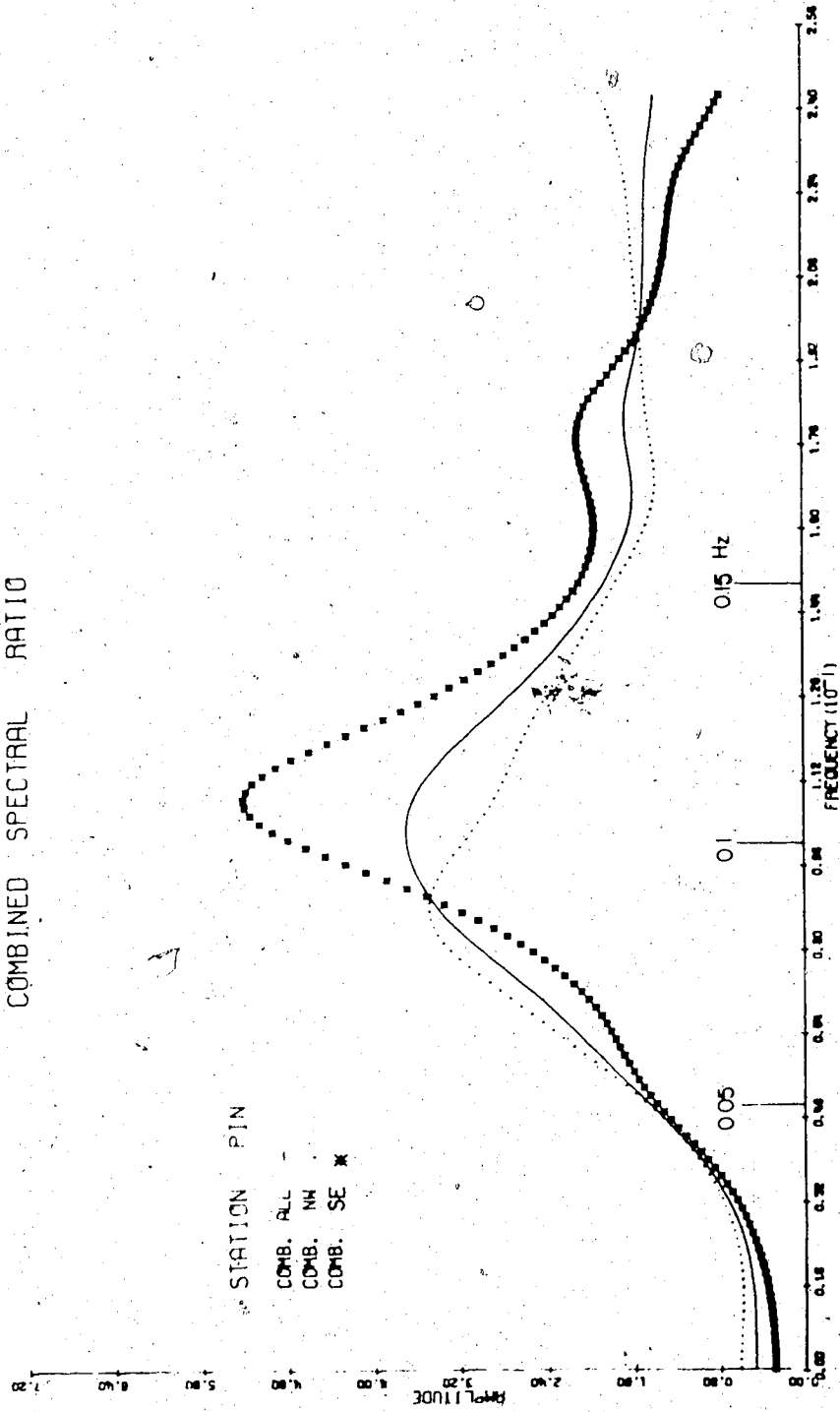
### 3. / PIN station

For this station, data free from predicted additional phases were found only for the SE sector. Events 48 and 68 yield a peak at about the same frequencies but 10 mHz difference exists in peak position. Event 73 has very low amplitude and did not produce a peak as other events. These differences cannot be explained using the theory discussed in this thesis. However, event 48 has a maximum amplitude and when combined spectra are joined (Figure 8), SE group produced a peak which has the same location and shape as in EDM station. Model 2 of EDM produces a

Figure V.8

Combined long period spectral ratios for PIN station. Event 83 has no resolution at low frequencies due to lower magnitude, therefore not included in the averages.

COMBINED SPECTRAL RATIO



very good fit to the observed combined spectra (Figure 8). Events belonging to the NW sector produced very poor results, the shape of spectra being distorted and shifted to lower frequencies. All events for the NW sector contain additional phases (Figure 8) and no dependable event has been found.

The short period band of the spectrum (Figure 9) has been found to be unstable. Peaks in the spectrum have shown variations from spectra to spectra. Peak at about 0.8 Hz has fairly well been produced by different events and the double peak at about 1.5 Hz is also a common feature of the spectrum. Comparison with EDM short period data shows that at this station the sedimentary layer is much thicker and this layer is much more complex due to a factor affecting the long period of the spectrum. Close peak position of the experimental spectrum suggests a thicker sedimentary layer. However, modelling of this spectrum using the theory mentioned in this thesis is difficult. Plane layering is the most likely one of the assumptions which has been violated. Rapid variation in the top 10-15 km region of the crustal sequence is apparent in all azimuths. Events from the SE sectors have relatively early arrival times and large azimuthal deviations for this quadrant (Figure 10). The anomalous variation of

Figure V.9

A few short period spectral ratios for PIN station and comparison with same models.

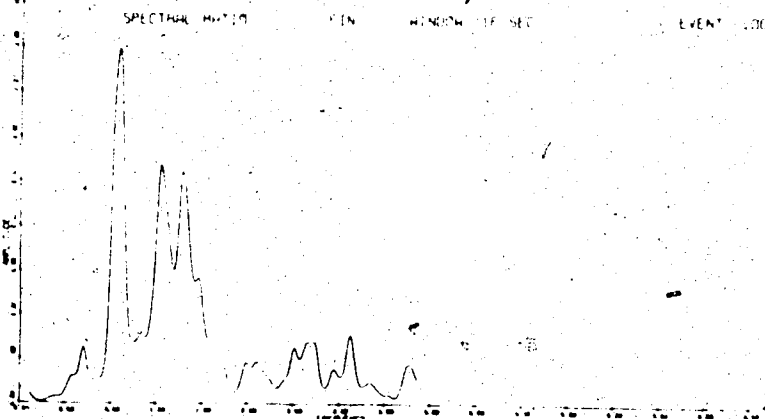
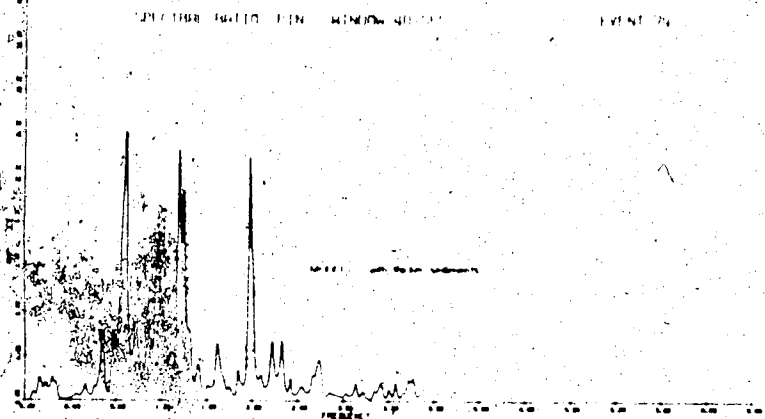
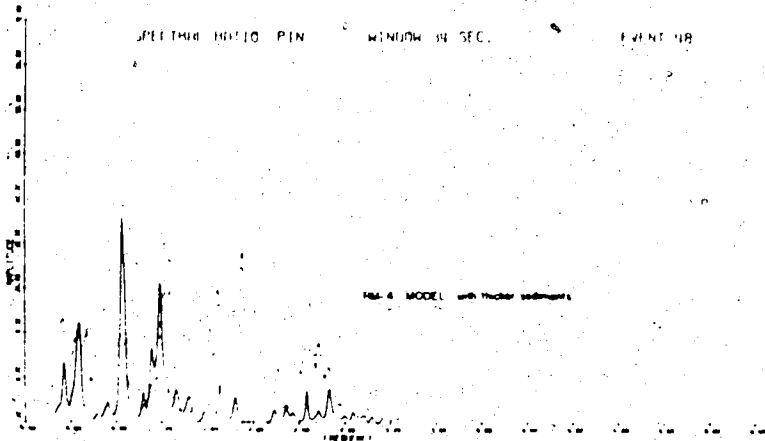
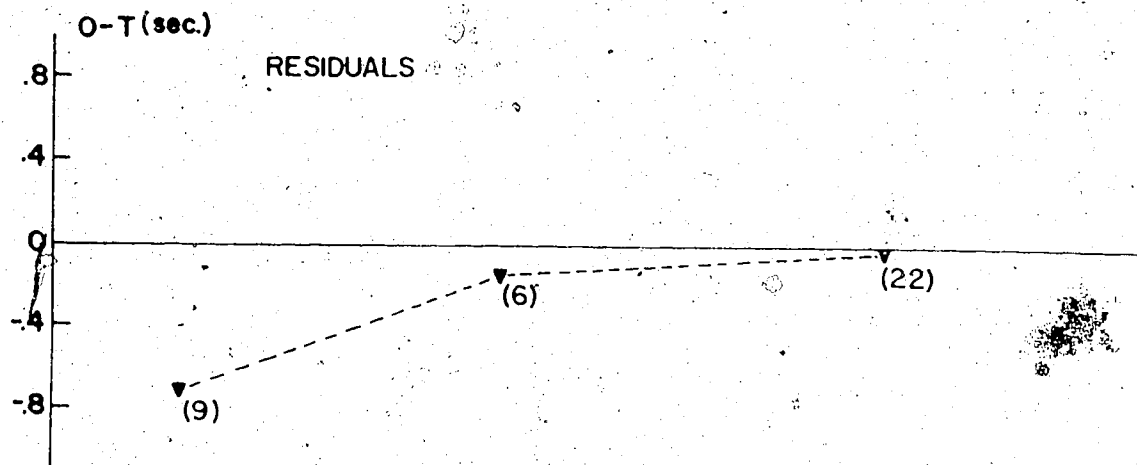
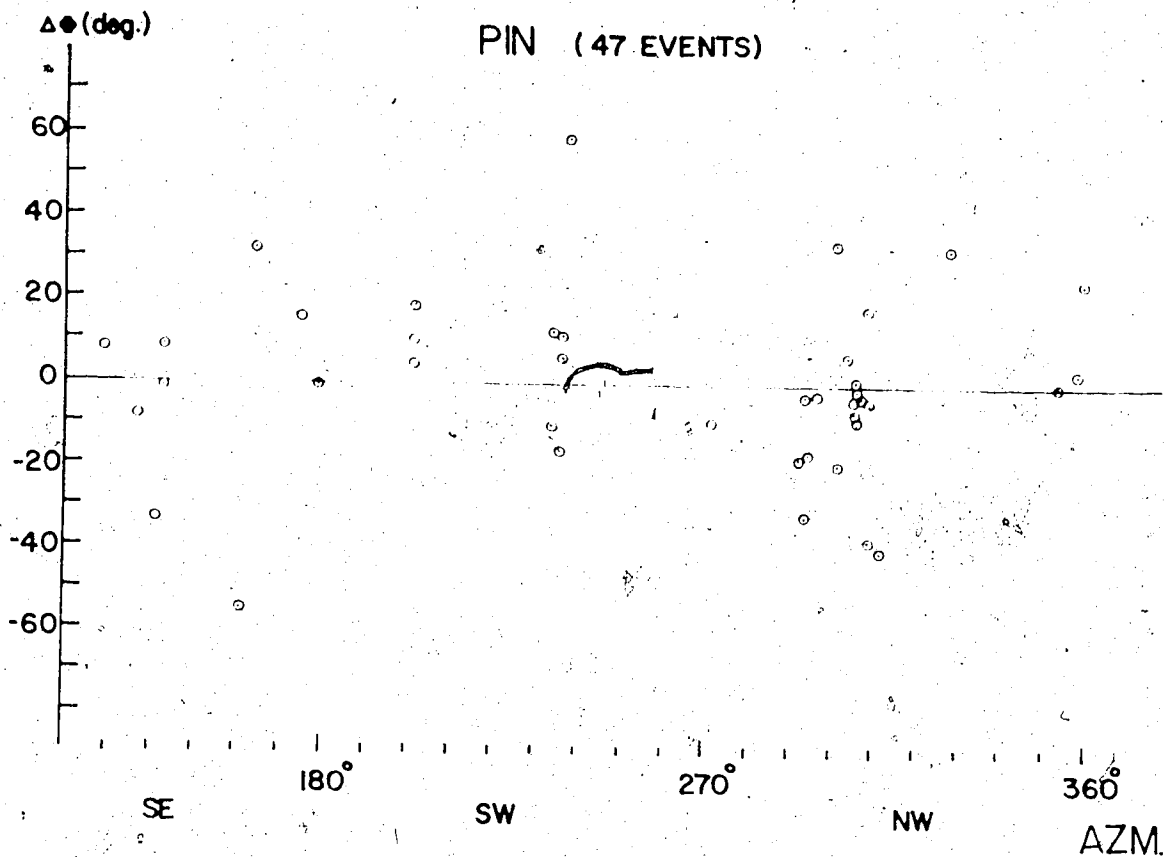




Figure V.10

Azimuthal deviation as a function of azimuth  
and residuals for PIN station.



the spectrum in this quadrant should be related to the scattering which seems to affect the wavelengths of about 30-60 km.

#### 4. RM stations (RM1 and RM2)

Long period spectral ratios at these stations have been characterized by a peak at centered around 0.18 Hz. In Figure 12, event 73 is clear from additional phases and shows a well resolved characteristic peak and a small peak at about 0.25 Hz. A large number of events showed a peak around 0.18 Hz (Figure 12-a,b) but not a second peak. Therefore, we will consider this peak as a real one. Event 73 exhibits a very low resolution at 0.09-0.1 Hz and shows a very small peak. However, other events generally show a larger peak at these frequencies, but all events other than event 73 have additional phases. On the other hand, event 73 has a lower magnitude which may cause lower resolution at these periods. Therefore, a small peak centered at about 0.1 Hz may also be accepted as a real one (Figure 13-c). As can be seen in Figure 13-b, major peak positions can vary more than 20 mHz for different earthquakes. Events 73 and 86 produced a peak at similar frequencies but event 84 has the same peak shifted to the higher frequencies. Events 84 and 86 have the same characteristics (Table I)

according to the earthquake data; additional phases are incident at the same time. For these earthquakes source mechanism has not been studied but record characters are similar; event 86 has 1 km deeper depth of focus. However, the large standard deviation in depth determination does not yield a solid comparison. Distorted long period spectral ratios due to one or more additional phases have generally lower amplitude and when combined spectral ratios were formed, general characteristics of the spectra were retained.

The crustal structure of regions close to the Rocky mountains is believed to be very complex. From the spectral analysis it can be seen that these stations produced completely different spectral ratios than at all other stations. In an attempt to model these peculiar spectral ratios using available theoretical tools, a different starting model was used. This model produces only one major peak for long periods. Parameters of the model were varied to obtain a spectrum similar to the experimental one that is a small peak at 0.1 Hz and a larger one at 0.18 Hz. First, the thicknesses of the layers were varied in turn until spectral ratios did not improve to give a better fit between experiment and theory. Next P and S wave velocities were changed to improve the comparison between observed and theoretical spectral ratios. This order of variation in parameter

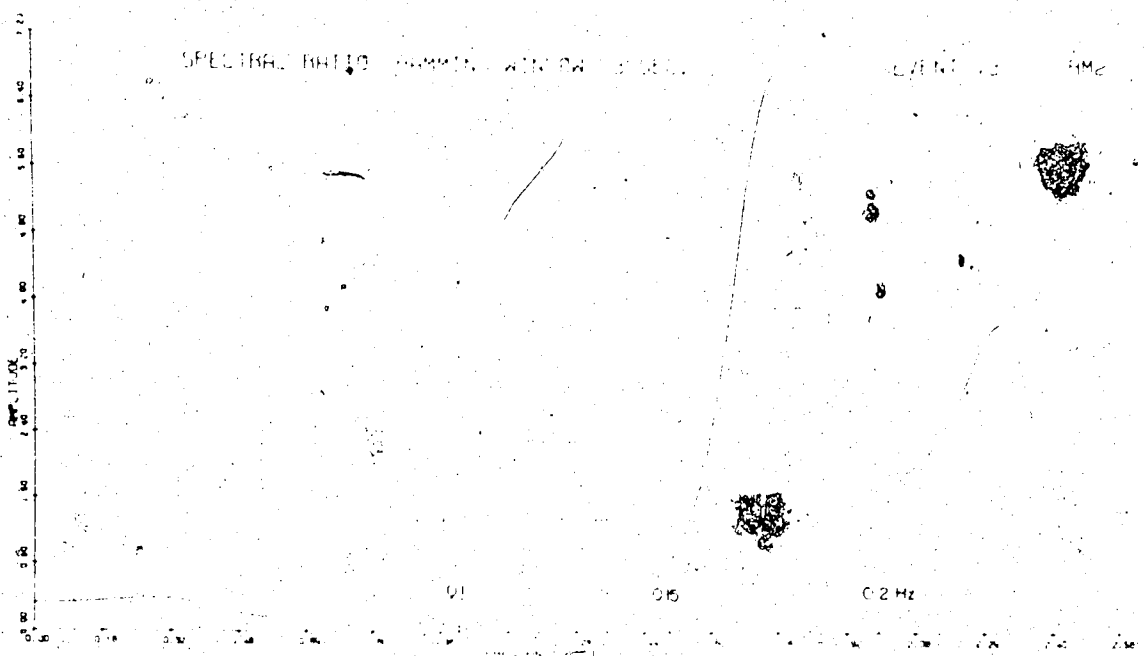
is not justified. However, such an order of variation in crustal parameters is necessary for the inversion of data using an empirical method. Model RM1 shown in Table III produced two peaks similar to those observed in the spectral ratios. However, the first peak at 0.1 Hz has a larger amplitude than the second peak. This model has a crustal thickness of 35 km. The simple layered crust as proposed for other stations does not produce a spectral ratio which has two peaks as in this experimental case. The amplitude of the second peak can be increased in two ways: first by lowering the P wave velocities only as in model RM2, which corresponds to a Poisson's ratio of 0.2 for the whole crust, secondly, by using a thicker sedimentary section (model RM4). It is well known that the sedimentary section of this region is very thick. In fact, a 2.8 km thick sedimentary section increases the amplitude of the second peak significantly to give a better fit between theory and experiment. In Figures 14 and 15, various models have been compared with experimental ratios. Events from the NW sector have larger major peak amplitudes than those from the SE sector. A dipping model like RM3 increases the amplitudes of both peaks. A model with extreme dipping interfaces has not been calculated because the spectral amplitudes

Table III

ALTACRT-1		Model RM1		Model RM2		Model RM3		Model RM4	
h (km)	V <sub>P</sub> (km/sec)	V <sub>S</sub> (km/sec)	P (gr/cc)	h (km)	h (km)	V <sub>P</sub> (km/sec)	Dip (deg)	h (km)	V <sub>P</sub> (km/sec)
2	3.06	1.77	2.21	2.0	2.0	3.06	0.0	1.4	3.45
-	-	-	-	-	-	-	-	0.9	5.3
-	-	-	-	-	-	-	-	0.5	4.9
10	6.1	3.52	2.7	5.0	5.0	5.9	+5.0	5.0	5.9
23	6.5	3.75	2.73	13.0	13.0	6.1	+5.0	13.0	6.1
10	7.15	4.13	3.20	15.0	15.0	6.75	0.0	15.0	6.75
-	8.08	4.66	3.45	-	-	8.08	0.0	-	8.08

Figure V.11

Event 73 recorded by RM2 station and its long  
period spectral ratio using Hemming window.



0.8 SEC.



Figure V.12

Some of long period spectral ratios for RM stations  
and their combined versions with respect to azimuth.

(a)

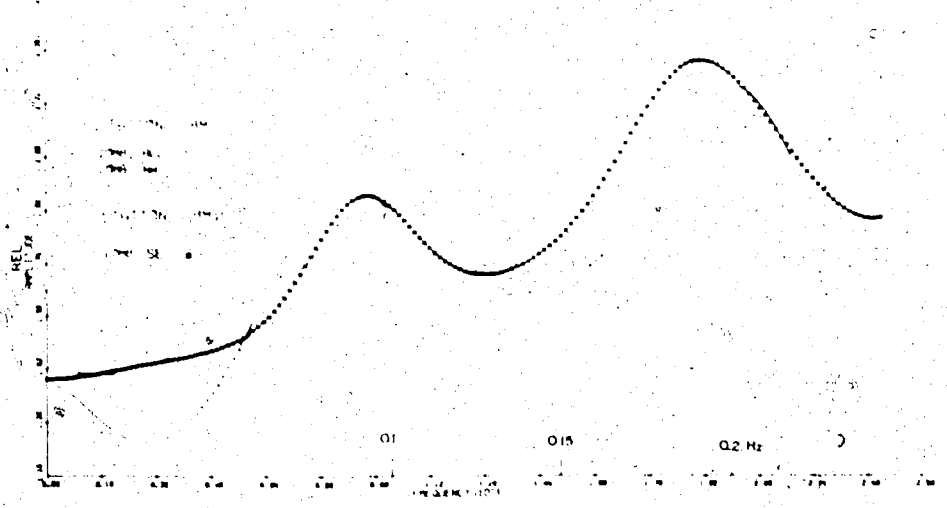
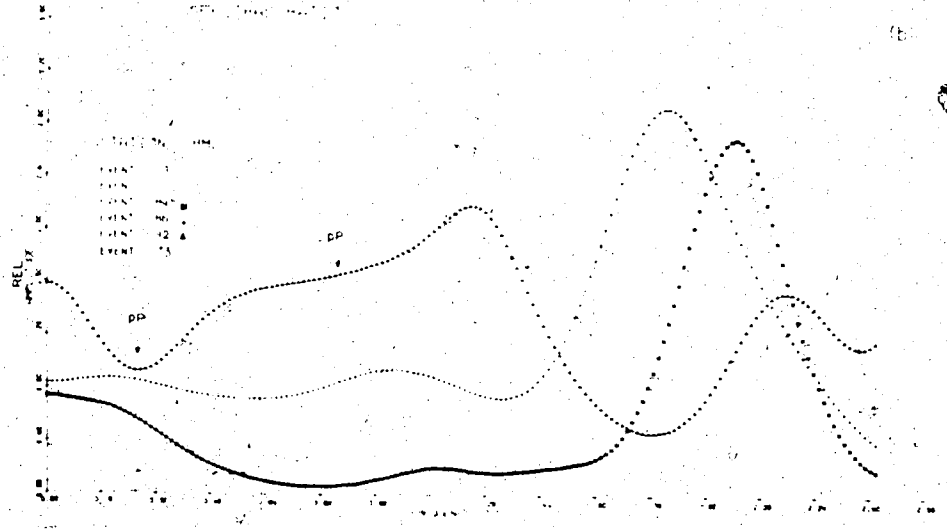
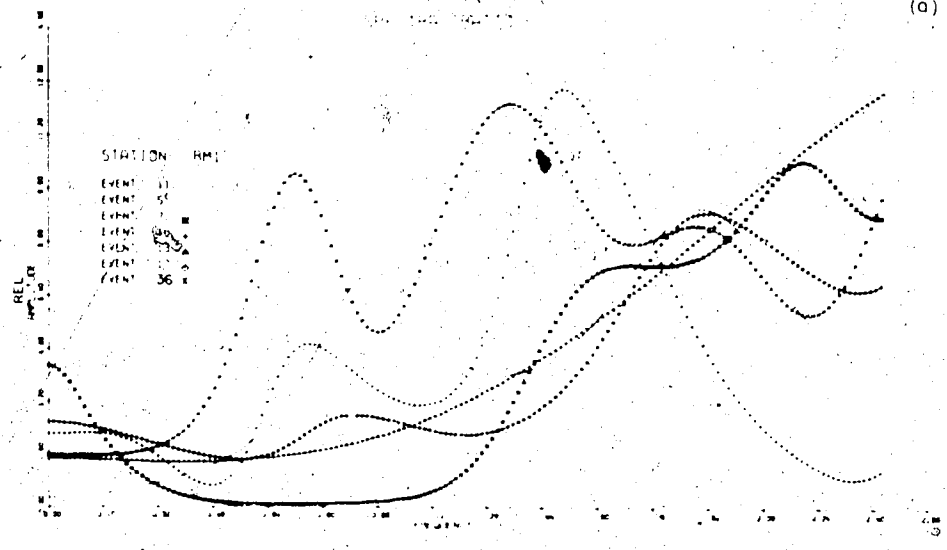


Figure V.13

Two events from SE sector and their comparison  
with models in Table III.

SPECTRAL RATIO DELTA 82-87 DEG. SE SECTOR

STATION RM1

EVENT 11. -  
EVENT 17. -

MODEL RM-4

RM-3

MODEL RM-2  $i=23^\circ$

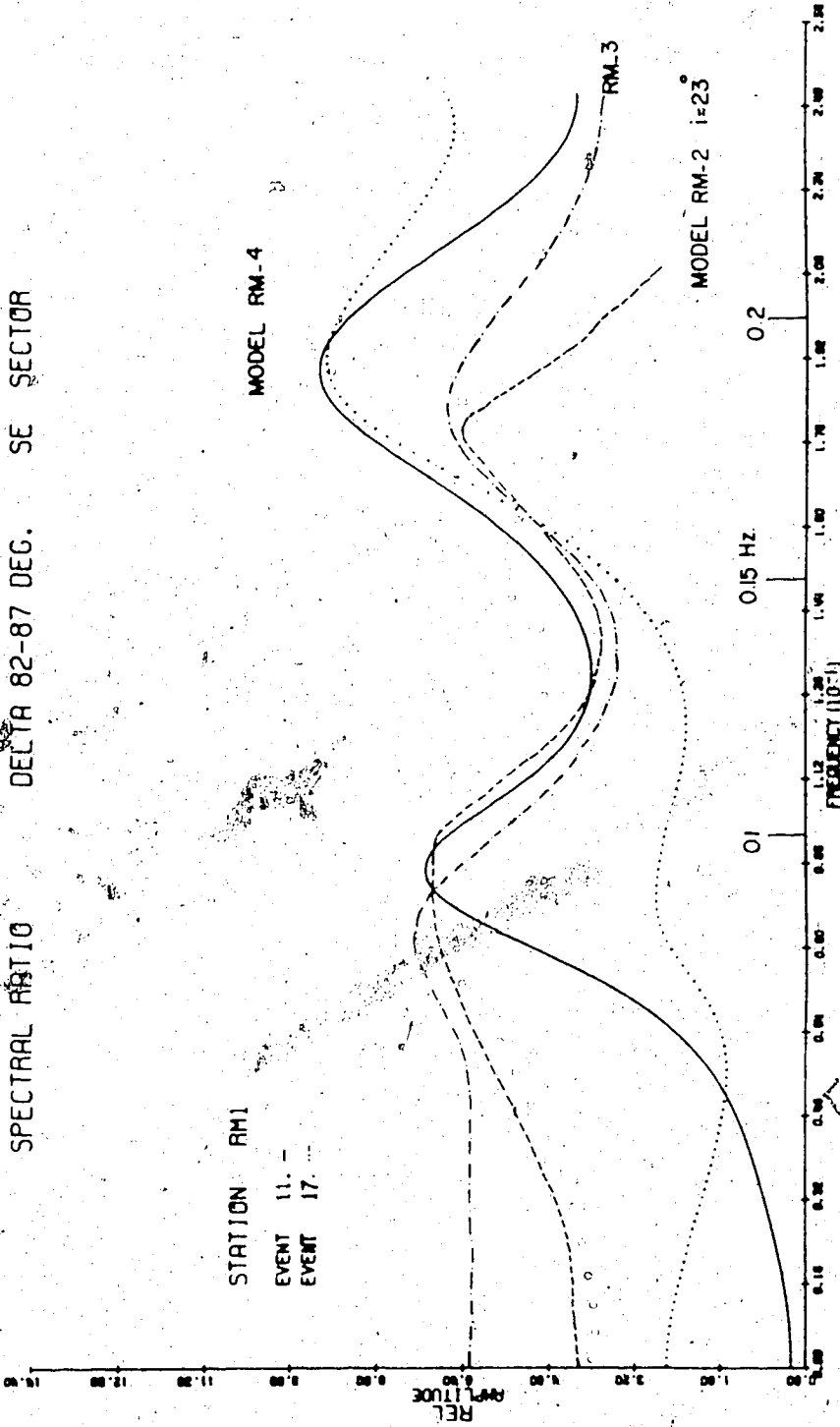


Figure V.14

Three long period spectral ratios and their comparison with RM models. Amplitudes in these graphs are true amplitudes.

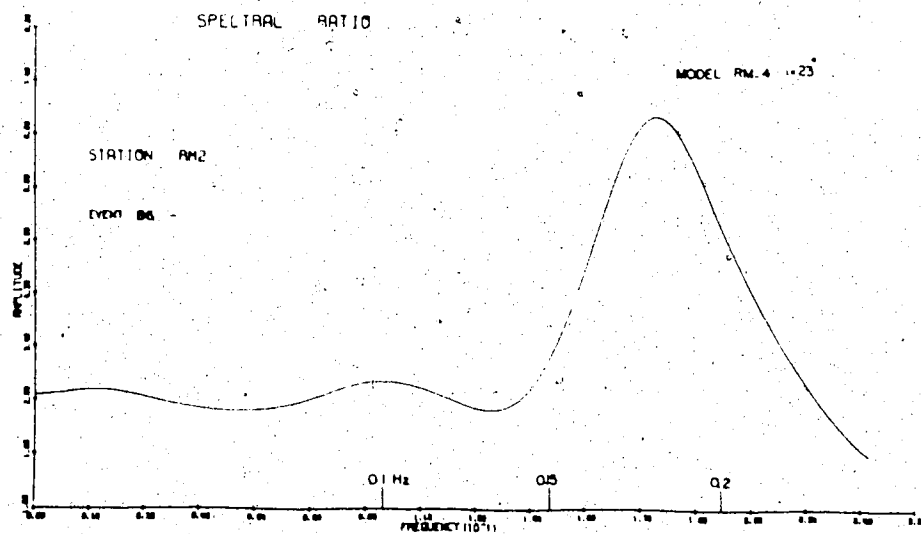
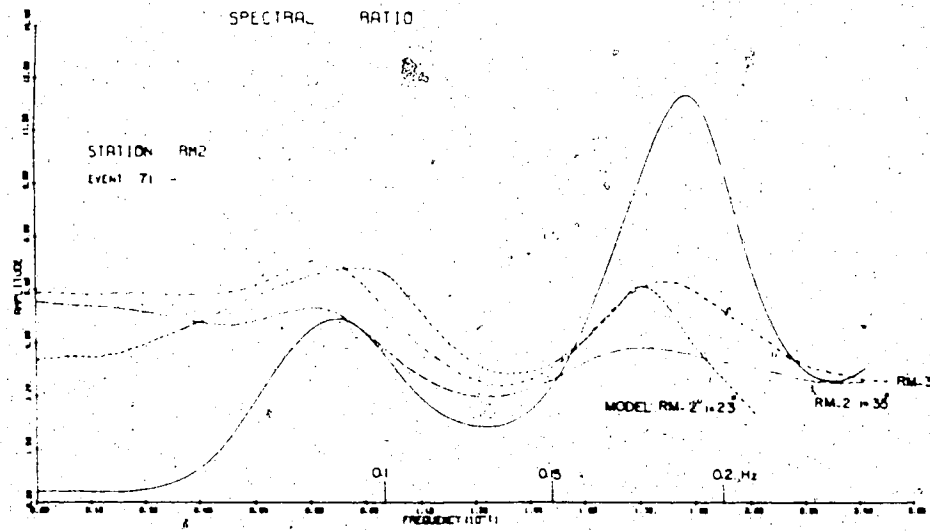
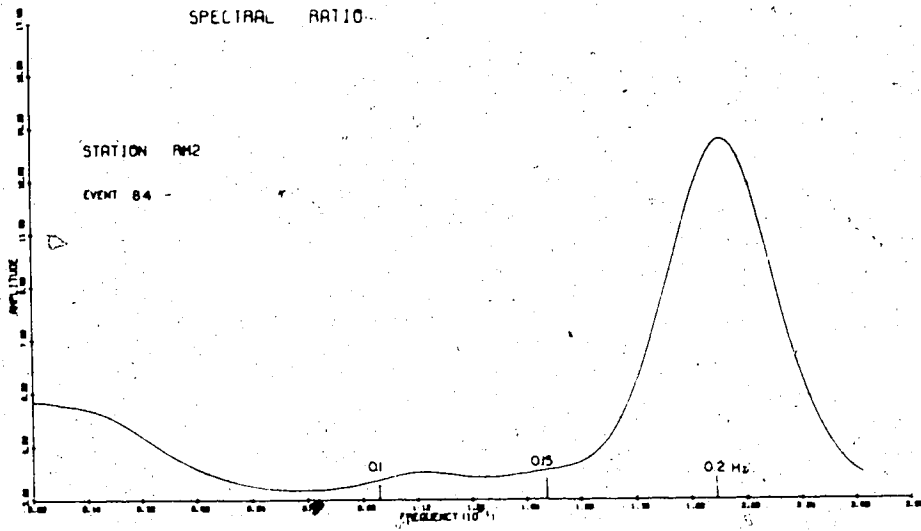
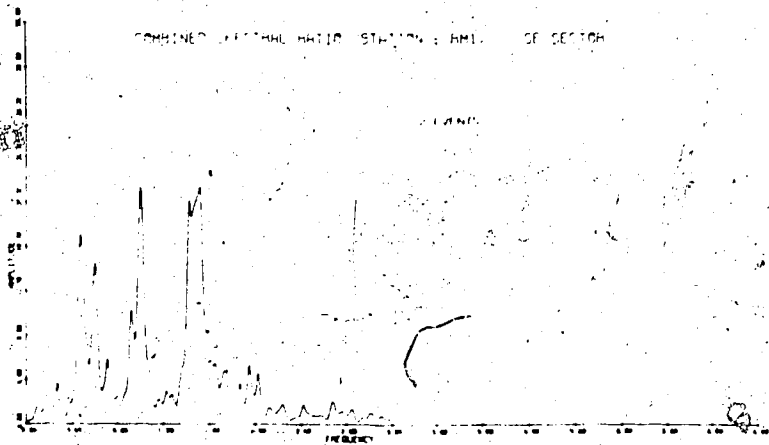


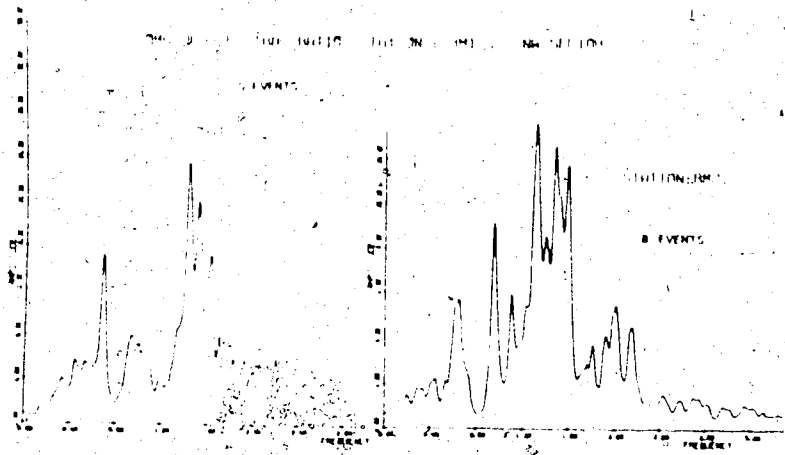
Figure V.15

Short period spectral ratios for RM stations and  
their classification with respect to azimuth.

COMBINED CENTRAL BATHY STATION: BH1 OF SECTION



COMBINED CENTRAL BATHY STATION: BH2 OF SECTION



COMBINED CENTRAL BATHY STATION: BH3 OF SECTION

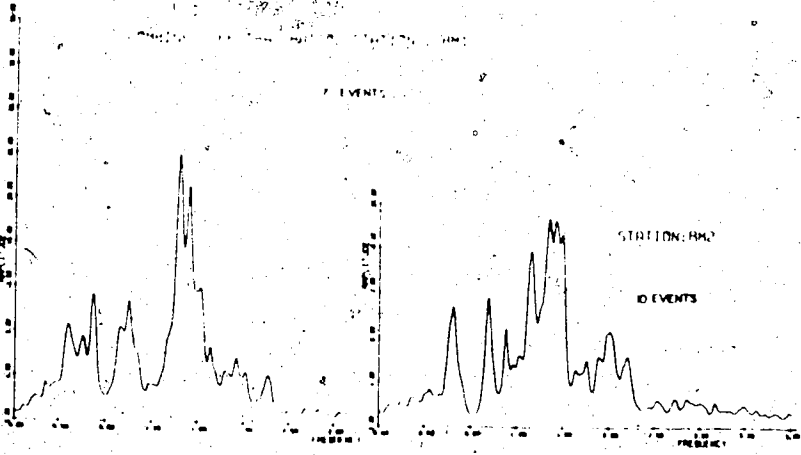
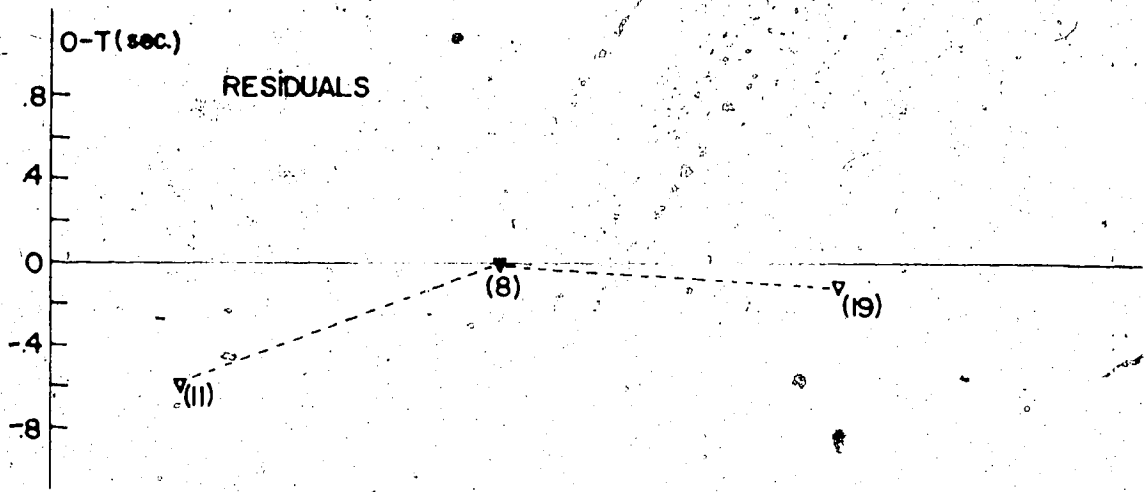
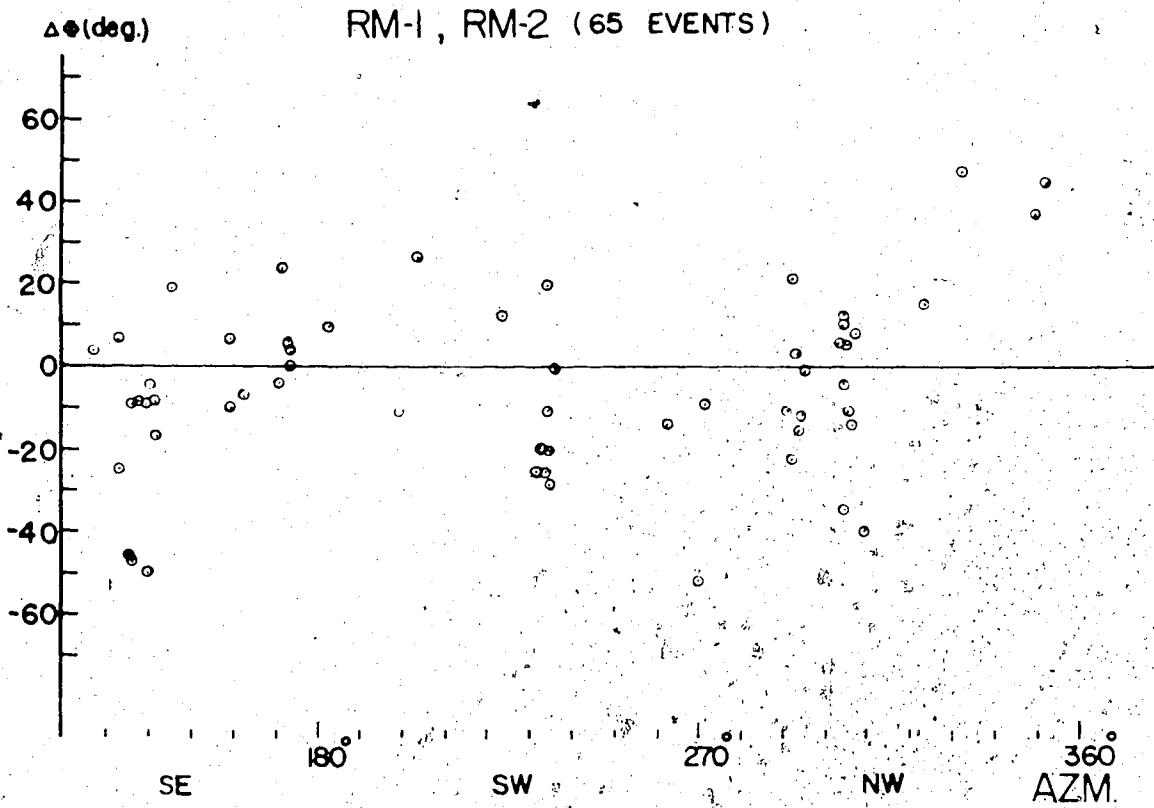




Figure V.16.

Azimuthal deviations versus azimuth and station residuals.



are contaminated by energy from additional phases. Amplitude differences for these two sectors can be explained in terms of differences in the thickness of the upper layers.

The spectral ratios at higher frequencies for those stations show closely spaced peaks similar to the PIN and TRO stations indicating the presence of a low velocity layer or a thick sequence of layers in the crust. Most of the energy has been concentrated in a small frequency band. Peaks are broad and the splitting of peak occurs frequently (Figure 15). Modelling of these short period spectral ratios are difficult using a plane layered model. However, a sedimentary section 3-3.5 km thick is indicated by the model experiment.

A number of seismic measurements has been carried out across the Rocky mountains, but most of them cover southern B.C. and Alberta. White and Savage (1965) estimated that there is a 31 km thick simple crustal section under the mountains. Gravity anomalies for a strip across the southern part of the Canadian cordillera suggest (Stacey, 1973) a thicker crust if this corresponds to the depth of compensation. As far as we know there are no deep seismic measurements around the RM stations. This region shows a high magnetic anomaly and a large positive Z residuals

on the geomagnetic components (Haines et al., 1971; Berry et al., 1971). Therefore, the best fitting model for spectral ratio studies can only be correlated with other stations of the array. A crust with a thickness of 35 km is concordant with the ones obtained for other stations. In addition, these spectral ratio studies favor a multilayered crustal model with relatively low velocities for P waves.

Azimuthal deviations for these stations do not show any particular pattern (Figure 16) but the arrivals from the SE sector are consistently earlier. This could be related to a thinning of the low velocity layer in the mantle under the plains away from the mountains or it could be effectively generated near the source region.

##### 5. TRO and DEL stations

The transverse component of ground motion at TRO and DEL showed very large amplitudes; sometimes larger than the vertical component (Figure 17). The azimuthal deviations show a definite pattern with azimuth (Figure 18-a). This pattern of azimuthal deviation be modelled with the use of dipping interfaces (Niazi, 1966; Zengeni, 1970). The zero crossings of azimuthal deviation will determine the direction of dipping structure. During the computation of azimuthal

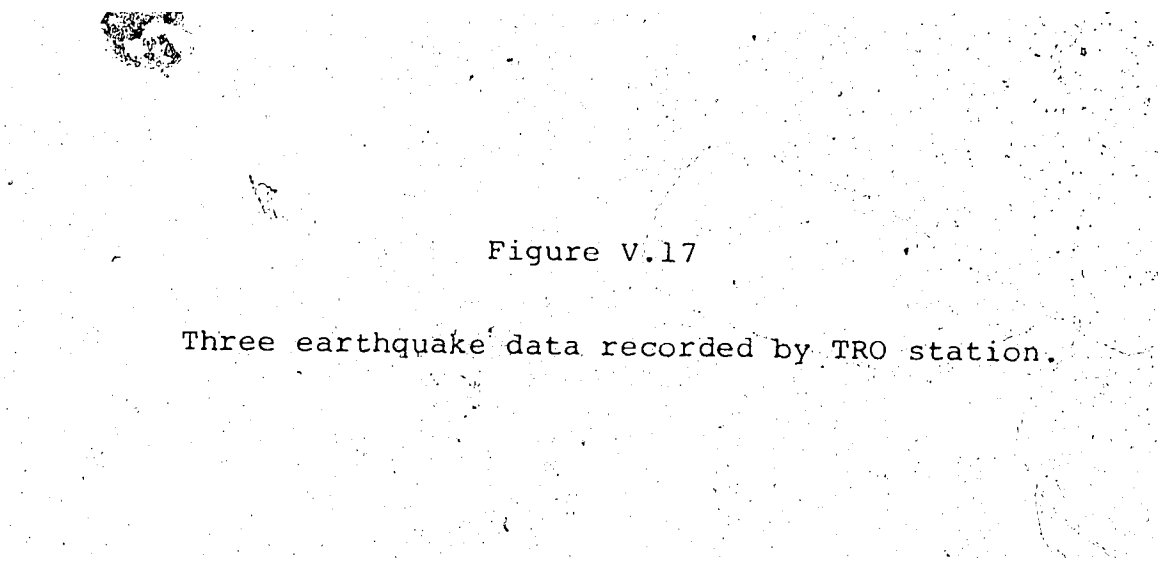
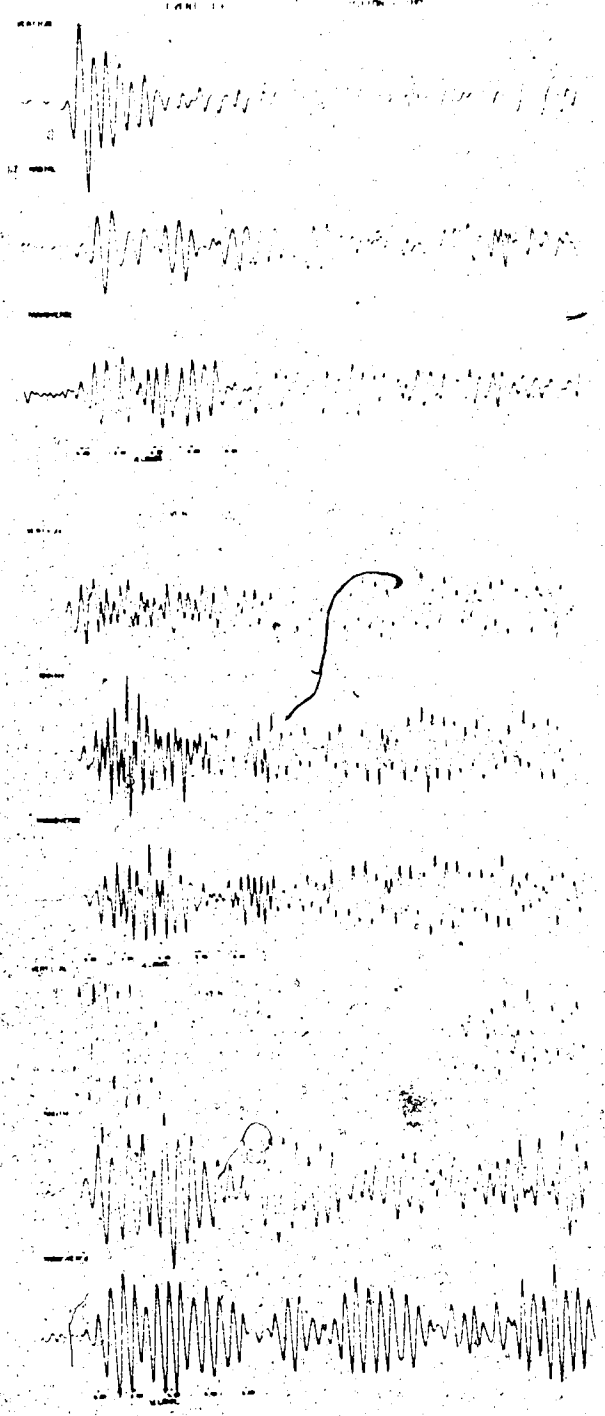
The image shows three distinct seismic waveforms recorded at the TRO station. Each waveform consists of a series of oscillations, with the most prominent feature being a sharp initial peak followed by a series of smaller, decaying oscillations. The waveforms are arranged horizontally, with the first on the left, the second in the middle, and the third on the right. The background is a light, textured gray, and the waveforms are rendered in a dark, high-contrast style.

Figure V.17

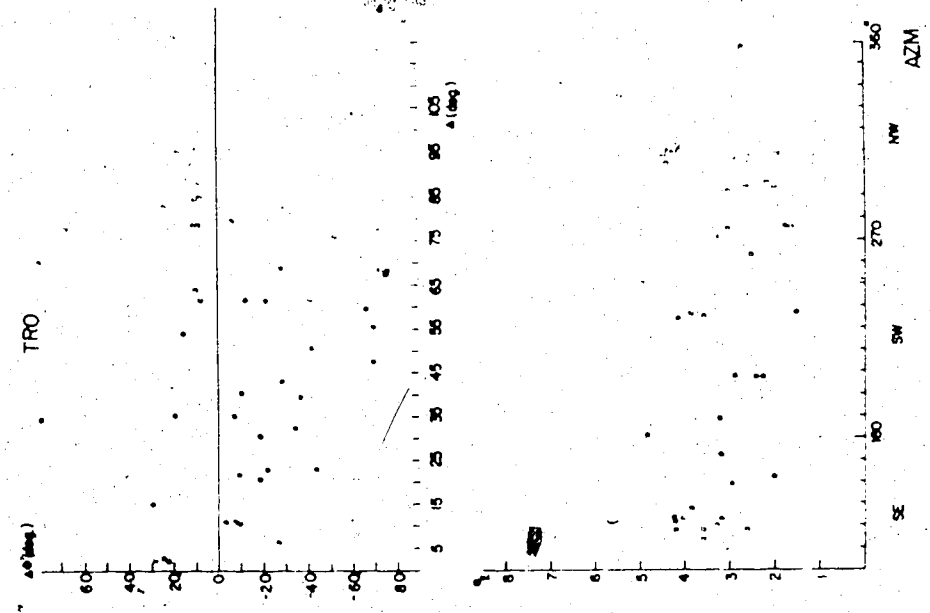
Three earthquake data recorded by TRO station.



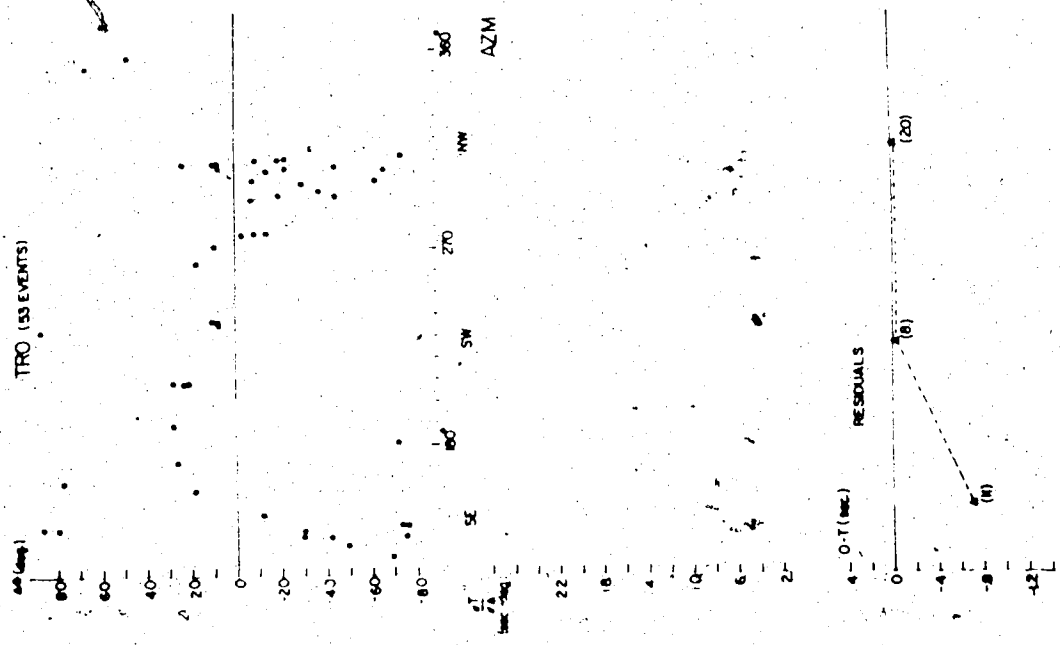
Figure, V.18

- a) Azimuthal deviations measured as function of azimuth, slowness measurements using all stations in the array and residuals for TRO.
- b) Azimuthal deviation as a function of distance and minimum of ratio of transverse energy to the total horizontal energy as a function of azimuth.

(b)



(a)



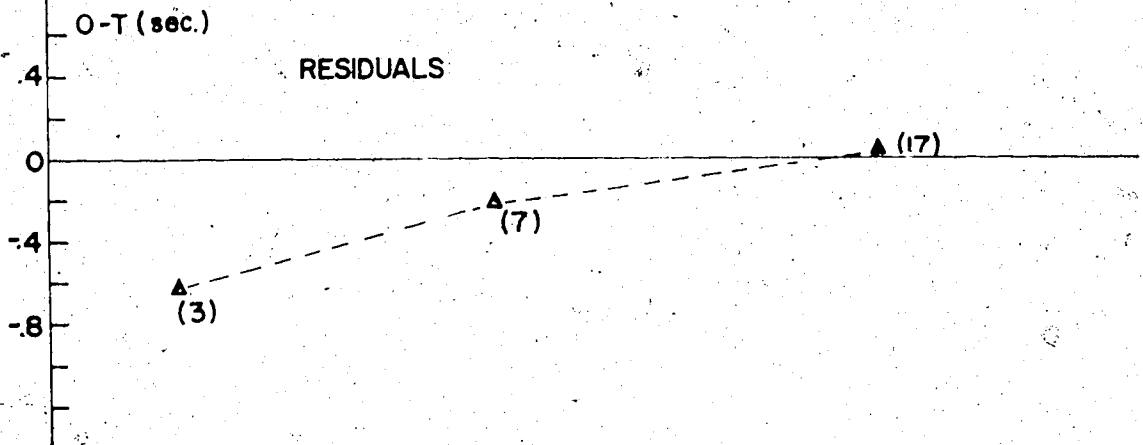
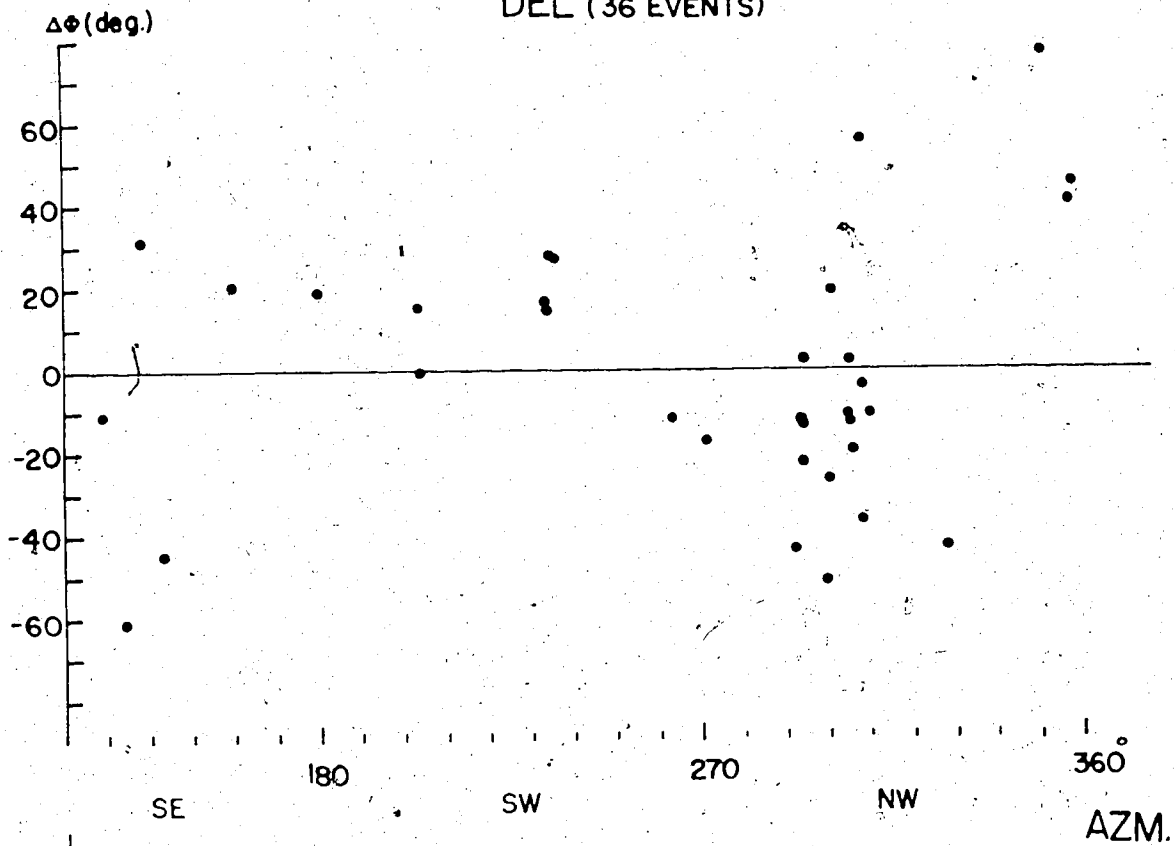


deviation, clockwise rotation was chosen as a positive. Therefore, the second zero crossing will be the dip direction. For both DEL and TRO the second zero crossing is at about  $290^\circ$  azimuth. A slowness measurement using all stations in the array has also been shown in Figure 19 (After Gutowski, 1974), in which a strong anomaly is clear and it suggests a dipping structure under the array. However, this anomaly can only be correlated to the azimuthal deviations observed at TRO and DEL stations. The azimuthal deviations showed no definite pattern with distance (Figure 18-b). Niazi's tables for determining the dip angle are not applicable because the azimuthal deviations are very large and not regular enough for a simply dipping layered model. Since the time residuals at these stations are small, any dipping or faulted interfaces must be near the surface and local in nature. A refraction study (Richards and Walker, 1959) does not indicate any anomaly in crustal structure in a north-south profile in central Alberta. If we assume the seismometers were positioned and operated with sufficient accuracy, this anomaly is not a large one because it is only observed by two stations and therefore a steeply dipping crust to the west under the array cannot be postulated.

Figure V.19

Azimuthal deviations measured as a function of  
azimuth and residuals for DEL station.

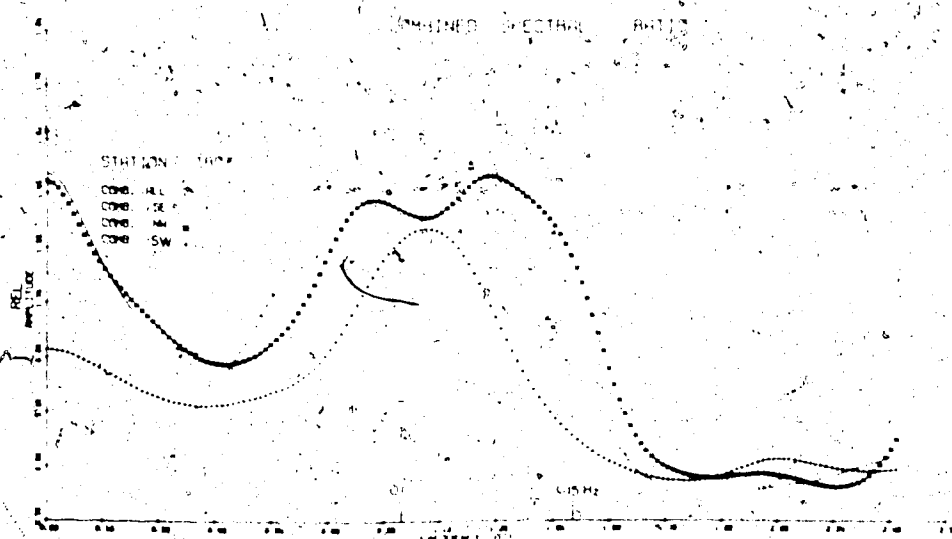
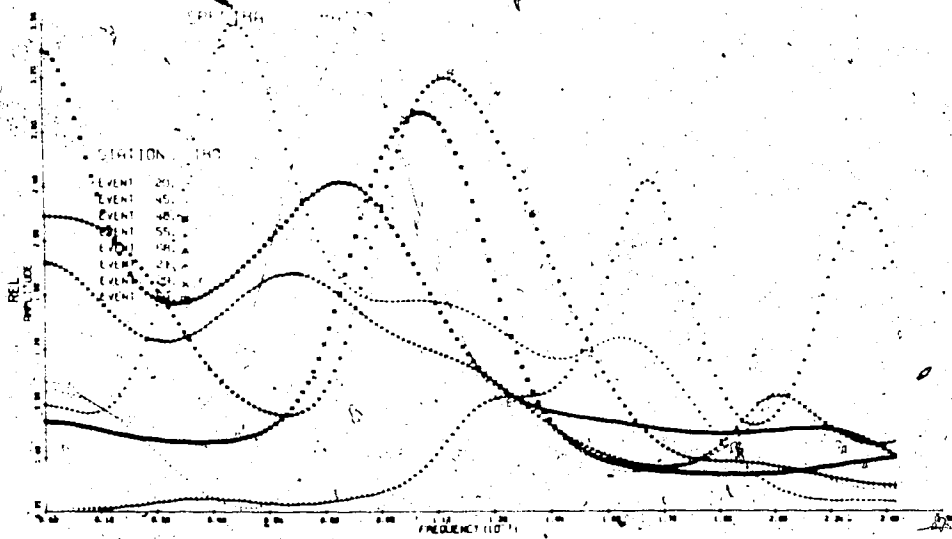
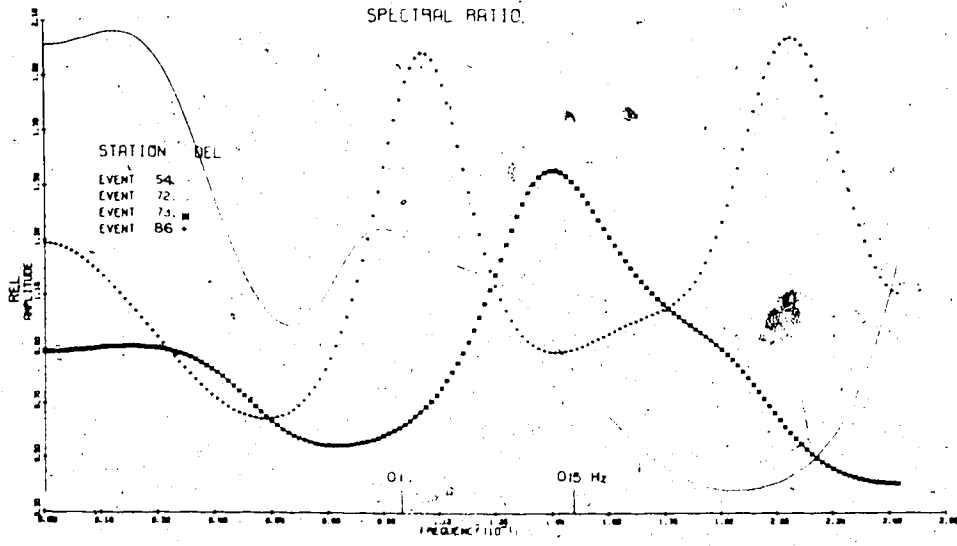
DEL (36 EVENTS)



Anomalous results were also noticed on the spectral ratios (Figure 20) which have very low amplitudes at these stations. Horizontal components on the seismogram (Figure 17) have large amplitudes and some phases cannot be correlated with the ones on the vertical components. Since horizontal motion is generally shear motion, the large arrivals on the horizontal components can be related to anomalous P to S conversions, possibly in the sedimentary layers. Combined spectral ratios for SE and SW sectors have a smooth appearance but they are well separated in frequency. The SW events can be modelled by a crustal section about 36 km thick but the SE events are best modelled by a 10 km thicker crust. Events from NW azimuth yielded a spectral ratio with two peaks (Figure 20). Splitting of this peak position occurs around  $290^\circ$  azimuth. Insufficient data from all azimuths makes it difficult to interpret spectral ratios in terms of dipping structure. The SE events favor either a thicker crust or slower transmission of waves whereas the SW events favor a thinner crust or faster transmission of waves through the same crustal structure. Either of these interpretations is compatible with the azimuthal deviations. The distance between TRO and DEL is about 20 miles and it is clear that this anomaly extends over at least this distance;

Figure V.20

Long period spectral ratios for TRO and DEL and their averages.



however, it is not seen at Pine Lake, which is 20 miles to the SW.

From the record character, large horizontal motion indicates anomalous conversion of P to S occurs. The most probable place will be the low velocity sedimentary layers. These layers should have highly irregular structure to account for the conversions. Therefore, a steeply dipping or possibly, more complicated thick sedimentary layers can be postulated to explain distortion in the long period waves while the exact cause of anomaly cannot be resolved at this time.

## 6. Conclusions

In section III, it has been shown that 35 seconds of P coda allows us to obtain sufficient resolution for the interpretation of long period spectral ratios. Most of the experimental long period spectral ratios showed only one dominant peak in the range, 0.05 to 0.2 Hz but there were some small peaks on each side of the major one. The disappearance of the small peaks in some earthquake data may be attributable to the presence of additional phases but there were some clear spectra from deep events which, even with a larger data window, also did not show these small peaks. This can be explained by the results obtained in section III, where

many model calculations with dipping interfaces showed very small or unnoticeable side lobes. Many long period experimental spectral ratios presented in this section had about 10-30 mHz shift in major peak position from event to event. These variations cannot be explained by additional phases alone and may also be due to interfaces, dipping as much as  $10^\circ$ .

By the amount of experimental data taken for spectra, we assume an incident plane wave which is dipping on the 60-100 km region of the Moho, from the station to the opposite direction of wave approach. Therefore, assumption of lateral homogeneity and no secondary sources is necessary in this part of the crust. For the crustal interpretation with a 2-3 km sedimentary layer, the model calculations assume that about a 20 km region near the station also possesses flat or simply dipping layers. Generally, the spectral ratios observed at short periods did not match the ones obtained by drilling and Sonic log data under a particular station. This would seem to indicate the rapid variations and the violation of basic assumptions in this method since short period waves average over large region of Precambrian crystalline basement.

EDM long period analyses indicate that the crustal thickness is about 36 km. The amount of uncertainty



is large because there are structural variations with azimuth and insufficient amount of uncontaminated data for all azimuths. Therefore, there are crustal variations in thickness of about 4 km or the velocity structure may vary from the mean of 6.5 km/sec. Short period spectral ratios for this station are well determined as indicated by their duplication on various events. The short period interference pattern for this station can be approximated sufficiently by a two layer sedimentary section. Uncontaminated events show much lower amplitudes than this model, but this may well be related to the soft layers in the sediments and lower velocities in the deep crust. A thin low velocity layer in the upper crust cannot be resolved in the frequency band available.

Dependable data for the PIN station shows similar long period spectral ratios to the ones determined for the EDM station. RM stations showed completely different long period spectral ratios and a model with a 35 km crust is suggested. The long period interference pattern can be modelled by using a larger number of layers than necessary for other stations. TRO and DEL data indicates a very heterogeneous structure. Azimuthal deviation measurements and record character suggest that this anomaly is due to a steeply dipping or more complicated structure (i.e. with faults) in the upper section.

The short period spectral ratios for PIN, TRO and DEL show no correlation with each other indicating a rapidly varying structure in the upper crust. Short period energy has been concentrated into a small frequency band at the RM stations and modelling of these spectra is difficult using the assumption of plane layering. However, the  $\frac{1}{2}$  spaced peaks indicate a sedimentary section 300 km thick, with possibly lower velocities in the southern part of the array.

## CHAPTER III

### SYNTHETIC SEISMOGRAMS

#### I. Seismograms for P waves

A time history of the surface motion of a layered media responding to a pulse can be obtained by convolving the impulse response with a source function. Hannon (1964) obtained a time series for a number of models using a low frequency pulse. He studied the effect of soft layers and variations in the angle of incidence on the surface motion. McCamy (1967) has made a comparison between experimental and theoretical seismograms calculated by the Haskell-Thomson matrix method.

The Haskell-Thomson matrix formulation yields a complete plane wave solution for a layered medium. Therefore, when a time synthesis is formed, all phases will be included provided that the sampling frequency is sufficiently small. In this thesis, synthetic seismograms were calculated for a number of Alberta crustal models by an inverse Fourier transform of the frequency components of the ground motion. A fast Fourier algorithm was used to obtain the time response of a layered medium:

$$X(T) = \frac{1}{N} \sum_{\omega=0}^{N-1} H(\omega) S(\omega) e^{2\pi i \omega T/N} \quad (1)$$

where  $\omega$  is the digital frequency index,  $T$  is the time index and  $N$  is the total number of digital points as a power of 2.  $H(\omega)$  is the complex transfer function obtained using the Haskell-Thomson method for the layered media in which seismic anisotropy and attenuation may exist.  $S(\omega)$  is a function representing the source pulse. The time index  $T$  is limited to  $T < N-1$ .

In Figure 1, an arbitrary source pulse function was chosen to be (Hron, et al., 1972)

$$S(t) = \sin(\omega_0 t) e^{-(\alpha \omega_0 t)^2} \quad (2)$$

where  $\omega = 2\pi f_0$ ,  $f_0 = 10$  Hz and  $\alpha$  is an attenuation constant, chosen to be 0.25. This function has a Fourier transform as follows:

$$S(\omega) = \frac{-i\pi}{\alpha \omega_0} \exp\left[-\frac{1}{4\alpha^2} \left(1 + \left(\frac{\omega}{\omega_0}\right)^2\right)\right] \sinh\left(\frac{1}{2\alpha \omega_0} \omega\right) \quad (3)$$

Ray methods may also be used to calculate the response of a layered medium. In the ray theory used in this thesis, the wave solution has been expanded into an infinite power series of terms containing reciprocal frequency combined with a vector which is only space-dependent (section III). The ray theory approach

is limited by the computational difficulties associated with the selection of phases in the partial ray expansion. However, a ray theory is more flexible than a matrix method, in that the solution is not restricted to plane parallel interfaces. A comparison between a ray and a wave solution has been carried out to evaluate the criteria used in selecting an optimum number of terms in the ray expansion (Figure 1). Using a number of test parameters outlined in section III, a reasonable match between two solutions was obtained for a flat layered media. In a ray solution containing 1380 rays for the construction of a seismogram the difference in amplitudes calculated by the two methods was less than 0.1 % for the first 3 seconds of time. The accuracy of the partial ray expansion decreases with later arrivals unless more rays with converted phases are allowed. The arrival times of all phases agree and no significant difference in amplitudes has been found. A major advantage of the partial ray expansion is that all phases are identified and may be listed on the Calcomp plot of the synthetic seismogram.

A high frequency source is desirable because the seismograms will have a high resolution enabling us to see differences between the two solutions clearly. However, as is often the case with many earthquakes the source has a larger period and duration. In that

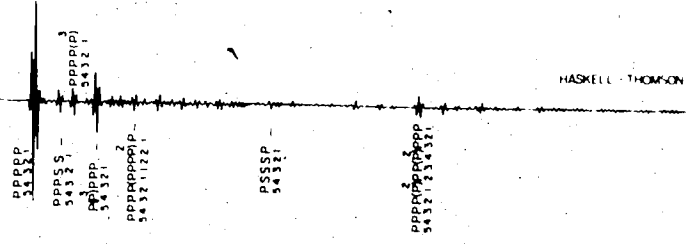
Figure I.1

Comparison of seismograms computed by Haskell-Thomson and ray theory for a plane P wave impinging on the bottom of the layered media (ALTACRT-3) with  $i = 70^\circ$  ( $\text{ALPHA} = 20^\circ$ ). In this diagram coding of rays is specified by the equation

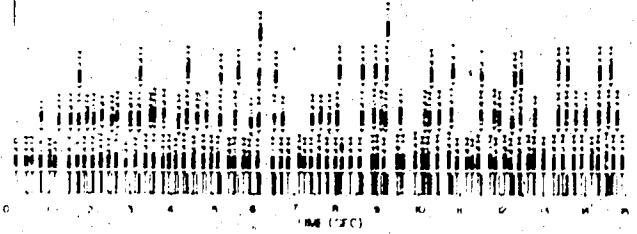
$$\text{NOFRAY} = 100000 \cdot \text{JRAY} + 1000 \cdot \text{JCONV} + \text{JC}$$

where JC is an integer which indicates the point of incidence at which phase conversions occur for any particular ray. JRAY is the ray number from ray table (section III) and JCONV is the number of conversions experienced by the JRAY.

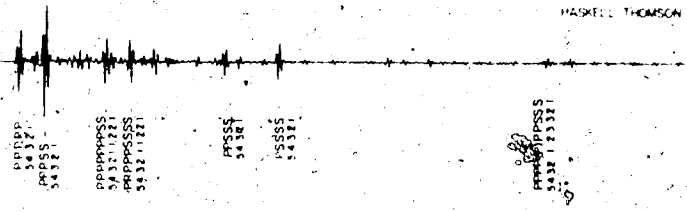
EXPERIMENTAL DATA FOR REFLECTION



ASYMPTOTIC RAY THEORY



EXPERIMENTAL DATA FOR REFLECTION



ASYMPTOTIC RAY THEORY

situation, interference of phases is important and in section III, it has been shown that the long period spectra obtained either by the ray or wave method are in reasonable agreement in position of peaks and amplitude. The fast Fourier inversion method of obtaining a seismogram, even for a high frequency pulse, requires 50 % less computing time when a partial ray expansion for the models used. However, the ray expansion enables us to interpret the various phases easily. For the model shown in Figure 3, there are 100,000 rays which have 13 segments in the layered media but only 0.031 % had amplitudes large enough that they had to be included. Rays with a large number of segments are very important for the long period spectrum. As shown in Figure 3, the number of rays incorporated in a dipping model generally is lower. This occurs because rays are eliminated by the program when they approach the vertex of the wedge. A dipping sedimentary layer as much as 10 degrees reduces the number of rays used in the solution. The long period spectrum may be unreliable. This restriction is reasonable in a sedimentary basin because layers seldom have the same dip for extended distances and wedging is only common near the edge of the basin. A coordinate system has been chosen with the +z axis being upward and +x axis in the direction



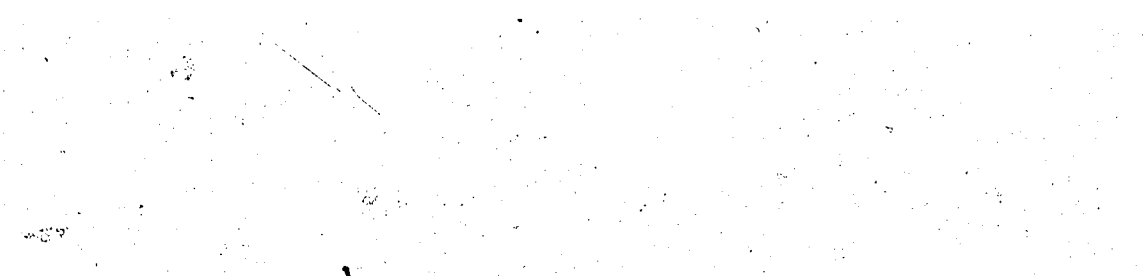
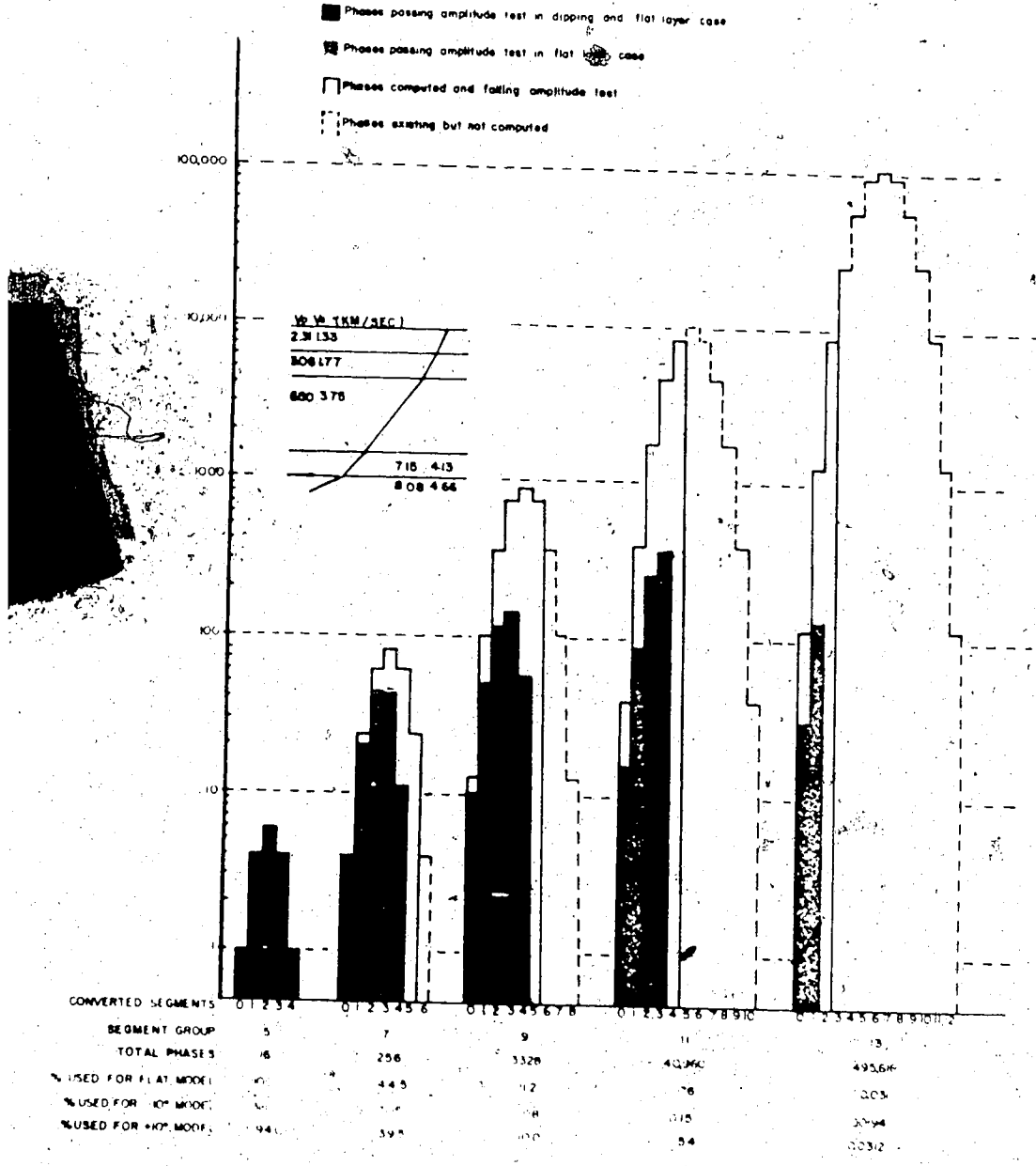
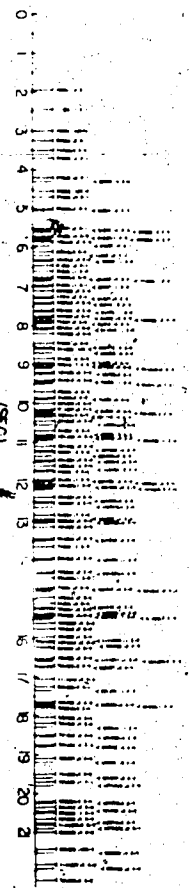
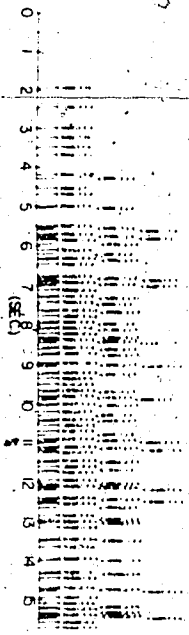


Figure I.2

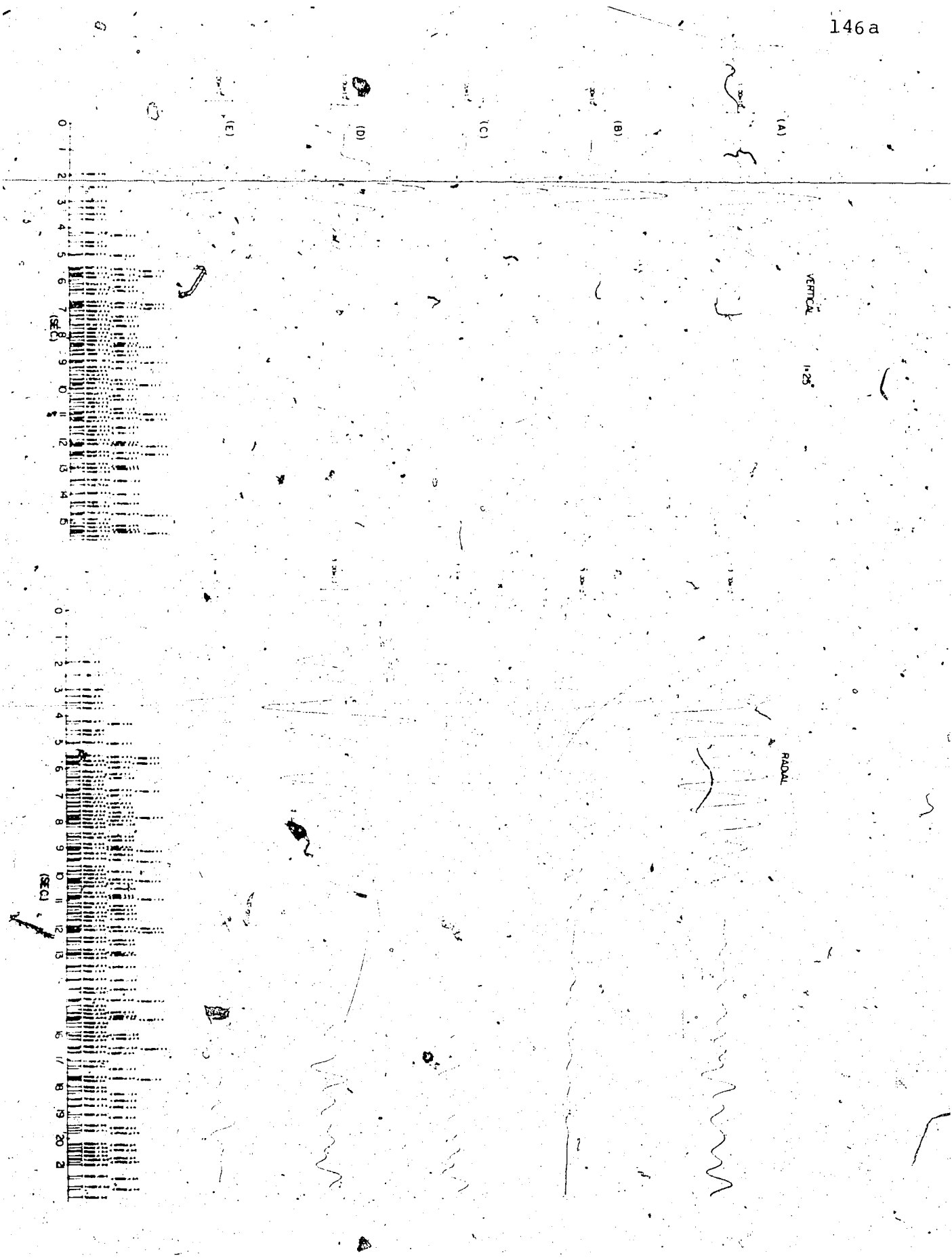
Existing rays and their use for a 4 layered  
crustal model over half space. Dipping model  
indicates only dipping Moho.





VERTICAL  
1:25

RADIAL



of phase velocity. The effect of a dipping sedimentary layer (Figure 3-B) is greatest when compared to a flat layer case (Figure 3-A). A low velocity sedimentary section produces large horizontal motion and introduces a large phase. Therefore, S motion represents an elliptical particle motion with an axis in the quadrant formed by negative vertical motion and positive horizontal motion or positive vertical motion and negative horizontal motion. Therefore, elliptical particle motion with various angles of tilt in the axis may occur. Steeply dipping thicker layers with higher velocity did not produce the same effect. Only minor differences exist for large time intervals.

For a flat layered model, a pulse with wavelengths larger than layer thickness usually is relatively transparent to the layer, although minor differences in amplitude are noticeable. For example, a number of seismograms have been constructed for Model-1 and Model-2 of section V. For frequencies centered around 1 Hz, there is not any significant change but only amplitude differences exist. For various models, both the matrix method and the ray method have been used simultaneously and they produced the same results for wavelengths which are 0.015-10 times of the layer thicknesses:

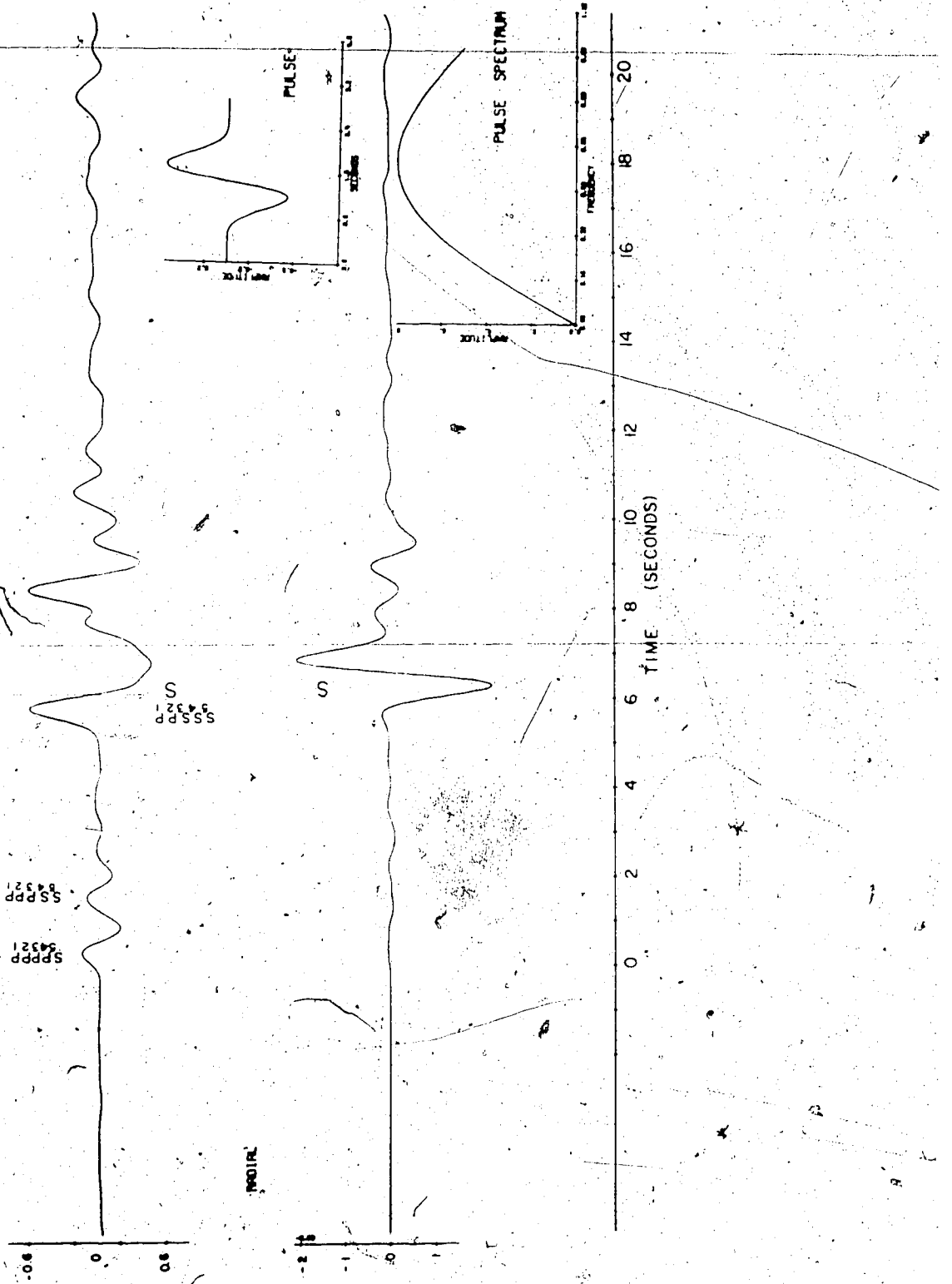
## II. Seismograms for S Waves

The time response of a layered media to a plane S wave incident at the base can also be calculated by the Haskell-Thomson matrix method (section II). For this case the wave and partial ray expansion techniques produced identical results within the limits of computational accuracy. In Figure 1, a low frequency seismogram (0.5 Hz) calculated by the matrix method has been shown for crustal model ALTACRT-3. This model has a two layered sedimentary section which is common in a continental crust. In this Figure, the main arrival on the vertical component has the second largest amplitude but an earlier arrival was identified as a conversion at the bottom of the sedimentary layer. However, the direct S wave has the largest amplitude on the radial component. On vertical component, the time difference between converted phase which has largest amplitude and the pure S<sub>v</sub> phase is delayed about 1 sec and it may be as large as 2 seconds depending on thickness and velocity of the sedimentary layers, and it was found to be not sensitive to dipping interfaces. On the vertical component of ground motion, a few other phases with significant amplitude exist about six seconds before the main phase. These precursors have been identified as conversions from S to P at the Moho and at intermediate

Figure II.1

Theoretical seismograms calculated using a Haskell-Thomson matrix formulation for a plane S wave incident at  $30^\circ$  on the crustal model ALTACRT-3. Incident pulse and its spectrum are shown in the insert.

VERTICAL PULSE 0.5 HZ. INCIDENT S 1=30 DEG. ALTA CRUST



layer. Obviously, these could be used as indicative phases for determining crustal thickness.

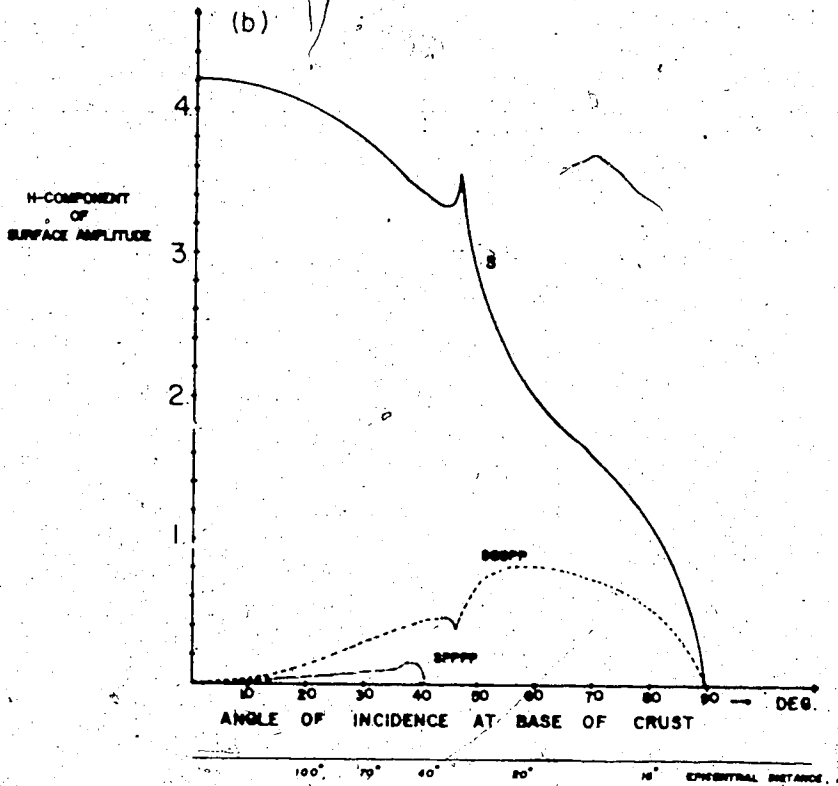
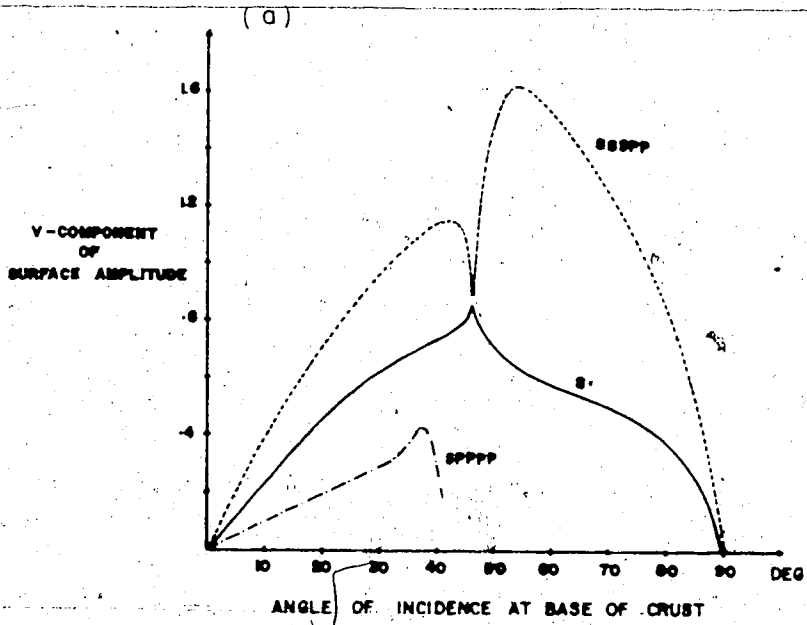
The interpretation of S arrival has been always a difficult task. Neuman (1930) noticed early longitudinal arrivals before the main S arrival for an earthquake at an epicentral distance of 2500 km. He interpreted this as a P phase and measured 4 seconds of time difference between this phase and  $S_g$  phase. Gutenberg and Richter (1931) could not identify any S arrivals for epicentral distances between  $9^\circ$ - $15^\circ$ . Byerly (1934) noted the difficulties in identification of S phases and he classified S waves as impressive (iS) and early phases (eS). Jeffreys and Bullen (1940) have noted that S waves are not satisfactorily readable up to  $25^\circ$  unless the source is very deep. In Figure 2, the amplitude of the vertical and the horizontal component of surface amplitudes has been shown for various epicentral distances. The converted phase at the bottom of the sedimentary section has the greatest amplitude on the vertical component at all distances. On the radial component, two phases have very close amplitudes for epicentral distances of about  $16^\circ$ .

The Haskell-Thomson matrix formulation will determine the response of a layered media to an input pulse for all frequencies when



Figure II.2

The vertical and horizontal component of surface displacement as a function of angle of incidence for S and the precursors, SPPP and SSSPP, from Moho and the base of the sedimentary layers.



$$k < \frac{\omega}{V_p} \quad (1)$$

where  $k$  is a wave number,  $\omega$  is angular velocity and  $V_p$  the maximum velocity in a layered media. This condition is equivalent to the phase velocity being larger than the maximum velocity in the media. This is always true for P waves. That is:

$$C > V_p \quad (2)$$

However, for S waves;

$$C = V_s \csc i_s \quad (3)$$

Therefore, for some epicentral distances conditions (1) and (2) are violated. The maximum wave number to be evaluated falls beyond the poles of matrix formulation in the complex  $k$  plane (Phinney, 1965) and they are imaginary for P waves, producing a damped motion in frequency. In the matrix elements, terms containing a sin or cos will be sinh and cosh.

Therefore, for these cases, the response can be calculated for wave numbers that occur before the first pole,  $k = \omega/V_p$  which corresponds to  $C = V_p$ .

The case where  $C < V_p$  produces a phase difference of  $\pm 90^\circ$  between the vertical and the horizontal components of S motion which corresponds to an elliptical particle motion, the axis of the ellipse being

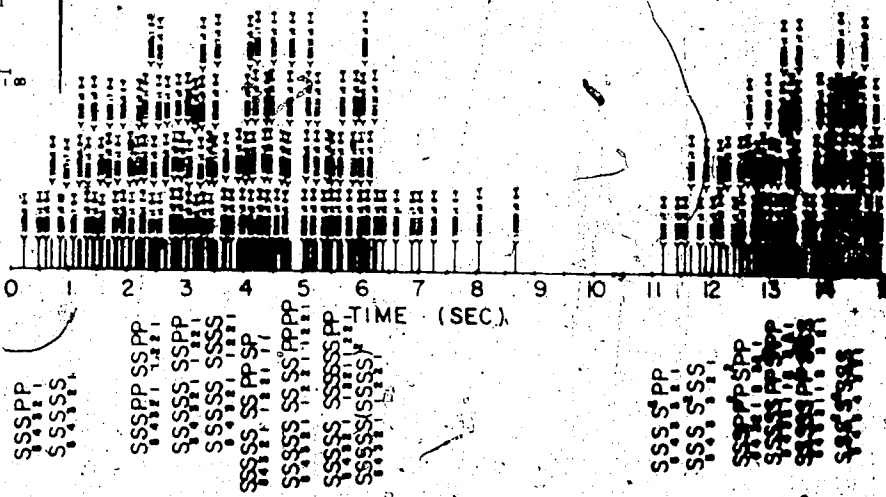
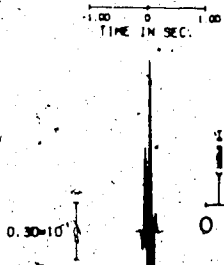
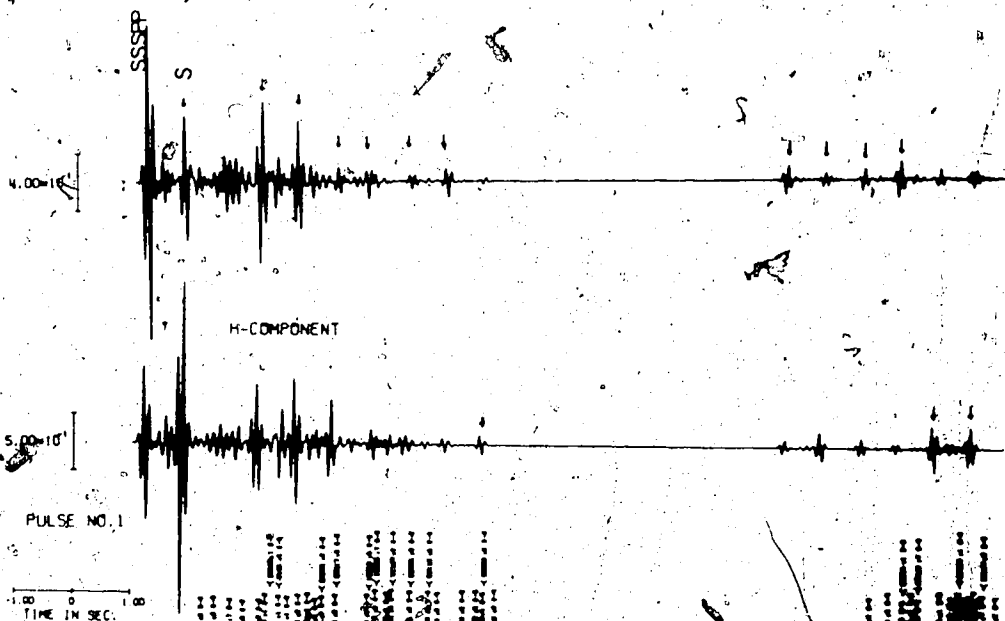
vertical and radial. This arises because the numerator of the transfer function for the horizontal component will be imaginary and the numerator of the transfer function for the vertical component will be real. The transfer function for S waves oscillates rapidly and produces a complicated particle motion. As far as we know, there have been no studies on the change of frequency of S waves with epicentral distance. But Nuttli and Whitmore (1962) have investigated the particle motion of S waves. They found that the interpretation can be done best when the phase velocity is larger than the maximum velocity in the crust.

The condition where  $C < V_p$  in a layer corresponds to the propagation of "trapped" modes for P waves but for the solution to exist the phase velocity must be greater than the S wave velocity in any layer. The ray theory approach should produce the same results as the matrix method. However, the ray approach used here does not predict the frequency characteristics of the surface motion. In Figure 3, seismograms still retain their high frequency character (10 Hz). For an angle of incidence of  $70^\circ$ , the phase velocity is less than the S wave velocities in a few layers. However, in Figure 3, the seismograms have a flat region between 7-11 seconds. These regions are due to rays which do not reach the surface since  $C < V_p$  in the

Figure II.3

Theoretical seismogram for a plane S wave incident at an angle of  $70^\circ$ . Among 10976 created rays, 1613 of them were used.

$i = 70^\circ$  S WAVE INCIDENT ON ALBERTA CRUST  
V-COMPONENT



model. In the ray method returning rays have not interacted with upgoing rays. However, this has been done in the wave solution producing an attenuation of S waves with a converted segments.

Precursors to the S or shear phase due to the presence of a crustal layer can introduce serious errors in interpretation if only the vertical component is available. The error may be as much as 1-6 seconds at all distances and is of particular importance when  $t_S - t_P$  times are used to determine epicentral distances, first motion studies and in the study of premonitory phenomena using the ratio  $t_S/t_P$  for earthquake prediction.

## BIBLIOGRAPHY

- Aki, K., Seismological evidences for the existence of soft thin layers in the upper mantle under Japan, J.G.R., 73, 585-594 (1968).
- Alpaslan, T., Spectral behavior of short period body waves and synthesis of crustal structure in western Canada, M.Sc. thesis, University of Alberta, Department of Physics, Edmonton (1968).
- Anderson, D.L., Elastic waves in layered anisotropic media, J.G.R., 66, 9 (1961)
- Anderson, D.L. and Archambeau, C., The anelasticity of the earth, J.G.R., 69, 2071-2084 (1964).
- Anderson, D.L., Recent evidence concerning the structure and composition of the Earth's mantle, Phys. and Chem. of Earth, 6, 1 (1965).
- Anderson, D.L., The anelasticity of the mantle, G.J., 14, 135-164 (1967).
- Babuska, V., Elastic anisotropy of the upper mantle and the Mohorovicic discontinuity, Studio Geophys. Geod., 14, 296-300 (1970).
- Backus, G.E., Long-wave elastic anisotropy produced by horizontal layering, J.G.R., 67, 4427 (1962).
- Backus, G.E., A geometrical picture of anisotropic elastic tensors, Reviews of Geophysics and Space Physics, 8, 3 (1970).
- Bakun, W.H., Crustal model parameters from P-wave spectra, B.S.S.A., 61, 4, 913-935 (1971).



- Berry, M.J., Jacoby, W.R., Niblett, E.R. and Stacey, R.A.,  
A review of geophysical studies in the Canadian  
cordillera, *Can. J. Earth Sci.*, 8, 788-801 (1971).
- Biot, M.A., The influence of initial stress on elastic  
waves, *J. App. Phys.*, 11, 522-530 (1940).
- Birch, F. and Bancroft, D., Elasticity and internal  
friction in a Quincy column of granite, *B.S.S.A.*,  
28, 243-254 (1938).
- Bonger, K.P. and Fuch, K., Crustal structure in south-  
west Germany from transfer ratio of long period  
body waves. International Upper Mantle Project,  
Scientific Report No. 27, Stuttgart, 1970.
- Born, W.T., The attenuation constant of earth materials,  
*Geophysics*, 132, 148 (1941).
- Brian, J.M., Surface wave attenuation and crustal anelas-  
ticity in Central North America, *B.S.S.A.*, 63,  
1057-1071 (1973).
- Brune, J. and Dorman, J., Seismic waves and earth struc-  
ture in the Canadian shield, *B.S.S.A.*, 53, 167-209  
(1963).
- Buchwald, V.T., Rayleigh waves in transversely isotropic  
media, *J. Mech. and App. Math.*, vol. XIV (1961).
- Bullen, K.E., An introduction to the theory of seismology,  
Cambridge University Press, 1963.
- Byerly, P., The earthquake of 1934 July 6: Amplitude and  
first motion, *B.S.S.A.*, 28, 12 (1938).

- Červený, V. and Ravindra, R., Theory of seismic head waves, University of Toronto Press, 1971.
- Cherry, J.T., et al, Shear waves recording using continuous signal methods, Geophysics, 33, 229-239 (1968).
- Christensen, N., Compressional wave velocities in metamorphic rocks at pressures to 10-K bars, J.G.R., 70, 24, 6147 (1965).
- Christensen, N. and Crosson, R.S., Seismic anisotropy in the upper mantle, Tectonophysics, 6, 2, 93-107 (1968).
- Cisternas, A., Betancourt, O. and Leiva, A., Body waves in a "Real Earth", part I, B.S.S.A., 63, 143 (1973).
- Clowes, R., et al, Seismic attenuation and the nature of reflecting horizons within the crust, J.G.R., 75, 6693-6705 (1970).
- Collins, F. and Lee, C.C., Seismic wave attenuation characteristics from pulse experiments, Geophysics, 21, 16-40 (1956).
- Corlet, A.V. and Emery, C.Z., Prestress and stress redistribution in rocks around a mine opening, Trans. Canadian Inst. Min. Met., 62, 188 (1959).
- Crampin, S., Higher modes of seismic surface waves: propagation in Eurasia, B.S.S.A., 56, 1227-1239 (1966).

- ~~159~~
- Crampin, S., The dispersion of surface waves in multi-layered anisotropic media, G.J.R. Astr. Soc., 21, 387-402 (1970).
- Crosson, R.S. and Christensen, N.I., Transverse isotropy of the upper mantle in the vicinity of Pacific fractured zone, B.S.S.A., 59, 1, 59-72 (1969).
- Cumming, G.L. and Kanasewich, E.R., Crustal structure in western Canada, final report contract No. AF19 (629)-2835, 1966.
- Donato, R.J., O'Brien, P.N.S. and User, M.J., Absorption and dispersion of elastic energy in rocks, Nature, 193, 764-765 (1962).
- Dorman, L.M., Anelasticity and spectra of body waves, J.G.R., 73, 12, 3877-3882 (1968).
- Doyle, H.A. and Hales, A.L., An analysis of the travel times of S waves to North American stations in the distance range  $28^{\circ}$  to  $82^{\circ}$ , B.S.S.A., 57, 761-771 (1967).
- Ellis, R.M. and Basham, P.W., Crustal characteristics from short-period P waves, B.S.S.A., 58, 1681-1700 (1968).
- Fedotov, S.A., The absorption of transverse seismic waves in the upper mantle and energy classification of near earthquakes of intermediate focal depth, Bull. (Izv.) Akad. Nauk. USSR, 6, 509-530 (1963).

- Fernandez, L.M., Master curves for the response of layered systems to compressional seismic waves, B.S.S.A., 57, 515-543 (1967).
- Futterman, W.I., Dispersive body waves, J.G.R., 67, 5279-5291 (1962).
- Ganley, D.C., A seismic reflection crustal model near Edmonton, Alberta, M. Sc. thesis, University of Alberta, Edmonton, 1973.
- Ganley, D.C. and Cumming, G.L., A seismic reflection model of the crust near Edmonton, Alberta, Can. J. Earth Sci. (1974) (in press).
- Garland, G.D. and Tanner, J.G., Investigation of gravity and isotropy in the southern Canadian cordillera, Pub. Dom. obs., 19, 5, 169-208 (1957).
- Gentlemen, W.M. and Sande, G., Fast Fourier transforms for fun and profit, Proc. of the Fall Joint Computer Conference, San Francisco, 563-578, 1966.
- Gilbert, F. and Backus, G.E., Propagator matrices in elastic wave and vibration problems, Geophysics, 31, 326-332 (1966).
- Gutenberg, B. and Richter, C.F., On supposed discontinuities in the mantle of the Earth, B.S.S.A., 21, 216-223 (1931).
- Gutenberg, B., Effect of ground on Earth's motion, B.S.S.A., 47, 221-249 (1957).
- Gutowski, P.R., Seismic array investigations of the upper and lower mantle, Ph.D. thesis, Department of Physics, University of Alberta, 1974.

- Haines, G.V., Hannaford, W. and Riddihaugh, R.P.,  
Magnetic anomalies over British Columbia and the  
adjacent Pacific ocean, *Can. J. Earth Sci.*, 8,  
387-391 (1971).
- Hannon, W.J., An application of the Haskell-Thomson matrix  
method to the synthesis of the surface motion due  
to dilatational waves, *B.S.S.A.*, 54, 2607 (1964).
- Harkrider, D.G. and Anderson; D.L., Computation of  
surface wave dispersion for multilayered aniso-  
tropic media, *B.S.S.A.*, 52, 2, 321-332 (1962).
- Hasegawa, H.S., Short-period P-coda characteristics in  
the eastern Canadian shield, *B.S.S.A.*, 60, 839-  
858 (1970).
- Hasegawa, H.S., Crustal transfer ratio of short and long  
period body waves recorded at Yellowknife,  
*B.S.S.A.*, 61, 1303-1320 (1971).
- Haskell, N.A., The dispersion of surface waves in multi-  
layered media, *B.S.S.A.*, 43, 17-34 (1953).
- Haskell, N.A., Crustal reflection of plane P and SV  
waves, *J.G.R.*, 67, 4751 (1962).
- HelMBERGER, D.V., The crust-mantle transition in the  
Bering sea, *B.S.S.A.*, 58, 179 (1968).
- Hess, H.H., Seismic anisotropy of the uppermost mantle  
under oceans, *Nature*, 203, 629-631 (1964).
- Hill, D.P., Velocity gradients and anelasticity from  
crustal body wave amplitudes, *J.G.R.*, 76, 3309-  
3325 (1971).

- Horton, C.W., A loss mechanism for the Pierre shale, *Geophysics*, 24, 667-680 (1959).
- Hron, F., Introduction to the ray theory in broader sense application to seismology, Laboratoire de physique de l'ecole normale Supérieure, 1968.
- Hron, F. and Kanasewich, E.R., Synthetic seismograms for deep seismic sounding studies using asymptotic ray theory, *B.S.S.A.*, 61, 5, 1169-1200 (1971).
- Hron, F., Criteria for selection of phases in synthetic seismograms for layered media, *B.S.S.A.*, 61, 765 (1971).
- Hron, F., Numerical methods of ray generation in multi-layered media. In "Methods in computation physics, vol. 12: Theoretical seismology", B.A. Bolt ed., Academic Press, New York and London, 1972.
- Hron, F., Kanasewich, E.R. and Alpaslan, T., Partial ray expansion required to suitably approximate the exact wave solution, *Geoph. J.*, (1974) (in press).
- Ibrahim, A., Determination of crustal thickness from spectral behavior of SH-waves, *B.S.S.A.*, 59, 1247-1258 (1969).
- Imamura, A., On the Earth-vibrations induced in some localities at the arrival of seismic waves, *Bull. Earthq. Res. Inst. (Tokyo)*, 7, 489-494 (1929).
- Ishii, H. and Ellis, R.M., Multiple reflection of plane P and SV waves by a dipping layer, *Geoph. J.*, 20, 11-30 (1970).

Ishii, H., Head and reflected waves from a SH line source in a dipping layer overlying an elastic medium. *Journal of Physics of the Earth*, 18, No. 1 (1970).

Jackson, D.D. and Anderson, D.L., Physical mechanism of seismic wave attenuation, *Rev. Mod. Phys.*, 30, 1178-1192 (1970).

Jeffreys, H. and Bullen, K.E., *Seismological Tables*, British Assoc. for Advancement of Science, Gray Milne Trust, London, 1940.

Jensen, O.G., Linear systems theory applied to a horizontally layered crust, Ph. D. thesis, University of British Columbia, 1970.

Joly, R.N., Investigation of shear waves, *Geophysics*, No. 4 (1956).

Kane, J., Teleseismic response of a uniformly dipping crust, *B.S.S.A.*, 56, 841-859 (1966).

Kaminura, K., The crust and upper mantle structure in Japan, *Bull. Earth. Res. Inst., Tokyo Univ.*, 44, 2, 511-518 (1966).

Khalevin, N.I. and Tavrín, I.F., On the subhorizontal stratification of the upper part of the Earth's crust in Urols; *Izv. Akad. Nauk. SSSR*, No. 3, 177 (1965).

Khalevin, N.I. and Koshkina, M.J., On the quasi-anisotropy of elastic properties of some rocks of Urols, *Izv. Akad. Nauk. SSSR*, No. 11, 734 (1966).

- Khatkevich, A.G., The theory of elastic waves in transversely isotropic media, Bull. (Izv.) Acad. Sci. USSR, Geophy. Ser. No. 9 (1964).
- Knopoff, L., The seismic pulse in material possessing solid friction: I plane wave, B.S.S.A., 46, 175 (1956).
- Knopoff, L. and Porter, L.D., Attenuation of surface waves in a granular material, J. Geophy. Res., 68, 6317-6321 (1963).
- Knopoff, L., Q. Rev. Geophy., 2, 625-660 (1964).
- Knopoff, L., Mantello e nucleo nella fisica fonetaria, Academic Press, 1971.
- Knott, C.G.; Reflexion and refraction of elastic waves with seismological applications, Phil. Mag. London, 48, 64-97, 567-569 (1899).
- Koefford, O., Oosterveld, M. and Galons, I., A laboratory investigation into elastic properties of limestone, Geoph. Prospecting, 11, 300-312 (1963).
- Kovach, R.L., Seismic surface waves: Some observations and recent development, Phys. Chem. Earth, 6, 251-314 (1965).
- Kraut, E.A., Anisotropic elastic waves, Rev. of Geophysics, 1, 401 (1964).
- Kuhn, V.V., The peculiarities of seismic waves in media with pinching out layers, Izvestia, No. 12, 1136-1147 (1961).



Kurita, T., Crustal and upper mantle structure in Japan from amplitude and phase spectra of long-period P waves, *Journal of Physics of the Earth*, 17, 1, 13-41 (1969).

Kurita, T., Attenuation of shear waves along the San Andreas fault in central California, *European Geophysical Society, first meeting, 1973.*

Lang, L.T. and Bery, J.W., Transmission and attenuation of primary seismic waves, *B.S.S.A.*, 59, 131-146 (1969).

Layat, C.A., Clement, A.C., Rommer, G. and Buffet, A., Some technical aspects of seismic refraction prospecting in Sahara, *Geophysics*, 26, 437-446 (1961).

Leblanc, G., Truncated crustal transfer functions and fine crustal structure determination, *B.S.S.A.*, 57, 719-733 (1967).

Lehmann, I., The Hindu Kush earthquake of March 4, 1949 as recorded in Europe, *B.S.S.A.*, 54, 1915-1925 (1964).

Lighthill, M.J., Studies on magneto-hydrodynamic waves and other anisotropic wave motion, *Phil. Trans.* A252, 397-430 (1960).

Love, A.E.H., A treatise on the mathematical theory of elasticity, Dover, 1944.

Lyakhovitsky, T.M. and Nevskey, M.V., Analysis of seismic wave velocity anisotropy in thin-layered periodic media, *Izv. Akad. Nauk. SSSR, Fiz. Zemli*, 9, 72 (1970).

Macdonald, G.J.F., Orientation of anisotropic minerals in a stress field, *Geol. Soc. Am. Mem.*, 79, 1 (1960).

Macelwane, J.B. and Schon, F.W., Introduction to theoretical seismology, St. Louis University, 1932.

Maxwell, J.C., On the dynamical theory of gases, Dover Publication, New York, 1866.

McCamy, K., An investigation and application of the crustal transfer ratio as a diagnostic for explosion seismology, *B.S.S.A.*, 57, 6, 1409-1428 (1967).

McCollum, B. and Snell, F.A., Asymmetry of sound velocity in stratified formations. Reprinted in *Early Geophysical papers, Soc. of Exp. Geophysicists* (1932), 212-217 (1947).

McDonald, T.J., Angona, F.A., Mills, R.L., Sengbush, R.L., van Norstrand, R.G. and White, J.E., Attenuation of shear and compressional waves in Pierre shale, *Geophysics*, 23, 421-439 (1958).

Mereu, R.F. and Jobidon, G., A seismic investigation of the crust and Moho on a line perpendicular to the Glenville front, *Can. J. Earth Sci.*, 8, 1553-1583 (1971).

Mikhlin, S.G., Linear equations of mathematical physics,  
Holt, Rinehart and Winston, Inc., New York, 1966.

Milne, A.R., Two seismic refraction measurements north  
Pacific ocean basin and Dixon entrance, B.S.S.A.,  
54, 1, 41-50 (1964).

Musgrave, M.J.P., On the propagation of elastic waves in  
anelotropic media, Proc. Roy. Soc., 226, 339-366  
(1954).

Nafe, J.E. et al, in Talwani, et al, J.G.R., 64, 1545-  
1555 (1959).

Nasu, N., Comparative studies of Earthquake motions above  
ground and in a tunnel, part I, Bull. Earthq. Res.  
Inst. (Tokyo), 9, 454-472 (1931).

Neuman, F., An analysis of S-wave, B.S.S.A., 20, 19-20  
(1930).

Niazi, M., Corrections to apparent azimuths and travel-  
time gradients for a dipping Mohorovicic discon-  
tinuity, B.S.S.A., 56, 491-509 (1966).

Nuttli, O. and Whitmore, D.J., An observational deter-  
mination of the variation of the angle of incidence  
of P waves with epicentral distance, B.S.S.A., 51,  
269-276 (1961).

Nuttli, O. and Whitmore, D.J., On the determination of  
polarization angle of S wave, B.S.S.A., 52, 95-  
108 (1962).

O'Brien, P.N.S., A discussion on the nature and magnitude  
of elastic absorption in seismic prospecting,  
Geoph. Pros., 9, 261-275 (1961).

- O'Neill, M.E. and Healy, J.H., Determination of source parameters of small earthquakes from P-wave rise time, B.S.S.A., 63, 599-614 (1973).
- Osipov, I.O., Features of variation of propagation velocities of elastic waves in anisotropic media, Izv. Acad. Sci. USSR, Geophy. Ser. No. 1 (1962).
- Peselnick, L. and Outerbridge, W.F., Internal friction in shear and shear modulus of Solenhofen limestone over a frequency of  $10^7$  Hz, J.G.R., 66, (2), 581-588 (1961).
- Phinney, R.A., Structure of the earth's crust from spectral behavior of long-period body waves, J.G.R., 69, 14, 2997 (1964).
- Press, F., Seismic wave attenuation in the crust, J.G.R., 69, 4417-4418 (1964).
- Rait, R.W., Anisotropy of the upper mantle, Geophysical Monographs, 13, Am. Geoph. Union, 1969.
- Richards, P.G., Elastic wave solution in stratified media, Geophysics, 36, 798-809 (1971).
- Richards, T.C. and Walker, D.I., Measurement of the thickness of the Earth's crust in the Albertan plains of western Canada, Geophysics, 24, 262-284 (1959).
- Ricker, N.A., Further developments in the wavelet theory of seismogram structure, B.S.A.A., 33, 197-228 (1943).
- Riznichenko, Yu.V., On seismic quasi-anisotropy, Izv. Akad. Nauk. SSSR, ser. XIII, No. 6 (1949).

Rogers, Jr., A.M. and Kisslinger, C., The effect of a dipping layer on P-wave transmission, B.S.S.A., 62, 1, 301-324 (1972).

Sato, R., Attenuation of seismic waves, J. Physics Earth., 15, 32-61 (1967).

Savage, J.C., Attenuation of elastic waves in granular mediums, J.G.R., 70, 3935-3952 (1965).

Savarensky, E.F., On the prediction of earthquakes, Tectonophysics, 6, 17-27. (1968).

Sezawa, K. and Kanai, K., Possibility of the free oscillations of strato excited by seismic wave, III. Bull. Earthq. Res. Inst. (Tokyo), 10, 1-18 (1932).

Sezawa, K. and Kanai, K., On the free vibrations of a surface layer due to an obliquely incident disturbance, Bull. Earthq. Res. Inst. (Tokyo), 15, 375-383 (1937).

Silaeva, O.I. and Bayuk, E.E., The nature of anisotropy of the elastic properties of rocks, Izv. Akad. Nauk SSSR, 12, 789-793 (1967).

Somerville, P.G. and Ellis, R.M., P-coda evidence for a layer of anomalous velocity in the crust beneath Leduc, Alberta, Can. Journal of Earth Sci., 9, 845-856 (1972).

Spencer, T.W., The method of generalized reflection and transmission coefficients, Geophysics, 25, 625 (1960).

- Spetzler, H. and Anderson, D., The effect of temperature and partial melting on velocity and attenuation in a simple binary system, *J.G.R.*, 73, 6051-6060 (1968).
- Sprenke, K.F., An application of the P-coda spectral ratio method to crustal structure in central Alberta, M. Sc. thesis, University of Alberta, Edmonton, 1972.
- Stacey, R.A., Gravity anomalies, crustal structure and plate tectonics in the Canadian cordillera, *Can. Journal of Earth Sci.*, 10, 615-628 (1973).
- Stonley, R., The seismological implications of anisotropy in continental structure, *Monthly Notices of Royal Astronomical Society, Geophysical Supplement*, 6, 222-232 (1949).
- Sumner, R.D., Attenuation of earthquake generated P waves along the western flank of the Andes, *B.S.S.A.*, 57, 173-190 (1967).
- Suyimura, A., A possible anisotropy of the upper mantle accounting for deep earthquake faulting, *Tectonophysics*, 5, No. 1, 25-33 (1967).
- Synge, J.L., *J. Math. Phys.*, 35, 323 (1957).
- Thomson, W.T., Transmission of elastic waves through a stratified solid medium, *J. Appl. Phys.*, 21, 89 (1950).

- Tsukuda, T., J. Phys. Earth, 20, 341-356 (1972).
- Tullos, F.W. and Reid, A.C., Seismic attenuation in Gulf coast sediments, Geophysics, 34, 516-528 (1969).
- Vanderstoep, D.M., Velocity anisotropy measurements in wells, Geophysics, 31, 900-916 (1966).
- Walsh, J.B., Seismic wave attenuation in rock due to friction, J. Geophys. Res., 71, 2591-2599 (1966).
- Walsh, J.B., New analysis of attenuation in partially melted rock, J.G.R., 74, 4333-4337 (1969).
- Weatherby, B.B., Born, W.T. and Harding, R.L., Granite and limestone velocity determinations in Arbuckle mountains, Oklahoma, Bull. Amer. Assoc. Petr. Geol., 18, 106-118 (1934).
- Whitcomb, J.H., Garmony, J.D. and Anderson, D.L., Earthquake prediction variation of seismic velocities before the San Fernando earthquake, Science, 180, 632-635 (1973).
- White, W.R.H. and Savage, J.C., A seismic refraction and gravity of the Earth's crust in B.C., B.S.S.A., 55, 463-486 (1965).
- Whitmarsh, R.B., Seismic anisotropy of the uppermost mantle beneath mid-ocean ridges, Nature, 268, No. 5141, 558-559 (1968).
- Wu, F.T. and Hannon, W.J., PP and crustal structure, B.S.S.A., 56, 3, 733-747 (1966).

Wuenchel, P.C., Dispersive body waves on experimental study, *Geophysics*, 30, 539-551 (1965).

Yegorkina, G.V., Use of recordings of converted seismic waves to study crustal anisotropy, *Izv. Acad. Nauk.*, 567-573 (1969).

Zengeni, T.G., A note on an azimuthal correction for  $dT/d\Delta$  for a single dipping plane interface, *B.S.S.A.*, 60, 299-306 (1970).



Wuenchel, P.C., Dispersive body waves on experimental study, *Geophysics*, 30, 539-551 (1965).

Yegorkina, G.V., Use of recordings of converted seismic waves to study crustal anisotropy, *Izv. Acad. Nauk.*, 567-573 (1969).

Zengeni, T.G., A note on an azimuthal correction for  $dT/d\Delta$  for a single dipping plane interface, *B.S.S.A.*, 60, 299-306 (1970).